ELECTRODEPOSITION OF CATALYSTS FOR PEM FUEL CELLS USING A POTENTIOSTATIC METHOD

Dissertation
zur Erlangung des Grades
des Doktors der Naturwissenschaften
der Naturwissenschaftlich-Technischen Facultät
der Universität des Saarlandes

von
Dan Iulian Durneata

Saarbrücken
2017

Tag des Kolloquium :	24.07.2017
Dekan :	Guido Kickelbick
Berichterstatter:	Prof. Rolf Hempelmann
	Prof. Guido Falk
Vorsitz :	Prof. Kaspar Hegetschweiler
Akad. Mitarbeiter:	Dr. Volker Huch

Für Licht braucht man Energie, genauso wie für Kreativität.

Mika Gustavson

ABSTRACT

The fundamental principle of proton exchange membrane fuel cells (PEMFC) is to electrochemically convert Hydrogen (H_2) and Oxygen (O_2) into electric energy, water and heat. The main advantage of this technology is to provide clean energy without any carbon dioxide emission. Thereby, one of the most important fuel cell (FC) components represents the electrocatalyst. Typically, they are prepared on the base of noble metals (Pt, Pd) and their alloys. Due to their high prices, the FC production costs are high and the FC marketing at a large scale is difficult. For this reason we have focused in this work on the catalyst layer and microstructure construction by using and combining spraying and the electrodeposition methods. Using the proposed techniques the catalyst loading is significantly reduced ($\leqslant 0.1\,\mathrm{mg\,cm^{-2}}$) without a noticeable PEMFC performance decrease. The performed tests on anode and cathode sides at a temperature of 80 °C indicated a superior performance in comparison with commercial catalysts. Due to the flexibility of the employed methods, it was possible to up-scale the process and to produce gas diffusion electrodes with an area of $225\,\mathrm{cm^2}$. The applied ageing procedure indicated high catalyst stability ($\leqslant 40\,\%$ current density losses at a voltage of $650\,\mathrm{mV}$) for all tested electrodes. Furthermore, a series of devices necessary for FC testing were produced and for each developed instrument, highly accessible controlling software's were programmed.

ABSTRAKT

Das grundlegende Prinzip von Protonenaustauschmembran-Brennstoffzellen ($PEM - BZ$) besteht darin, Wasserstoff (H_2) und Sauerstoff (O_2) elektrochemisch in elektrische Energie, Wasser und Wärme umzuwandeln. Ein großer Vorteil dieser Technologie besteht darin, saubere Energie ohne Kohlenstoffdioxid-Emission zu liefern. Eine der wichtigsten BZ-Komponenten stellt dabei der Elektrokatalysator dar. Typischerweise werden diese durch Edelmetalle (Pt, Pd), bzw. deren Legierungen dargestellt. Aufgrund der hohen Preise dieser Edelmetalle sind die BZ-Produktionskosten sehr hoch und die Markteinführung in großem Maßstab wird erheblich erschwert. Aus diesem Grund lag der Fokus in der vorliegenden Arbeit auf der Katalysatorschicht- und Mikrostrukturkonstruktion. Hierzu wurden sowohl Sprüh- wie auch Elektroabscheidungsverfahren verwendet und kombiniert. Mit Hilfe dieser Verfahren konnte die Katalysatorbeladung ohne signifikante Leistungsabnahme der PEM-BZ deutlich reduziert werden ($\leqslant 0.1\,mg\,cm^{-2}$). Die durchgeführten Versuche an der Anoden- und Kathodenseiten bei einer Temperatur von $80\,°C$ haben im Vergleich zu den handelsüblichen Katalysatoren eine überlegene Leistung gezeigt. Aufgrund der Flexibilität der eingesetzten Methoden war es möglich, den Prozess zu skalieren und Gasdiffusionselektroden mit einer Fläche von $225\,cm^2$ herzustellen. Das angewandte Alterungsverfahren zeigte dabei eine hohe Katalysatorstabilität ($\leqslant 40\,\%$ Stromdichteverluste bei einer Spannung von $650\,mV$) bei allen getesteten Elektroden. Weiterhin wurde eine Reihe von Geräten, welche für BZ-Tests erforderlich sind, eigens hergestellt und jeweils eine frei zugängliche Steuerungssoftware programmiert.

PUBLICATIONS

Paper

- A. EGETENMAYER, I. RADEV, D. DURNEATA, M. BAUMGÄRTNER, V. PEINECKE, H. NATTER AND R. HEMPELMANN, Pulse electrodeposited cathode catalyst layers for PEM fuel cells, International journal of hydrogen energy, **(2017)**, accepted
- T. DIER, D. RAUBER, D. DURNEATA, R. HEMPELMANN AND D. VOLMER, Sustainable Electrochemical Depolymerisation of Lignin in Reusable Ionic Liquids, submitted in Scientific reports, **(2017)**, waiting for revision
- M. SCHMITT, R. HEMPELMANN, S. INGEBRANDT, W. MUNIEF, D. DURNEATA, K. GROSS AND F. HEIB, Statistical approach for contact angle determination on inclining surfaces: "slow-moving" analyses of non-axisymmetric drops on a flat silanized silicon wafer, International journal of adhesion and adhesives, 55 (**2014**), pp. 123-131

Oral presentation

- D. DURNEATA, H. NATTER AND R. HEMPELMANN, 3D fuel cell electrodes architecture prepared by a layering structuring process, Fuel cells science and technology **(2016)**, Glasgow (UK)

Posters

- D. DURNEATA, H. NATTER AND R. HEMPELMANN, Catalyst layer pore structuring for proton exchange membrane fuel cell electrodes, Bunsentagung (**2016**), Rostock (Germany)
- R. ENGSTLER, D.DURNEATA, H. NATTER AND R. HEMPELMANN, In situ method for efficient catalyst layer production with very low catalyst loading, Bunsentagung (**2016**), Rostock (Germany)
- D. DURNEATA, H. NATTER AND R. HEMPELMANN, Optimization of Pt electrochemical deposition parameters on PEM-FC, GDCh Electrochemistry **(2014)**, Mainz (Germany)
- D. DURNEATA, F. ARENA AND R. HEMPELMANN, Optimized MEA preparation parameters for the use of cross-linked sPEEK membrane in HT-PEMFCs, GDCh Wissenschaftsforum Chemie **(2013)**, Darmstadt (Germany)
- F.ARENA, J. MITZEL, D. DURNEATA and R. HEMPELMANN, Permeability and diffusion measurements on polymer exchange membranes for fuel cell applications (PEM-FC), Euromembrane (**2012**), London (UK)

ACKNOWLEDGEMENTS

This thesis marks the culmination of my PhD journey which I started in September 2012 at the Institute of Physical Chemistry, Saarland University. What was achieved in this period would not have been possible without the support and encouragement of family, friends, colleagues and supervisors.

Firstly, I would like to thank Professor Rolf Hempelmann and PD Dr. Harald Natter for their support and guidance during the entire PhD. I have always felt so lucky to be their student and to pursue my PhD under their supervision.

I would like to thank the members of the research group; colleagues, academics and administrators, for their help with the various aspects of the work and other matters during the project period.

I'd like to give special thanks to Dipl. -Ing. Rudolf Richter and the colleagues from the workshop Jens, Norbert and Peter which have made possible the planing and construction of many devices developed during this thesis. They have sustained all the time my ideas and have provided technical support on each question.

My gratitude and appreciation are extended to the following people for their support: Vinoba Vijiaratnam, Florian Heib, Daniel Rauber, Mohaned Hammad, Julia Baumgarten, Anette Britz and Konstantin Weisshaar.

I would like to acknowledge and thank Francesco Arena and Jens Mitzel for helping me on my research and providing me with powerful advices. Their professionalism has motivated me to work harder in order to approach their expertise.

A special thank to Silvia Kuhn for the extra TEM and SEM appointments. Also I want to thank Silvia for the daily discussions in the kitchen, which sometimes was totally crazy.

An exclusive appreciation to Elfi Jungblut which has measured countless samples for me. Without her help, I could not evaluate and improve the samples obtained in actual work.

Not at least I want to thank for the entire support on the sample preparation and characterization to my two student worker Roxanne Engstler and Gabriela Prada. We have suffered and enjoyed together the bad and the good results collected during this PhD journey.

Finally, I would like to say a massive THANK YOU to my dear wife, without her I would not have managed to get here.

CONTENTS

LIST OF FIGURES

LIST OF TABLES

ACRONYMS

BP	Bipolar plate
CCM	Catalyst-coated membrane
CCS	Catalyst-coated substrate
CHP	Combined heat and power
CL	Catalyst layer
CPE	Constant phase element
CV	Cyclic voltammetry
DC	Direct current
DHE	Dynamic hydrogen electrode
DMFC	Direct methanol fuel cell
DP	Dew Point
ECSA	Electrochemical active surface area
EEPROM	Electrically erasable programmable read-only memory
EIS	Electrochemical impedance spectroscopy
FC	Fuel cell
FCEV	Fuel cell electric vehicle
GDE	Gas diffusion electrode
GDL	Gas diffusion layer
GUI	Graphical user interface
HDA	Hydrogen depolarized anode
HOR	Hydrogen oxidation reaction
ICP – OES	Inductively coupled plasma optical emission spectroscopy
IPA	Isopropyl alcohol
ISECD	In-situ electrochemical catalyst deposition
LV	LabVIEW
MEA	Membrane electrode assembly
MFC	Mass flow controller
MPL	Microporous layer
OCV	Open circuit voltage
ORR	Oxygen reduction reaction
PEM	Proton exchange membrane
PEMFC	Proton exchange membrane fuel cell
PID	Proportional integral derivative
PPT	Pulse plating technique
PS	Particle size
PV	Photo voltaic
RH	Relative humidity
ROM	Read-only memory
RTD	Resistance temperature detector
SEM	Scanning electron microscopy
SPEEk	Sulfonated poly(ether-ether ketone)

SRAM	Static random-access memory
SSR	Solid state relay
TEM	Transmission electron microscopy
TPB	Triple phase boundary
USART	Universal synchronous/asynchronous receiver transmitter
USB	Universal serial bus
VI	Virtual instrument
WE	Working electrode
WP	Working package

SUPPLIERS & INSTITUTIONS

Arduino	Arduino (Italy)
Atmel	Atmel Corporate (San Jose, USA)
Bandelin	Badelin electronic GmbH & Co. KG (Berlin, Germany)
Bio – Logic	Bio-Logic SAS (Claix, France)
Bronkhorst	Bronkhorst High-Tech B.V. (AK Ruurlo, Netherlands)
Brooks Instrument	Brooks Instrument (Hatfield, USA
Conrad	Conrad Electronic SE (Hirschau, Germany)
DLR	Deutsches Zentrum für Luft- und Raumfahrt (Stuttgart, Germany)
DOE	Department of energy (Washington DC, USA)
Drollinger	Drollinger Metalveredelungswerke GmbH (Birkenfeld, Germany)
DuPont	E.I. du Pont de Nemours and Company (Wilmington, USA)
Eisenhuth	Eisenhuth GmbH & Co. KG (Osterode am Harz, Germany)
Erichsen	Erichsen GmbH & Co. KG (Hemer, Germany)
Eurotherm	Invensys Eurotherm (Ashburn, USA)
FEM	Research Institute for Precious Metals and Metal Chemistry (Schwäbisch Gmünd, Germany)
Freudenberg	Freudenberg FCCT KG (Weinheim, Germany)
FTDI	Future Technology Devices International Limited (Glasgow, United Kingdom)
Fumatech	FuMA – Tech GmbH (Bietigheim-Bissingen, Germany)
Gamec	Gamec Analysentechnik (Illingen, Germany)
Horst	Horst GmbH (Lorsch, Germany)
IKA	IKA Werke GmbH & Co. KG (Staufen, Germany)
JM	Johnson Matthey (London, United Kingdom)
Julabo	Julabo GmbH (Seelbach, Germany)
Jumo	Jumo GmbH & Co. KG (Fulda, Germany)
Landgraf	Landgraf Laborsysteme HLL GmbH (Langenhagen, Germany)
Michell	Michell Instruments Ltd. (Cambridgeshire, United Kingdom)
Microchip	Microchip Technology Inc. (Chandler,USA)
Neslab	Neslab Instruments Inc. (New Hampshire, USA)
NI	National Instruments Corporation (Austin, USA)
Perma Pure	Perma Pure LLC (Lakewood, USA)
PKP	PKP Prozessmesstechnik GmbH (Wiesbaden, Germany)
RS	RS Components GmbH (Mörfelden-Walldorf, Germany)
SGL	Carbon SE (Wiesbaden, Germany)
Simrit	Freudenberg Simrit GmbH & Co. KG (Weinheim, Germany)
Swagelok	B.E.S.T. Fluidsysteme GmbH (Frankfurt, Germany)
TI	Texas Instruments Incorporated (Dallas, USA)
Timcal	Timcal Graphite & Carbon Ltd. (Bodio, Switzerland)

Toray	Toray K.K. (Tokio, Japan)
Umicore	Umicore AG & Co. KG (Hanau, Germany)
USaar	Saarland University (Saarbrücken, Germany)
Velleman	Velleman nv (Gavere, Belgien)
ZBT	Fuel cell research center ZBT GmbH (Duisburg, Germany)

1

IN-SITU ELECTROCHEMICAL CATALYST DEPOSITION PROJECT

The earth population is steadily increasing, with catastrophic results on our planet. In the entire world new energy sources are investigated and adopted to supply the consumers. However, to hold our home clean and to stop the greenhouse emissions clean energy sources and storage systems are required. Nowadays, we are living in the battery era, which due to its flexibility and price are applied in many domains. They are present in all usual devices, from telephones or cars to the high advanced submarines or data centers. Anyhow, it possess a limited storage energy capacity in competition to the generated power and therefore cannot be used as permanent storage solution. One of the simplest and elegant method is to convert the energy excess in chemical energy, which is stable and can be always attainable. So a system is for example H_2, it is abundant on our planet and can be extracted from the water through the electrolysis process. The H_2 conversion in electrical energy takes place usually in a fuel cell (FC).

FC are highly efficient electrochemical devices that convert the chemical energy of a fuel directly into electricity, water and heat. Because the FCs does not combust the fuel, they are quiet, pollution-free and more efficient that combustion technologies ($\geqslant$55 %) [4]. FCs are mostly used as stationary energy supplies and nowadays as power provider for cars. In order to make this new technology more attractive for other industries, a massive material and production costs reduction is required. Not at least, improvement of the performance and life-time is mandatory.

1.1 GENERAL INTERESTS

In order to accomplish these high requirements, new materials for FC components have to be investigated. An appropriate attention should be given to the catalyst, which represents 47 % of the entire stack costs [4]. The use of alternative electrocatalysts could decrease the FC production costs and not at least improves its marketing. Some metals such as Ru, Co, Ni or Pt alloys could represent the solution.

To attain these requirements, through the in-situ electrochemical catalyst deposition (ISECD) project new methods to produce the electrocatalyst have been investigated. So, using two different electrochemical processes the catalyst is deposited directly on the commercial gas diffusion layers (GDL).

In the first procedure, the catalyst deposition is achieved from a galvanic bath using a pulse plating technique (PPT). This is suitable to produce catalysts from noble metals (e. g. Pt, Au) or simple alloys (e. g. PtRu) over large GDE areas, in a continuous process. During this technique the metal is deposited from an aqueous solution, directly into the microporous layer (MPL). Subsequently, a penetration with a proton conductive ionomer is necessary.

In the second approach, which is developed in this work, the catalyst is potentiostatic deposited, under dry conditions. This allows the production of electrochemical active catalysts (e. g. Pt or Pt alloys as Co, Cr and Ni), without the undesired H_2 evolution during the deposition process. For this procedure the precursor and the ionomer are firstly introduced in the MPL network. Thus, for a precisely precursor distribution a spraying device is constructed. Along that, to attain a optimum precursor reduction the electrodeposition cell is improved. In addition, the catalyst stability and activity tests are performed in a self-developed test station. In this way a complete electrochemical characterisation of the prepared catalyst structure is possible.

The principal advantage of both methods is the minimization of noble metal consumption during the GDE production, through a high catalyst transfer rate. This implies a high deposition efficiency at the same time with low noble metal loadings and high FC performances. Moreover, for both methods the catalyst structure is created mostly at the triple phase boundary (TPB). This implies a simultaneous catalyst contact with the ion conductor (ionomer), the electron conducting phase (carbon network), as well as to the reactants.

1.2 PROJECT PARTNERS

The attainment of the proposed goals is based on a coordinated collaboration between the participating research groups. In order to complete all requirements, three research centers cooperate in the project In-situ electrochemical catalyst deposition (ISECD).

- Research institute for precious metals and metal chemistry (FEM)
- Saarland University, department of Physical Chemistry (USaar)
- Fuel cell research center ZBT GmbH (ZBT)

These three research partners have deep knowledge in the area of noble metals (FEM), electrochemical coating (FEM, USaar) and fuel cell technology (USaar, ZBT). The FEM is responsible for the galvanostatic deposition of noble metals. USaar is focused on the potentiostatic deposition of the electrocatalyst in the GDL. Furthermore, the ZBT with its experience in FCs characterization, complete the GDE and membrane electrode assembly (MEA) production process. Along that, they are responsible for the ageing tests of the prepared GDEs.

In order to accomplish the objectives successfully, as can see in Table 1, the project is divided into ten distinct working packages (WPs). These contain the main topics, which are considered over the entire project period. In the focus is the development of above mentioned methods for the catalyst deposition and the semi-automation concept for industrial mass production.

Research Institute for Precious Metals and Metal Chemistry

Saarland University

Fuel cell research center

Figure 1: The ISCED project consortium.

	Electrochemical methods to produce gas diffusion electrode for PEM fuel cells (ISCED)																															
	Time and work plan		Current Month/Year																													
			1	2	3	4	5	6	7	8	9	10	11	12	13	14	15	16	17	18	19	20	21	22	23	24	25	26	27	28	29	30
WP	Description	RC																														
1	Elaboration of target quantities for GDE manufacturing with regard to the catalyst proprieties for cathode and anode applications (loading, crystallite size, penetration depth for Pt and Pt-alloys).	1,2,3																														
2	Expand technical concepts for the two different electrochemical preparation processes (ISECD).	1,2																														
3	Construction, development and commissioning of deposition cells and additional components for two different catalysts electrochemical production methods.	1,2																														
4	Characterization and optimization of coating parameters for two different electrochemical production methods in order to achieve the WP 1 targets (with electrochemical methods, ICP-OES, SEM, TEM, FIB, Raman, Rheology, XRD).	1,2																														
5	Development of a procedure to activate and contact the GDE with ion conductor by adding an additional layer.	2,3																														
6	Processing the polymer activated GDE and MEA characterization (structure, performance, CV, EIS).	2,3																														
7	Iterative structure optimization of the GDE as well as the polymer extra layer based on fuel cell measurement of prepared MEA.	1,2,3																														
8	Transfer the successful developed method from Pt to powerful Pt alloys such as Pt_3Co in order to improve the cathode performance.	1,2,3																														
9	Processing the Pt alloys GDE to MEA and characterization in fuel cell test bench.	1,2,3																														
10	Comparative evaluation of the two different electrochemical producing methods with regard to device costs, production cost and the power density vs platinum loading.	1,2																														
	RC1: FEM, RC2: Usaar, RC3: ZBT		2014									2015												2016								

Table 1: Gantt chart of the project "In-situ electrochemical catalyst deposition"

2 RENEWABLE ENERGIES - EXPLORE FUEL CELLS

The search for low-carbon heating and electricity alternatives to natural gas and petrol which are affordable for stationary and mobile applications has been speedup in the last years. This transition is sustained by the environmental constraints and attractiveness of economic and environmental opportunities that will be open during the renewable energy transition [5]. Also, the ability to provide energy without dependency on weather, time and seasons should be considered [6].

2.1 RENEWABLE ENERGIES AND ITS APPLICATIONS

Around the world, the fossil fuels are the dominant energy source. They are used to heat most of our homes, fuel our cars and trucks and generate most of the electricity that is utilized today. But, our high demand on fossil fuel comes as a heavy cost to the climate. In December 2015, 195 countries adopted in Paris the first universal climate agreement. They agreed to hold "the increase in the global average temperature to well below 2 °C above pre-industrial levels and to pursue efforts to limit the temperature increase to 1.5 °C above pre-industrial levels, recognizing that this would significantly reduce the risks and impacts of climate change". In order to limit global warming to 1.5 °C, a global CO_2emission reduction of 80 % or higher should be achieved until 2050 [7].

To reach this ambitious target, all polluting fuels must be replaced with clean energy sources and leave most of the world's fuel reserves in the ground. Moreover, the switch to renewable energy could improve our health, by preventing the air pollution, and increase our safety by protecting us from the hazards of dangerous fuels. Furthermore, the water consumption can be diminished, by adapting renewable energy. Most of the renewable energy sources use small water quantities in the electricity production, leaving more water available for homes and the preservation of healthy aquatic ecosystems [8].

2.1.1 *Renewable energy sources*

Renewable energy comes from sources that are naturally replenished in a relatively short time frame. Sunlight, wind, water and geothermal heat are the most known renewable energy sources which are present on earth.
Bioenergy: comes from trees and crops grown for their energy content and forms by-products such as sewage, straw, manure, animal and vegetable fat and rubbish. These energy sources are referred as biomass feed-stocks. Biomass can be burned to produce heat or can be turned into biofuels that can be the substitutes for fossil fuels in transport.

Geothermal energy: uses the heat extracted from the ground to form steam, which is transported by pipes to geothermal power stations. These geothermal fluid is turned into steam that drives turbine generators and produce electricity. This type of energy does not depend on weather conditions, making it consistent and reliable, but unfortunately it is not present on all countries.
Wind energy: results from the wind actions on the turbine blades, which are connected to generators producing electricity. Wind turbines are easy to install and do not produce greenhouse gas emissions, a fact that makes the wind power one of the most environmental friendly forms of electricity generation. Even if this energy source does not pollute the environment, many people's are complaining about the noise produced by the rotors. Therefore, most of the wind turbines are built on the sea, far away from houses.
Solar energy: represents the conversion of sun energy using solar panels, also known as photo-voltaic (PV) panels, to electricity. The generated electricity is injected into the electricity grid where each one can use the current generated by this renewable energy source. Otherwise, it can be stored in batteries or other chemical storage systems (e. g. H_2, methane). Another technology is solar water heating, which uses the sun to heat water. Solar technology is silent and unobtrusive and can be used all around the countries. Therefore, most of the PV panel are installed on house roofs. The main barrier to its uptake is the cost.
Hydro-electricity: uses gravity to drive water from streams, rivers or dams through turbines, converting the kinetic energy into electricity. This technology burns no fuel, so the pollution is minimal and requires low operation and maintenance costs. However, hydro-power facilities can have large environmental impacts by changing the environment and affecting land use, homes and natural habitats in the dam area.

Most of produced electric power from the renewable energy sources is consumed instantaneously. The electricity generation is in general carefully timed, so it occurs at the same time it is demanded. When the proper amount of electricity cannot be provided at the request time, the grid is overloaded, at worst this may lead to service interruptions [1]. Moreover, the power demand varies from time to time and the price of electricity changes accordingly. In case of high electrical energy consumption, the power suppliers must complement the base-load power plant (such as coal-fired and nuclear) with less cost-effective but more flexible forms of power-generation, such as oil and gas-fired generators [1], which affect the environment in a negative way.

An optimum solution is to store electricity at peak-off times in storage devices (over night) and discharge it at peak times. Furthermore, the use of storage devices decreases the gap between day and night-time and allows a flatter electricity generation, with improvements in operating efficiency and cost reduction. Figure 2 shows a range of technologies and a rough variety of application where they can be used, depending on the generated electricity [9]. For applications where the energy is required for short time the flywheel and the battery are a quite good option, but when the energy is necessary to be stored over many months, transformation to synthetic natural gas or to hydrogen are the better choices. Another aspect is the storage cost (cost per kWh), which is low for the storage technology presented on the right side of the Figure 2 (synthetic natural gas, H_2) and high for the left one (lead acid battery and flywheel energy storage).

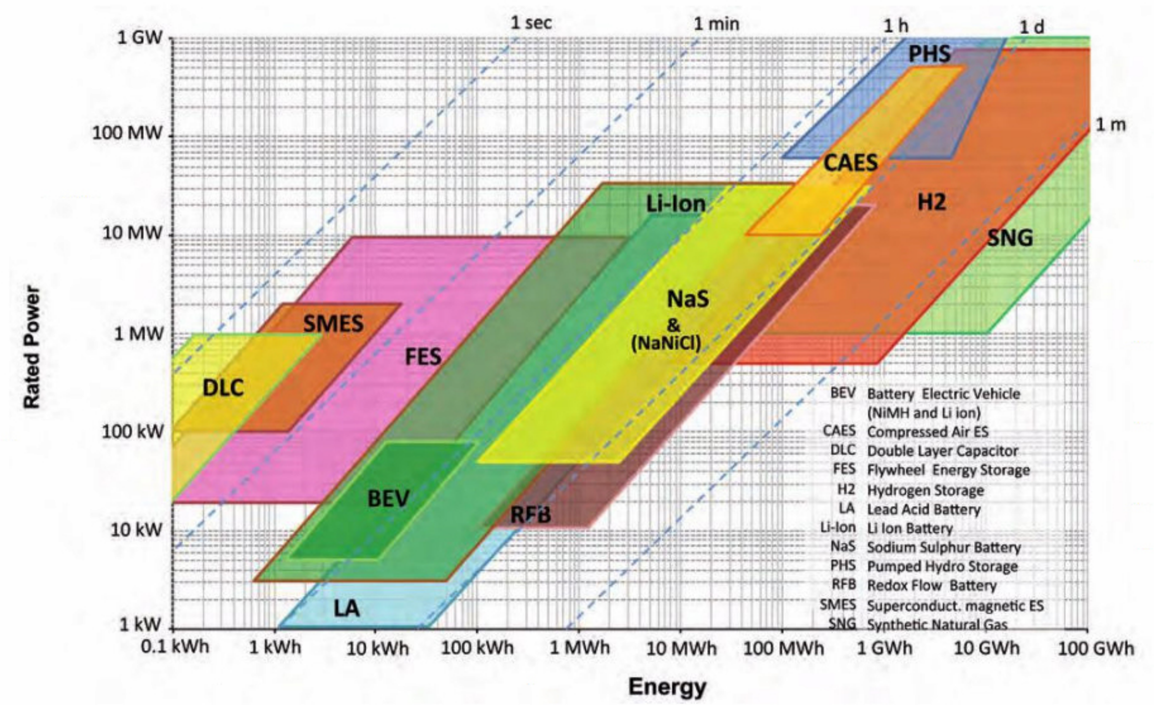

Figure 2: Comparison of storage technologies with respect to power and energy storage duration [1].

Most of the technologies presented in Figure 2 are electrochemical devices, but the storage of large amounts of energy in electrochemical devices may be too expensive and requires too much space [1]. An alternative is the transformation of electricity into hydrogen or synthetic methane gas at the peek-off time and distribute it within the existing natural gas grid [10]. In this way the hydrogen is stored under pressure, what can be done practically for an unlimited time and can be transformed and used any time over the country for electricity production. Furthermore, smaller amounts of hydrogen can be stored in above-ground tanks or bottles under pressure up to 900 bar [1] (e. g. for fuel cell electric vehicle (FCEV) refuelling).

To transform the stored H_2 into electricity a fuel cell (FC) is needed. This device converts the gas back in its initial state together with O_2 from air. The electrochemical reaction of the hydrogen and oxygen produces not only electricity, but also water and heat, which can be released or captured (see Section 2.2). Consequently, the FC represents a highly efficient energy converter.

2.1.2 *Hydrogen Production*

Hydrogen is an energy carrier similar to electricity, able to bank renewable intermittent sources and to provide fuel for transport and heating. Hydrogen can be produced or extracted using fossil or renewable energy sources. This unique

flexibility gives H_2 the potential to become a central integrating element in our energy system [10]. Hydrogen can be produced using diverse domestic resources including fossil fuels such as coal (preferentially with carbon dioxide sequestration), natural gas and biomass or using nuclear and renewable energy sources for splitting the water. This great potential for supply diversity is an important reason why hydrogen is such a promising energy carrier.
Hydrogen can be produced in large central plants, semi-centrally, or in small distributed units located at or very near to the point of use, such as hydrogen refuelling stations or stationary power sites [11]. Researchers are developing a wide range of technologies to produce hydrogen economically from a variety of resources in environmental friendly ways.
Natural Gas Reforming: the methane in natural gas is reacted with water (in the form of high-temperature steam) to produce carbon monoxide and hydrogen. The process takes place in a temperature range of $700-850\,^{\circ}C$ and at pressures between $3-25\,bar$. Usually, the heat is supplied from the combustion of the methane feed gas [11]. In order to increase the hydrogen quantity, these gases are reacted with water again, in a process called water shift reaction [12].

$$\begin{aligned} CH_4 + H_2O + heat &\rightarrow CO + 3\,H_2 \\ CO + H_2O &\rightarrow CO_2 + H_2 + heat \end{aligned} \tag{1}$$

Another method, called partial oxidation, produces hydrogen by burning methane in air. Both, steam reforming and partial oxidation produce a "synthesis gas", which is reacted with additional steam to produce a gas stream with higher hydrogen content.

$$CH_4 + {}^1\!/_2\,O_2 \rightarrow CO + 2\,H_2 + heat \tag{2}$$

The total reaction is exothermic and increases the reactor output temperature up to $950-1100\,^{\circ}C$. Moreover, the gas pressure in this case can be more than $100\,bar$. This method is the most efficient, cheapest and common for hydrogen production [11]. Although it consumes fossil fuels and emit CO_2, this process is used to produce about $95\,\%$ of the hydrogen used today in the U.S. [12]
Renewable Electrolysis: implies the water electrolysis whereby water is split into hydrogen and oxygen by the application of electrical energy [11]. This technology provides carbon oxide free hydrogen that can be used directly in FC.

$$H_2O + electricity \rightarrow H_2 + {}^1\!/_2\,O_2 \tag{3}$$

The total energy amount needed to split water and to produce H_2 increases slightly with temperature, while the required electrical energy decreases. In order to minimize greenhouse gas emissions, the required electricity for water electrolysis can be generated using renewable energy technologies (see Subsection 2.1.1), coal and natural gas with carbon dioxide sequestration. Three main types of electrolysis technology exists.
Alkaline water electrolyzers use an aqueous KOH solution as an electrolyte which is pumped through the electrolytic cells. This type of electrolyzers are suited for stationary application and are available at operating pressures up to $25\,bar$.

Polymer electrolyte membrane electrolysis requires no liquid electrolyte, a fact that simplifies its design. The main component is an acidic polymer membrane, which can be operated up to several hundred bar.

$$\begin{aligned} \text{Anode}: \quad & H_2O && \rightarrow 1/2\, O_2 + 2\, H^+ + 2\, e^- \\ \text{Cathode}: \quad & 2\, H^+ + 2\, e^- && \rightarrow H_2 \end{aligned} \tag{4}$$

The main advantages are the increased safety, more compact design due to higher densities and operation pressures.
High temperature electrolyzers are based on the high temperature fuel cell technology (see Subsection 2.3). The high temperature ($\geqslant 1000\,°C$) improves the overall process efficiency (the electrical energy needed is considerable less compared to low temperature electrolysis). A main advantage of this technology is its high dynamics to react on the available energy amount produced by renewable energy sources. According to Hydrogen Europe, in order to produce one kg H_2 about $55\,kWh$ electricity is necessary based on an assumed FC efficiency rate of 60 % [10].
Gasification: is a process where the coal or the biomass are converted into gaseous components by applying heat, pressure, air/oxygen and steam. The resulting synthesis gas contains hydrogen and carbon monoxide. Employing carbon capture and storage, hydrogen can be produced directly from coal with nearly-zero greenhouse gas emissions. The hydrogen generation via coal gasification is significantly more efficient than burning coal to produce electricity [12].
Biomass: can also be processed to produce renewable liquid fuels, such as ethanol, bio-diesel or bio-oil, which are relatively convenient to transport. These can be reacted at high temperatures and can be combined with a high temperature steam to produce hydrogen at or near the point of use [12].
High-Temperature Thermochemical Water-Splitting: use high temperatures generated by solar concentrators (mirrors that focus and intensify sunlight) or nuclear reactors to drive a sequence of chemical reactions which split the H_2O into hydrogen and oxygen. The intermediate produced chemicals are recycled within the process [12].
Photo-biological: this method is based on two steps: photosynthesis and hydrogen production, catalysed by hydrogenates (Equation 5). Certain microbes, such as green algae and cyanobacteria, produce hydrogen by splitting water in the presence of sunlight as a byproduct of their natural metabolic processes. Other microbes can extract hydrogen directly from biomass [11].

$$\begin{aligned} \text{Photosynthesis}: \quad & 2\, H_2O && \rightarrow 4\, H^+ + 4\, e^- + O_2 \\ \text{Hydrogen Production}: \quad & 4\, H^+ + 4\, e^- && \rightarrow 2\, H_2 \end{aligned} \tag{5}$$

Long-term basic and applied research is still required in this field, but if successful, this can be a long-term solution for renewable hydrogen production. Another option is to reproduce these two steps using artificial photosynthesis [11].
Photo-electrochemical: Hydrogen can be produced directly from water using sunlight and a special class of semiconductor materials as photo-catalyst. These highly specialized semiconductors absorb sunlight and use the light energy to completely separate water molecules into hydrogen and oxygen. Furthermore, these devices

offer some flexibility, as the output can be electricity from photo-voltaic cells or hydrogen from electrolyzer [11]. Based on the energy amount invested for hydrogen production, Acar et al. [13] have compared the H_2 price for all above specified technologies. They have found that the most advantageous methods for hydrogen production are natural gas reforming and gasification. With regard to renewable energy sources which can be applied to perform the water electrolysis, they give the highest production cost per kg of hydrogen.

For the future, a balance between the small scale production, which is expensive and the mass scale central production is necessary. Depending on the application, multiple advantages are considered as distribution, local utilisation, high efficiency, reliability and low production costs.

2.2 ADVANTAGES OF FUEL CELLS

Fuel cells are the most efficient method to convert hydrogen into electricity and heat. They are a modular technology that can be scaled up from powering private homes to large office blocks and even industrial complexes. It contains no moving parts, means that they are quiet and no regular maintenance is necessary. Due to the fact that the use of fossil fuels for electricity production has many negative consequences, the interest in FCs has increased during the past decades. They have all proprieties of traditional power systems, moreover, they can be used as portable power source, giving a better flexibility in multiple applications. This can be the key to bring the FCs in application for portable, transport or stationary sector.
Portable sector: This category includes the powering of numerous devices for longer time, as long the fuel is supplied. Some of these devices include recharges for laptops, cell phones, etc. [14]. The military also has a need for high power, long-term devices for soldier equipment. FCs can be easily manufactured with greater power and less weight. Other military advantages include silent operation and low heat signatures [15, 16].
Transportation market: Because the fossil fuels will continue to become scarce and the price will inevitably increase, FCs are promising systems which can be applied with success to the automotive sector. Furthermore, the legislation for the exhaust gases is becoming stricter. Many countries are passing laws to further reduce the environmental emission and to sell a certain number of zero emission vehicle annually [17, 18]. Fuel cell electric vehicles (FCEVs) have the ability to be more efficient than vehicles powered by other fuels [19]. Moreover, fuel cell electric vehicle (FCEV) have a significant potential to reduce emissions from the transport sector [12]. Comparing to the battery electro vehicles, the FCEV can be very fast refuelled and have a higher mileage (~ 482 km). In April 2014, five automakers - BMW, Daimler, Honda, Hyundai and Toyota - joined to launch the HyFive project, agreeing to develop 110 FCEVs in several European cities [20].
Stationary power generation: Stationary FCs are often used as primary or backup power for large energy infrastructures [21]. With an efficiency of 50 % for the electric generation they can produce enough electricity to power a house or a small business. The heat produced by the fuel cells can generate additional electricity through a turbine, provide heating directly to nearby buildings or facilities and even cooling with the addition of an absorption chiller [22]. Many utilities and companies are adopting FC in order to reach mandatory air pollution goals [7]. The main three uses for stationary FCs are combined heat and power (CHP), uninterruptible power supplies and primary power units. Nowadays, almost 10 % of the 500 Fortune companies use fuel cells for stationary power generation. Among 100 top companies in Fortune list, 25 % use fuel cells as backup solution [20].

Fuel cells are still more expensive than competing technologies, but this gap is rapidly decreasing as the technology is improved. This fact should not be so important considering the positive impact of FCs on the climate. During years, the increase in carbon dioxide amount and other greenhouse gases produced by burning fossil fuels has affected not just our life but also the climate. As result, since 1850 the global average temperature has increased by 0.76 °C. In addition, it has

an effect on the weather, on the ocean acidification level, arctic glaciers, extreme weather events, animal habitats and species population level. In the same time, it has numerous negative consequences for human communities, especially impoverished people.
A further benefit of FC usage is the power grid stability, since the electricity is generated at the point of use and does not depend on the grid. Because FCs does not need conventional fuels, such as oil or gas they can reduce the economic dependence on oil producing countries and provide a energy security for the user nation. Furthermore, since hydrogen can be produced anywhere where water and a power source exist, the fuel generation can be distributed and does not have to be grid dependent.
Not at least, FCs can be combined with other energy technologies, such as batteries, wind turbines, solar panels and super-capacitors, assuring a high flexibility on the energy production at zero emission level.

2.3 Types of fuel cells

A fuel cell is an electrochemical device that converts the fuel's chemical free energy into electricity, without the limitation of the Carnot efficiency. In contrast to a battery, a FC is an open operating system, which produces electricity from externally supplied fuel and oxidant. Just as there are different types of batteries, there exist many FC technologies to produce electricity. These technologies can be distinguished by the operation temperature and the assembled material types, which affect the tolerated fuels purity and the required peripheral equipment.

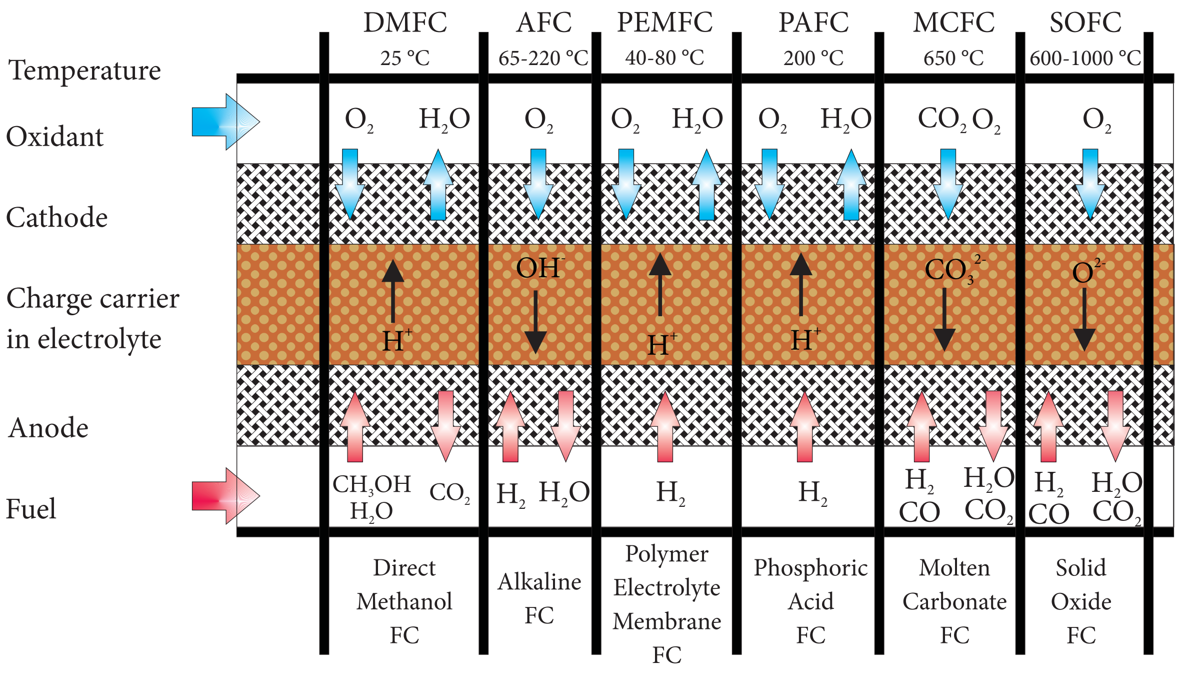

Figure 3: Main view of fuel cells types. The classification is made according to their electrolyte, operation temperature and catalyst type.

The FCs can be classified according to the required catalyst type, the electrochemical reaction that takes place in the cell and other factors (Figure 3). All these features affect the FC application field.

DMFC - Direct Methanol Fuel Cell

Instead to oxidize a gas at the anode, it is highly desired to design a fuel cell that convert directly a liquid fuel into electricity. In addition it is desired to retain a high power/weight ratio. Methanol possesses many advantages as fuel: it is a liquid, cheap and plentiful, in principle renewable from biomass. Moreover, the only products of the combustion are CO_2 and H_2O.

The DMFC has a good electrochemical performance and refilling is done by squirting in liquid or by replacing the cartridge. This enables continuous operation without downtime. Noble metal nanoparticles (especially Pt), supported on carbon black are most commonly employed at the anode. Another intensively explored catalyst is the Pt-Ru system due to its high catalytic activity towards methanol oxidation reaction in acidic media [23]. The basic problems currently faced by the DMFCs are: (1) poor electrode kinetics for the anode reaction, particularly at low temperatures, making it highly desirable to identify improved catalysts and to work at temperatures as high as possible; (2) the utilized perfluorosulfonic acid membranes suffer from a significant permeability towards methanol [24].

AFC - Alkaline Fuel Cell

Generally, an solution of potassium hydroxide is used as electrolyte. A plain variety of non-noble metals can be employed as catalyst. AFCs offers an electrochemical efficiency of about $60-70\,\%$ at a operating temperature of $65-200\,°C$. In fact, even the small amount of CO_2 in the air affect dramatically the cell performance and durability, through carbonate formation. The water management is simple and no compressors or other peripherals are required. The manufacturing and operating costs are low, especially for stacks.

Alkaline cells with liquid electrolytes can run in a recirculating mode; this fact that allows the electrolyte regeneration and to reduce the effects of carbonate formation. However, the recirculating mode introduces issues with shunt currents [25]. The liquid electrolyte systems also suffer from additional concerns including wettability, increased corrosion and difficulties handling in differential pressures.

AFC have been used in the Apollo spacecrafts to provide electricity and drinking water [26, 15].

PEMFC - Proton Exchange Membrane Fuel Cells

PEMFCs are the most developed technology and commonly used as fuel cell systems. They power cars, serve as portable power sources and provide backup power in place of stationary batteries in the offices. The compact design of PEMFCs assures a high energy-to-weight ratio and a quick start-up when hydrogen is applied.

A thin polymer sheet is used as electrolyte, which conducts protons between anode and cathode. This particular characteristic allow this FC type to work at low temperatures (typically $80 - 100\,°C$ and $50 - 90\,\%$ efficiency). The low operating temperature and the acidic media requires the utilization of noble metal catalysts (Pt).
Due to the high price of platinum, this is often cited as a cost concern. However, the platinum quantity for $1\,kW$ residential system is very low: $0.1 - 0.2\,g$ [4]. Nevertheless, the platinum usage implies the adoption of pure hydrogen gas as fuel. It is easily poisoned by sulphur and carbon monoxide. Additionally, the lower fuel grades can cause the membrane decomposition or clogging [27]. Furthermore, the PEMFCs needs a complex water management system. Too much water causes FC flooding and when is too dry, supplementary water must to be inserted. Thus the electrolyte is humidified and its ionic conductivity is increased.

For transport applications the PEMFCs have a service life of $2000 - 4000\,h$ and for stationary applications about $40000\,h$ [28, 29]. In comparison to the batteries where the voltage decrease suddenly after a number of cycles, the stack performances fade slower (state-of-the-art $\sim 10\mu V/h\,cell$). Additionally, the stack replacement is a major expense [30].

PAFC - Phosphoric Acid Fuel Cell

PAFC is one of the mature fuel cell types employed in commercial use and is considered the "first generation" of modern FCs. Typically, the PAFC is used for stationary power generation, but they have been used to power large vehicles such as city buses [24]. Since 1970 this FC technology is employed in large scale commercial CHP systems ($100 - 400\,kW$ electric) [31]. The electrolyte is based on liquid phosphoric acid at temperatures of $180 - 250\,°C$. Platinum with typical loadings of $2.4\,g\,kW^{-1}$ for anode and $5.2\,g\,kW^{-1}$ for cathode is used as electrocatalyst [31]. In comparison to PEMFCs, PAFCs are more tolerant towards impurities from the fossil fuels, that have been reformed into hydrogen. PAFCs energy efficiency exceeds $85\,\%$ in the case of electricity and heat co-generation. Its performance decreases significantly when PAFC are used only for electricity generation ($37 - 42\,\%$).
PAFCs are also less powerful than other fuel cells, at the same weight and volume. As a result, these fuel cells are typically large and heavy. In comparison to other FC types, PAFCs requires a higher Pt loading, a fact that make them expensive.

MCFC - Molten Carbonate Fuel Cell

MCFCs are high temperature fuel cells used in large industrial CHP plants. MCFC use natural gas and coal-gas as fuel. The electrolyte is a mixture of molten carbonate salt suspended in a porous, chemical inert ceramic lithium or aluminium oxide matrix. Due to the high working temperature (~$650\,°C$), non-noble metals (Ni, Fe) can be utilized as catalyst. Moreover, natural gas and other hydrocarbons can be internally reformed as in SOFCs. MCFCs benefit from relative cheap electrocatalysts and the simple auxiliary equipment. However, they suffer from short lifetime and

low power density. This fact can be compensated by coupling with a turbine. So, when the waste heat is captured and used, the overall fuel efficiency is $\geqslant$85 %.
Instead of recycling carbon dioxide, from anode to cathode, the fuel cell can be feed with carbon dioxide on the cathode from the power plant exhaust. These exhaust gases contain about $5 - 15$ % carbon dioxide, diluted by other gases, mostly nitrogen. The fuel cell would selectively take up the carbon dioxide, use it to form CO_2 ions and then emit it in a concentrated CO_2 stream at the anode. The gases emitted there can reach up to 70 % carbon dioxide. Most of the residue are water vapors, which can be easily condensed. Thus, a pure stream of carbon dioxide is produced. This one can be further pressurized and stored in the underground.

SOFC - Solid Oxide Fuel Cells

Solid oxide fuel cells benefit from high electric efficiency and fuel flexibility. They are well known and its development is ongoing since 1960s. Characteristic for this FC technology is the oxygen-ion conducting, the solid electrolyte and the operating temperature ($500 - 1000$ °C). At high temperatures the reaction at the electrodes is fast, a fact that allows the use of cheaper catalysts (Ni, La). Due to the high operating temperature, this FC type tolerates substantial more sulphur than other cell types. In addition, they are not poisoned by carbon monoxide, which can even be used as fuel. This property allows SOFCs to use as fuel natural gas, biogas and gases made from coal.
Unfortunately, the high temperature operation has also disadvantages. The cell starts quite slow and requires significant thermal shielding to retain the heat and protect the staff. Therefore SOFCs are typically used for stationary power supplying. Furthermore, all cell components must be compatible. The physical proprieties, such as the thermal expansion and dimensional stability in reducing and oxidizing environment are crucial [24]. The development of low cost materials with high durability is the main technical challenge facing this technology.

3 INTRODUCTION INTO PROTON EXCHANGE MEMBRANE (PEM) FUEL CELL

As an future alternative, the H_2 powered PEMFC can replace the internal combustion engine. It posses a series of advantages as fast start-up, low operating temperature, high fuel efficiency and it is environmentally friendly. In the last years several car manufactures (Toyota, Hyundai, Honda, Nissan and Daimler) have introduced H_2 fed FC vehicles on the road. However, some concerns related to the catalyst, membrane cost, durability, membrane proton conductivity, water management and catalyst activity still exist. In order to apply the PEMFCs in multiples sectors and to make them affordable and durable, further R&D needs to be done.

3.1 PEM FUEL CELL ELECTROCHEMISTRY

PEMFCs are distinguished from other FC types by its low operation temperature ($80 - 100\,°\mathrm{C}$) and its electrolyte represented by a polymer membrane. As shown in Figure 4, a PEMFC is composed of a proton exchange membrane sandwiched by an anode and a cathode. This assembly is called membrane electrode assemble (MEA) and represents the PEMFC heart.
At the anode, hydrogen is oxidized to form protons and electrons whereas oxygen is reduced at the cathode. The protons are transported from anode to cathode through the electrolyte membrane, while electrons are carried to the cathode over the external electronic circuit. At the cathode, oxygen reacts with protons and electrons, forming water and producing heat. Both, the anode and cathode include a catalyst to speed up the electrochemical process, as shows in Figure 4. On the PEMFC operation two half reactions are involved:

$$\begin{array}{llll}
\mathit{Anode}: & H_2(g) & \rightarrow 2\,H^+(aq) + 2\,e^- & E° = 0V \\
\mathit{Cathode}: & 1/2\,O_2(g) + 2\,H^+(aq) + 2\,e^- & \rightarrow H_2O(l) & E° = 1.23V \\
\hline
\mathit{Overall}: & H_2(g) + 1/2\,O_2(g) & \rightarrow H_2O(l) + \mathit{electric} & \mathit{energy} + \mathit{heat}
\end{array} \tag{6}$$

where E° is the standard reversible potential.
The theoretical cell potential is the difference between the two half reaction potentials. For a FC which is supplied with H_2 and O_2 under standard state condition the ideal reversible cell potential E_r of Equation 6 is 1.23 V. It is calculated from the Gibbs free energy:

$$\Delta G = -z\,F\,E_r \tag{7}$$

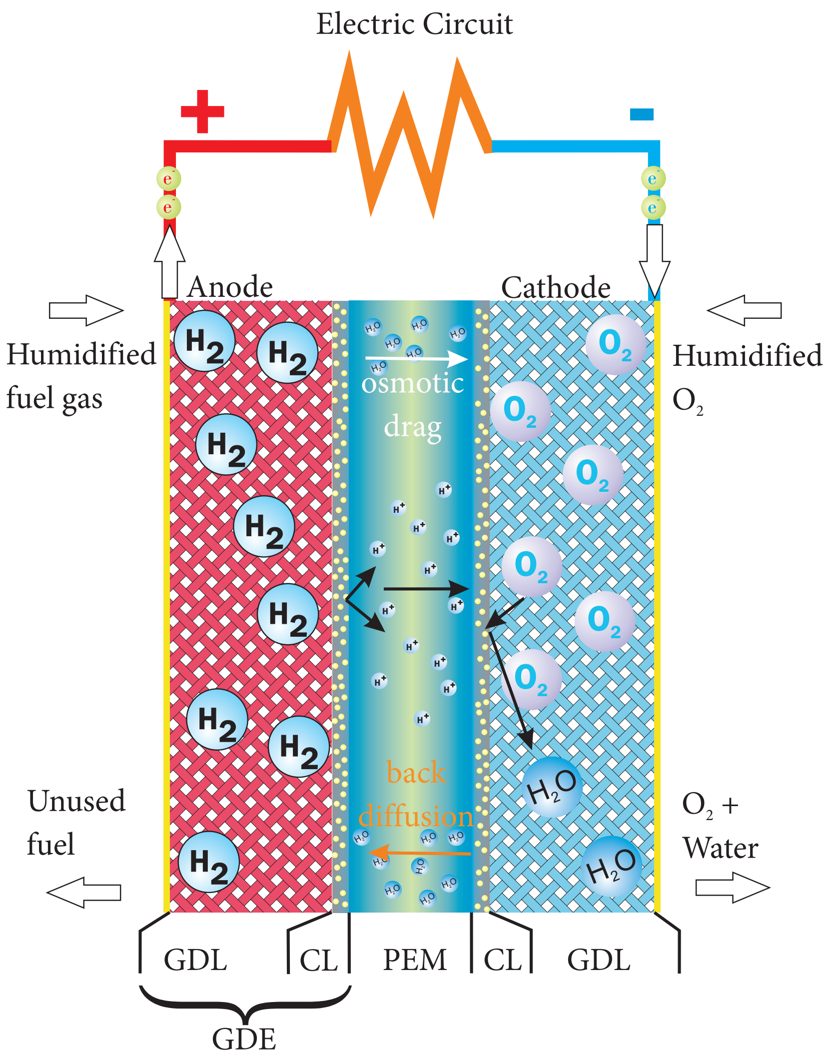

Figure 4: Schematic diagram of a H_2/O_2 PEMFC configuration, showing components, operation mechanism, reactants and mass balance across the cell.

where z represent the number of electrons transferred per mol of consumed fuel ($z = 2$) and F is Faraday's constant (96485 C/mol).

At standard temperature and pressure, this is the highest voltage obtainable from a hydrogen-oxygen operated FC. In order to obtain a higher voltage, several cells have to be connected together in series. It is advantageous to operate the fuel cell at pressures above atmospheric pressure, typically between $1-3$ bar [32]. Then the change in Gibbs free energy as related to the pressure can be written as:

$$dG = V_m \, dp \tag{8}$$

where V_m is the molar volume ($m^3 \, mol^{-1}$) and p is the pressure in bar. Writing this for an ideal gas, the Nernst equation is obtained:

$$E = E_r + \frac{RT}{zF}\left(\frac{p}{p_0}\right) \tag{9}$$

where E is the actual cell voltage, E_r is the standard reversible voltage, R is the universal gas constant ($8.314 \, J mol^{-1} \, K^{-1}$), T is the absolute temperature in K, z is the number of electrons consumed in the reaction and F is Faraday's constant.

When an electrical load connects the two cell electrodes, the current flows as long as H_2 and O_2 gases are supplied to sustain the reaction. For very low currents, the cell voltage can be higher than 0.9 V, corresponding to an efficiency higher than 60 % [19]. This performance is significantly higher compared to most complex heat engines, such as steam engines or internal combustion engines. In their case a maximum of ~45 % thermal efficiency can be achieved [15].

3.2 VOLTAGE LOSSES

The discussion in last section was focused on the theoretical output voltage of the PEMFC, which is in the ideal case approximately 1.23 V. In reality this voltage is never reached, it is not even approached. Not even the open circuit voltage (OCV), the cell voltage without applying current, reaches this value due to the presence of several voltage losses (Figure 5). The single FC provides a voltage depending on the operating condition such as temperature, applied load, fuel/oxidant flow rates, gases pressure and humidity. A standard method to characterize the FC performance is the polarization curve. This represents the cell voltage behaviour versus applied current density [33].
When electrical energy is drawn from the FC, the cell voltage drops from the OCV due to several irreversible losses. The loss is defined as the deviation of actual cell voltage (E_{ir}) from the maximum (reversible) FC voltage (E_r).

$$E(i) = E_r - E_{ir} \tag{10}$$

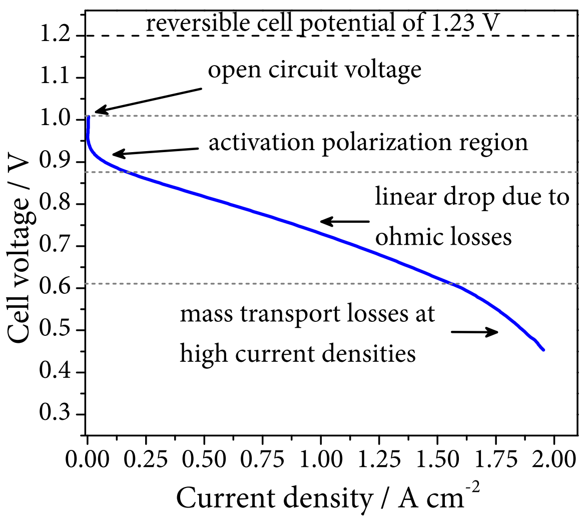

Figure 5: Generalized polarization curve for a fuel cell.

Thus, the actual measured OCV is lower than the theoretical value due to mixed potentials caused by gas crossover across the electrolyte and internal currents. The three major losses classifications, which result in the non-linear drop of the cell voltage with increasing current are (1) activation losses, (2) ohmic losses and (3) mass transport/concentration losses [15].
The activation losses are caused by the reactions kinetics taking place on the catalyst surfaces. This energy is necessary to assure that the reaction tends toward the

formation of water and electricity. This loss is dominant at small current densities in low temperature FCs [15] and is a measure for catalyst effectiveness [34]. This type of voltage loss is complex because it involves the gaseous fuel, the solid metal catalyst and the electrolyte [35]. The activation losses can also be expressed simply as Tafel equation:

$$\Delta V_{act} = a + b\ln(i) \tag{11}$$

where

$$a = -\frac{RT}{\alpha F}\ln(i_0) \quad \text{and} \quad b = \frac{RT}{\alpha F} \tag{12}$$

Then the complete equation for anode and cathode activation over potential can be represented by:

$$\upsilon_{act\_anode} + \upsilon_{act\_cath} = \frac{RT}{zF\alpha}\ln\left(\frac{i}{i_0}\right)\bigg|_{anode} + \frac{RT}{zF\alpha}\ln\left(\frac{i}{i_0}\right)\bigg|_{cath} \tag{13}$$

where n is the number of exchange electrons per mole of reactant, F is Faraday constant and α is an unit-less parameter, named charge transfer coefficient. It is used to describe the amount of electrical energy applied to change the rate of electrochemical reaction [15, 36].
The exchange current density i_0 is the electrode activity for a particular reaction at equilibrium [37]. In PEMFC the anode i_0 for hydrogen oxidation is very high compared to the cathode i_0 for oxygen reduction. In many cases the influence of i_0 at the anode is neglected [38, 39, 40]. The fuel crossover/internal current loss is associated with the losses that occur thought the electrolyte. Typically, the electrolyte should transport only the protons from anode to cathode, see Figure 4. Nevertheless, a certain amount of H_2 and O_2 always diffuses through the polymer material [41, 42]. This imply a mixed electrode potential and a lower cell voltage. Additionally the membrane is not a perfect isolator and very small electronic currents cross the membrane also resulting in cell voltage reduction.
As in any electrical device the most common source of loss are the ohmic losses. This occurs due to the electron flow resistance through the electrode material and the H^+ protons flow in the ionomer (electrolyte and catalyst layer (CL)) [22]. Generally, this voltage drop is directly proportional with the current density [36]. It represents the major source of voltage losses in low and high temperature FC [15]. Along the electrolyte, other FC components such as the CL, the GDL, the bipolar plates (BPs), the interfaces contacts and the terminal connections, contribute to the total electrical resistance.
Thus, the ohmic voltage loss can be written as:

$$\Delta\upsilon_{ohmic} = IR_{ohmic} = I\left(R_{elec} + R_{ionic}\right) \tag{14}$$

R_{ionic} represent the ionic resistance of the electrolyte and R_{elec} includes the total electrical resistance of all conductive components. R_{ionic} dominates the reaction in Equation 14 because ionic transport is more difficult than electrons transport.

Thus, the FC performance improves if the FC resistance is decreased. In practice, it is helpful to compare resistances on a per-area basis using the current density:

$$\upsilon_{ohmic} = i\,(ASR_{ohmic}) = i\,(A_{cell} R_{ohmic}) \tag{15}$$

where i is the current density, ASR_{ohmic} is the FC specific area resistance, A_{cell} is the active area of the FC, R_{ohmic} is the total ohmic cell resistance and represents the sum of electronic and ionic resistances. The mass transport or concentration losses result from the change in reactants concentration at catalyst surface [14]. This loss occurs in both, low and high temperature FCs and is only prevalent at high current densities [43, 44]. Several processes may contribute to concentration polarization: slow diffusion of the reactants in the electrode pores, solution/dissolution of reactants/products into/out of the electrolyte or diffusion of reactants/products through the electrolyte to/from the electrochemical reaction sites [22].

Summarized, the operating voltage of a FC can be represented as the deviation from ideal voltage caused by the different polarization phenomena:

$$E(i) = E_{rev} - \upsilon_{act\_anode} - \upsilon_{act\_cath} - \upsilon_{ohmic} - \upsilon_{conc\_anode} - \upsilon_{conc\_cath} \tag{16}$$

where υ_{act}, υ_{ohmic}, υ_{conc} represent activation, ohmic and mass concentration polarization. It can be observed in Equation 16 that activation and concentration polarization occur at anode and cathode, while the resistive polarization represent ohmic losses through the entire fuel cell.

3.3 STATE-OF-THE-ART MEMBRANE ELECTRODE ASSEMBLIES (MEA)

Each component in the PEMFC plays an unique role in the fuel cell functioning. In the past decades, as result of extensive research, the PEMFC performances has been significantly improved. The evolution from 1960 to the present day in PEMFC component development is amazing. In 1967, when PEMFC have make its entrance on the Gemini project, the standard platinum loading was $28\,mg\,cm^{-2}$ and today it decreased down to $0.4\,mg\,cm^{-2}$ [45].

In state-of-the-art MEA, a perfluorosulfonic acid membrane is used as electrolyte (regularly $Nafion^{TM}$ ($10 - 125\,\mu m$)), which is pressed between two GDE, each one with a catalyst layer ($\sim 1 - 10\,\mu m$ thick). The CL include the electrocatalyst (typically Pt) supported on high surface area carbon (graphite, carbon nanotubes [46], graphene [47] and carbon black[48]). In order to hold all CL components together, ionomer ($Nafion^{TM}$) is added as binder and as proton conducting medium.

An important challenge in PEMFC development is the decrease of material cost, while maintaining the same performance and the durability of currently used components. In order to replace the internal combustion engine with the PEMFC, the cost level for a FC systems should not exceed $49/kW [32].

3.3.1 *Proton exchange membrane (PEM)*

A proton conducting membrane generally has a functional group (usually sulfonic acid) attached to the polymer backbone. The membrane needs to be non-electron conductive and should have low permeability for H_2 and O_2 [49]. For

PEMFCs, the standard used membranes are commercially mature perfluorosulfonic acid (PFSA) foils, such as Nafion™ (DuPont), Fumapem© (Fumatech) and Aciplex© (Asahi Glass Chemical). All show a similar structure. Most of them were originally developed for chlor-alkali electrolysis, but they also demonstrate a good proton conductivity as electrolyte in PEMFCs. Apart from this property, the good chemical, morphological and thermal stability is presented by these membranes.

Nafion™ was discovered in late 1960s by Walther Grot at DuPont [50]. Figure 6 shows an example of Nafion™ general chemical structure. It contains a polytetrafluoroethylene (PTFE)-like backbone connected with a perfluorocarbon unit and a hydrophilic sulfonic acid group (-SO_3H) [51]. In the middle of 1990 the most used membranes were Nafion™ 117, Nafion™ 115 and in the last years Nafion™ 112 and Nafion™ 211 [52]. It is known that the performance of the proton exchange membrane is related to the membrane proton conductivity, which increase as the gas humidity growth [33]. In order to use Nafion™ in FC at temperatures above 80 °C, they can be doped with electrolytes, e. g.ionic liquids [53] or inorganic oxides (SiO_2, TiO_2, ZrO_2) [54].
Although the FCs efficiency increases with the temperatures, membrane issues, such as membrane dehydration [55], reduction of ionic conductivity [56, 57], decrease affinity for water [26], loss of mechanical strength via softening of the polymer backbone and increased parasitic losses through high fuel permeation [49] are accentuated.

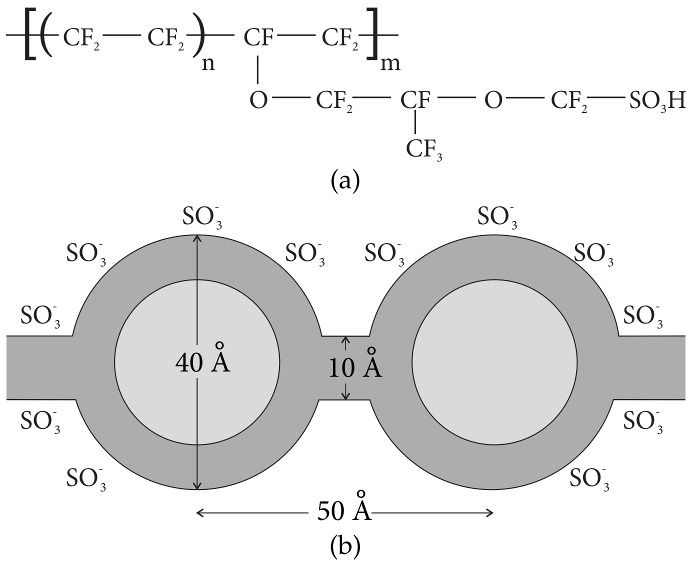

Figure 6: (a) Nafion™ chemical structure and (b) cluster-network model of Nafion™ according to Gierke et al. [2]

Many alternatives to replace the Nafion™ were proposed. Astill et. all have proposed a sulfonated poly(ether-ether ketone) (SPEEk) membrane which is less hydrophobic than Nafion™. Due to its hydrocarbon backbone and the large content on sulfonic acid groups it is expected to retain more water [58]. Furthermore, in order to use this membrane type in PEMFC at temperature over 100 °C many authors have modified the SPEEk membranes with diverse composite. In order to prevent the membrane dry at the anode side and to increase the pathway for protons, Sambandam et al. has functionalized his samples with silica composite [59].

However, in order to attain the cost and durability targets, great effort must be further invested [60].

3.3.2 *Gas diffusion electrode (GDE)*

In a PEMFC all electrochemical reactions take place in the electrode, at the cathode the oxygen reduction reaction (ORR) and at anode the hydrogen oxidation reaction (HOR). These reaction are catalyzed by Pt or by Pt-alloys ([61, 62]) or in the last years by developed nanotube-graphene [63]. Most of the catalysts used for ORR are very expensive and limited on the terrestrial crust. Furthermore, in order to provide enough catalytic sites the electrode structure should be very well designed. Explicitly that means that there must be good:

- access for reactants to the catalyst,
- connection between the electrolyte and the catalytic sites,
- efficient removal of water formed in the cathode to the gas channel,
- electric connection with the catalyst and bipolar plate,
- transfer of heat produced during the reaction to the bipolar plate.

The electrode is usually divided into at least two sub-layers: the active CL which is in contact direct with the membrane and the GDL next to the bipolar plate, as shown in Figure 7.

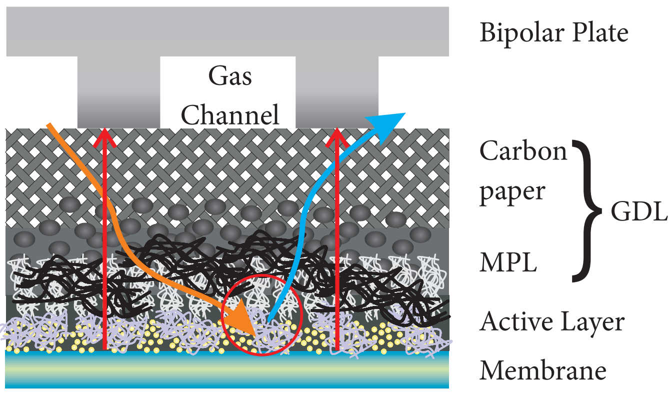

Figure 7: Schematic drawing of PEMFCs electrode structure and bipolar plate. The active layer contains a mixture of ionomer, Teflon, catalyst and carbon support.

3.3.3 *Gas diffusion layer (GDL)*

The GDL is situated in direct contact with the bipolar plate and does not contain any catalysts or proton conducting material. This layer provide a uniform supply of gases, electric potential and temperature distribution, under the gas channels and the ribs of the bipolar plate. It has a thickness in the range of $200 - 400\,\mu m$ and consists of macro-porous electrically conducting material [64]. Typically these layers are formed from carbon fibers as papers or woven cloths [65]. In addition, GDLs are typically wet-proofed with a PTFE (Teflon) coating to ensure that the pores do not become congested with liquid water [66, 67]. Because water is formed at the cathode, a thin ($\leqslant 50\,\mu m$ thick) MPL is usually placed between the GDL and the CL. This assist the water removal from the cathode to the flow field (Figure 7). The MPL contains Teflon and carbon black, is porous and is supposed to improve the interface contact between the CL and the GDL and not at least to control the humidity in the electrode.

3.3.4 *Catalyst layer (CL)*

The CL contains as the name already says the electrocatalyst, dispersed on a electric conducting carbon support. Here the electrochemical reaction (see Section 3.1) takes place. This layer also contains a proton-conducting ionomer, usually recast Nafion™ [48, 68], which is in contact with the Pt or Pt-alloy catalyst [69, 70]. Despite the CL has so many components, there remains enough void space to transport the gas and water [34].

The performances of the PEMFC is mostly controlled by the micro-structure of the CL [71]. Conventionally, the PEMFC CL is prepared by spreading a suspension of carbon-supported platinum catalyst, solvent and binder onto a GDL, followed by a drying process [72]. A wide range of methods can be used to assembly the catalyst layer: spraying [73], decal transfer [34], painting [74], rolling [75], sputter deposition [76], ink-jet printing [77], doctor blade coating [47] and screen printing [67, 78].

The two most common technique for deposition of CL used in research are spraying [73] and doctor blade coating [47]. Prior to this process, a ink is prepared by mixing Pt/C catalyst powder and ionomer in mixtures of aqueous/alcohol solvents. In order to homogenize the suspension, different methods are used (mechanical mixing, sonicating, or ball milling) for an extended period of time [79]. The prepared ink is subsequently sprayed or printed onto the membrane (catalyst coated membrane (CCM)) [77] or directly on the GDL (catalyst coated substrate (CCS)) [80]. The process temperature largely depends on the solvent boiling point, which usually does not exceed 100 °C.

A standard catalyst loading of $0.4\,mg\,cm^{-2}$ is adopted in practice [81].

3.3.5 *Bipolar plate*

Along the MEA, the bipolar plates (BPs) are a key component of PEMFC, with a multi-functional character. They distribute the reactants uniformly, conduct current from/to cell, remove heat from the active area and prevent leakage of gases and coolant [82]. Presently several types of materials are being used in BP production : non-metal (non-porous graphite/electro-graphite), metals (non-coated and coated) and composites (polymer-carbon and polymer-metal). Traditionally, the most commonly used BP material is graphite, because it has excellent chemical stability in the FC environment [82]. Even if this material is suitable for PEMFC applications, the production costs are quite high. The only suitable way to process the graphite is the machining, a fact which increases the costs.

Using metals as material for BP can be a great advantage. It provides a good mechanical stability, electrical and thermal conductivity and can be easily stamped to desired shape to accommodate in flow field channels. A positive fact about metal BP is that it can significantly reduce the volume and the weight of the stacks. However, its chemical stability is limited in the fuel cell environment, especially in contact with the acidic electrolytic membrane [83]. A direct connection between the metal and the electrolyte can be avoided by using a coating or a gasket at the cell edges (so called sub-gaskets) [31].

An alternative for BP are polymer composite materials. They are light weight and can be moulded into desired shape and size, are rigid and provide chemical resistance [84, 85]. Furthermore, the polymer composite BPs can be manufactured by either injection moulding or compression moulding, leading to substantial BPs producing cost reduction [86]. A major problem of this BPs type is that their bulk conductivity is limited, due to the non-conductive polymer matrix [87]. By increasing the graphite content a better conductivity is reached but in the same time the mechanical performances are reduced. However, the electrical conductivity of these composites is still below the DOE target [88].

Even though a significant progress haves been made for metal coated and polymer graphite composite materials, they are not yet able to attain the long-term reliability and power densities achievable by non-porous graphite as BP. A further research on both materials is necessary.
By optimizing all FC component a cost reduction can be achieved. This will permit to apply the fuel cells in many domains over all around the world.

3.4 CATALYSTS FOR PEM FUEL CELL

One of the main impediment to commercialize the FC is the high costs, due to the catalyst [89]. Research on cost reduction of cathodic electrocatalyst up to now was focused on the optimization of existing Pt catalysts by decreasing their particle size, controlling their structure and morphology or increasing their uniformity [90, 46]. Significant effort were devoted to replace the expensive Pt catalyst with Pt-alloys with new electronic structures [91, 92, 93]. Not at least inexpensive Pt-free catalysts consisting of earth abundant element are examined [94, 95, 96].
Usually the electrocatalyst used in the FC can be prepared using various methods. A list of the most used method on the catalyst preparation is presented in the following.
Chemical synthesis: is the main preparation technology to create nanocrystalline catalysts. It involve the reduction of a metal salt precursor with reducing agents for the preparation of alloys or Pt catalysts. One of the simple methods involves the use of H_2PtCl_6 x $6H_2O$ as precursor and formic acid as a reducing agent. After heating the formic acid at 80 °C and adding drop-by-drop the precursor, under vigorous stirring for 30 min the catalyst particles are obtained. This one is anchored to a carbon support, traditionally is represented by carbon black, carbon nanotubes and multilayered graphene [46, 97, 47]. In order to reduce the time and the temperature of the reaction Zheng et al. has prepared Pt nanoparticles through a room temperature hydrogen gas reduction in a ethylene glycol/water mixed solvent. After

investigation they have found that by changing the solvent from water to an ethylene glycol/water mix, the size of Pt nanoparticles changes from 10 nm to 3 nm. Also, a shape transitions from polyhedral to spherical was observed. Furthermore, by a 1:1 volume ratio mixture of ethylene glycol/water the created particles were uniformly dispersed with an average size of ~3 nm.
Recently, the formation of a thin Pt shell on the core of transition metal nanoparticles (e. g. nano-particle with core-shell configuration) is well known to significantly improve the utilization of Pt, thus decreasing expensive Pt usage while maintaining the ORR activity and lowering the cost of PEMFCs [98, 99, 100, 101]. Sun et al. have prepared NiPt hollow spheres with an ultra-thin shell ($2-3$ nm) by a facile wet chemical process. They have studied the growth mechanism and have discovered that the K_2PtCl_6 concentration has a remarkable effect on the morphology and structure, as well as in the phase of the NiPt nanoparticles. Without K_2PtCl_6, only sphere like amorphous products could be obtained [93]. As it can be observed by using chemical methods, catalyst with very well define shapes and sizes can be prepared. Furthermore, the advantage of low temperatures and short synthesis time are a positive point for the chemical methods.
Physical technologies: are processes where the precursor material suffer no chemical transformation. The physical methods include sputtering, ion or electron beam deposition, laser ablation and various types of irradiation [102, 23]. A variety of Pt nanoparticles have been fabricated, including nano-structured films and nanoparticles. Through this procedure a very thin CL is produced at the MPL surface. Although the deposited catalyst loading is low, these kinds of methods cannot be utilized on the industrial scale.
Electrochemical technologies: usually proceed through the reduction of metal precursor with complexes ligands as Cl, NH_3, NO_2 and H_2O by applying a current or a potential. Parameters as time, deposition potential and solution composition can be manipulated in order to obtain well defined nanoparticles or films [103, 104]. One of the big advantage of this method is the deposition selectivity according to the reducing potential. Thus, it is possible to produce core-shell particles only by applying a sequence of pulses. Kulp et al. have prepared, using a pulsed electrodeposition, core-shell particles, containing in the centre Cu and platinum as shell [101, 105]. Additionally, this technique provides a precise catalyst loading control [106, 107]. However, the structure and properties of the deposited metals depend on many parameters, including electrolyte composition, current density and electrode geometry [108]. Typically, the electrodeposition takes place in a electrolyte bath, which contains the necessary metal precursor [109]. As substrate can be used each type of electrical conductor (graphene, carbon nanotubes or carbon particles). One of the advantage of this technique is the low energy consumption and the easy control of the loading mass of Pt [48].
Microfluidics for the production of ORR catalyst: in conventional colloidal synthesis for a precise control over the size, shape and composition, nanoparticles are usually made in batch reactor [94]. The capacity of such process is typically limited to tens of mg and thus not sufficient for industrial applications. In order to increase the productivity of this systems a continuous production process based on the microfluidic reactor is proposed [110]. Miniaturization of the macroscopic reaction

vessels has a number of advantages, which include fast heat and mass transfer rate and effective use of reagents [94].

3.5 RESEARCH GOALS

The goal of this thesis is to prepare GDEs for PEMFC, with as low as possible catalyst loading and a high performance. Therefore, using an electrochemically method the noble metal precursor is deposited on a commercial GDL. This configuration grant the in-situ platinum catalyst production, directly in the MPL structure, at the triple phase boundary. To attain the work goals an base investigation of the main parameters that affect the platinum electrodeposition process is performed. Along that, using a spraying method, the CL architecture is shaped.

To facilitate the PEMFC investigation in a semi-automatically way, with a minimum operator impact, a new PEMFC testing platform is developed. The construction details are illustrated in Chapter 4. Along that, a high accurate spraying system is developed, having at the base a commercial 3D printer system. The created device is able to coat GDLs with distinct materials, following a pre-programmed pattern. Additionally, it makes possible the 3D CL structuring, by intercalating the ionomer with the carbon support and the precursor. For a better electrodeposition process management, a new deposition cell is produced. It has an improved design and makes possible a precisely temperature and humidity control. The construction steps and the employed materials are presented in Chapter 5.

Nevertheless, to improve the GDEs performances an in-depth spraying and deposition parameters investigation is required. In Chapter 6 the influence of multiple spraying and deposition parameters on the anode performance are examined. Among the parameters are included the spraying gas pressure, coating temperature, solvent composition and spraying order. Additionally, for the electrodeposition process the pulse shape and deposition humidity are considered. Using the optimized methods, new GDEs are produced and tested in PEMFC cathode. Chapter 7 presents the final results. This introduce a new CL networks, with crucial effects on the PEMFC operation. Also the feasibility to use other commercial GDLs for the electrodeposition procedure is examined. Another point in this chapter is the electrodeposition technique upscaling.

The produced GDEs are compared with a commercial platinum catalyst. The performance tests are recorded in a H_2/air FC configuration, at an absolute pressure of 2.5 bar. Chapter 8 summarize the obtained results and give an overview for future work.

4 CONSTRUCTION OF AN PEM FUEL CELL TEST STATION

Generally, the PEMFC performance depends not only on the catalyst electrochemical properties, structure of the GDE and electrolyte properties, but also on its components such as the gas leads and gas distributors. In order to understand the influence of FC components on its performance, a complete characterization, in terms of electrochemical properties is required. Along them, variation of the operational parameters can provide further information about factors and conditions which affect the cell performance. Knowing the FC behaviour, with well defined parameters, gives the possibility to determine the viability for future applications.
When the long time stability is examined, the FC characterization process can take days (shorts measurements) or even months and years. More than, a multitude of techniques has to be applied and the cell response needs to be recorded. In addition, the fuel cell housing should resist to the corrosive medium and remain stable over the time. Due to the complex analysis and multitude of parameters, it is recommended to perform the FC test in an automatic way, with as little as possible user intervention.

In focus of this chapter stay the development of a completely new PEMFC test station together with a control software. The developed test platform proves the concept of completely standalone automation fuel cell tests. Along that, a short description of the most used PEMFC testing techniques is presented. Not at least, a new cell design for PEMFC testing is introduced.

4.1 METHODOLOGY FOR FUEL CELL TESTING

Different types of diagnostic tools to analyse the PEMFC electrochemical parameters and as well as a variety of analytical instrument methods to record gas, water, temperature and current distribution are existing. In addition, even special cell designs to visualize flow patterns to obtain localized information of the cell are studied [33]. This helpful tools are intensively used to perform cell design optimization or particular configurations. The most used methods to characterize the FC performance are electrochemical techniques, including the cyclic voltammetry (CV), polarization curves, electrochemical impedance spectroscopy (EIS) and current interruption methods.

4.1.1 *Polarization curves*

This method is commonly used to examine the FC current-voltage characteristics. During this method the potential is shifted away from its equilibrium value, leading to an electrochemical reaction. A good cell should provide a polarization curve with high current density at high cell voltage. High current densities are expected

at low ORR overpotentials. This can be obtained only when the voltage losses are small (see Subsection 3.2). By measuring polarization curves, the influence of parameters such as electrode composition, gas flow rate or relative humidity (RH) can be monitorized.
In actual work, the current-voltage characteristics are measured in current and voltage mode.
In the galvanostatic mode, the current is varied in steps from 0 A up to a maximum value where a cell voltage $\geqslant$ 350 mV is maintained. This imply more attention from the user, which need to monitor and modify permanently the upper current value, in order to hold the cell voltage in the limit.
In potentiostatic mode the voltage is linear swept from the OCV to 350 mV. In this way the user does not need to supervise the machine and during the polarization curve the maximum current can be reached. The limit of 350 mV is imposed in order to not corrode the graphite flow fields [111].

4.1.2 *Cyclic voltammetry*

It provides useful information about catalyst and electrochemical reactions. Furthermore, it supplies data over the catalyst activity and the potentials at which they occur. The three-electrode configuration is the most widely used, due to the stability of the reference electrode during the measurement (see Subsection 4.1.4).

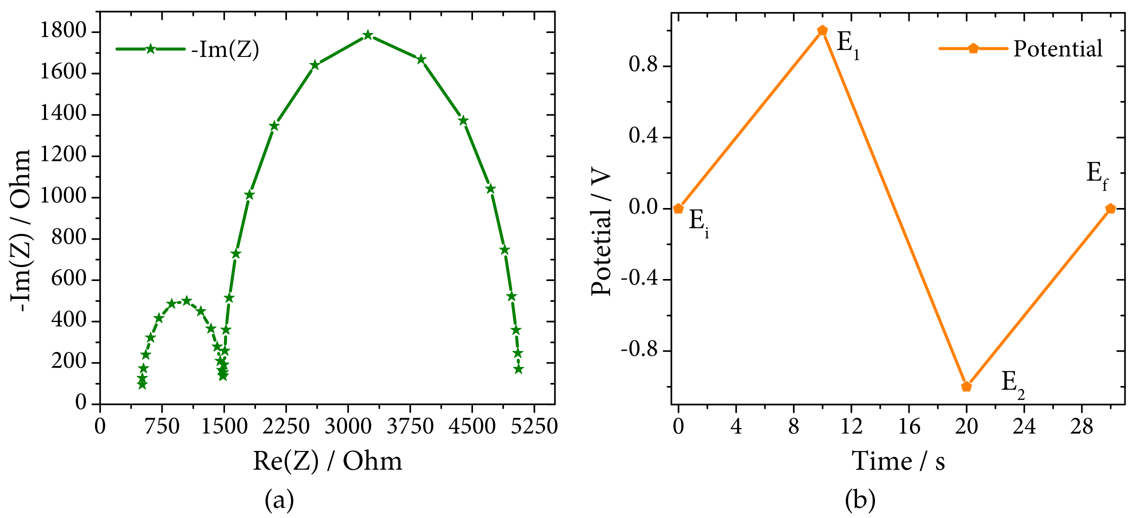

Figure 8: (a) Typical Nyquist plot for an electrochemical system and (b) the potential sweep profile for a cyclic voltammetry measurement.

During CV the WE potential is swept between two limits at a known sweep rate and the corresponding current is recorded as a function of the varying potential. The same sweep rate is normally chosen for the forward and reverse sweep.
FCs are two-electrode electrochemical systems where the CV is usually carried out by connecting the counter electrode and the reference electrode at the anode and the WE at the cathode of the cell. Due to low overpotential of hydrogen oxidation and reduction on platinum the FC anode can be used as a dynamic hydrogen electrode (DHE) [112, 41]. Additionally, the two electrode configuration is quite easy

to implement compared to a three-electrode connection for PEMFC. The results are typically represented as a dependence of current versus the potential. Most of the performed measurements are made in a potential range of $50 - 1000\,\mathrm{mV}$ with a scan rate of $50\,\mathrm{mV\,s^{-1}}$.
From this measurement, the catalyst electrochemical active surface area (ECSA) can be calculated using:

$$\mathrm{ECSA} = \frac{Q_H}{Q_{H_2,ads}\, L_W\, A_g} \tag{17}$$

where, $Q_{H_2,ads}$ is the hydrogen adsorption charge on a polycrystalline platinum surface ($210\,\mu\mathrm{C\,cm^{-2}}$ [37]), L_W is the cathode loading of the membrane electrode assembly ($\mathrm{mg_{Pt}\,cm^{-2}}$), A_g is the geometric area of the electrode ($\mathrm{cm^2}$) and Q_H is the integrated area (expressed in units of μC) under the hydrogen desorption region in the CV curve. A simple way to verify if the ECSA values are reasonable, is to compare with the average platinum particle size, as measured for instance by TEM [113]. Assuming that the platinum particles are perfectly spherical, its size from ECSA can be calculated:

$$\mathrm{ECSA} = \frac{6 \cdot (1 - S)}{\rho_{Pt} \cdot d} \tag{18}$$

where, S is an dimensionless factor which represent the faction of platinum surface covered by carbon (commonly 0.3) and $\rho_{Pt} = 21.45\,\mathrm{g\,cm^{-3}}$ is the density of platinum [113].

4.1.3 *Electrochemical impedance spectroscopy*

It is an useful technique that provide information about the potential losses. It measures the FC impedance frequency dependence, by applying a small sinusoidal alternating potential/current as a perturbation signal and record the FC response.

The EIS benefits of some advantages such as:

- measurements can be made at OCV or under load,
- a multitude of parameters can be determined by performing just a single experiment,
- the measurement is non-invasive (the system is not substantially disturbed from its operations conditions),
- microscopic informations about the FC system which can help to find the optimum structure, and the appropriate operating conditions can be provided.

Generally, the impedance spectrum of an electrochemical system can be presented in Nyquist and Bode plots. These are impedance representations as a function of the frequency [114]. The Nyquist plot displays the experimental datasets by representing the real and imaginary part of the impedance (Z_{re}, Z_{im}) at a particular frequency (Figure 8a). Typically the EIS result is a semicircle, with the high-frequency part giving the electrolyte resistance (for a fuel cell, mainly the membrane resistance) and the semicircle width indicating the charge-transfer resistance [115].

In order to extract physically meaningful proprieties of the electrochemical system, the researchers use electrical circuits to model the recorded data. The circuits are composed of ideal resistors (R), capacitors (C) and inductors (L). Since we are dealing with a real system that do not necessarily behave ideally, very often specialized circuit elements such as constant phase element (CPE) and Warburg element (Z_W) are necessary [116].

In actual work, the impedance spectra are recorded with a HPC − 803 booster from Bio-Logic SAS (Claix, France) (Bio − Logic) in a range of 10 kHz − 1 Hz. Using an equivalent circuit for a single PEMFC the frequency cell response is fitted (Figure 9a). The fit is performed using the software Ec-Lab (Version11.2) provided by Bio − Logic. The adopted circuit contains resistance elements specific for the proton exchange membrane (R_M) and anode ($R_{ct,a}$) resistances. Due to the porous structure of the electrodes, the circuit include a CPE ($C_{dl,a}$) in parallel with the anodic resistance. At cathode, a transmission line circuit ($G_{a,c}$) is used to simulate the catalyst layer and the porous network [117, 118, 119, 120]. Along that, the circuit incorporate a inductance, which is the equivalent of the connecting wires used to connect the cell with the potentiostat. To simplify the response of the electrode, the impedance experiments are performed under nitrogen as opposed to oxygen [121].

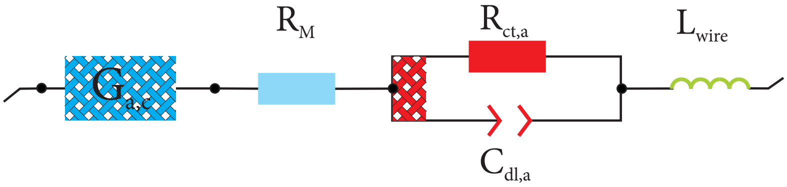

(a)

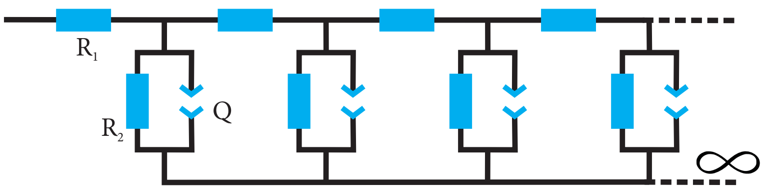

(b)

Figure 9: (a) Equivalent circuit of the PEMFC anode and cathode simulated with pores. (b) Gerischer element represented by a semi-infinite short-circuited uniform distributed RRQ transmission line.

In order to completely understand which parameter influence the FC performance it is necessary to test the FC using all presented techniques. Therefore an efficient and flexible way to couple this ones together with gases flows and temperatures control is necessary.

4.1.4 *Potentiostat/Galvanostat setup*

In electrochemistry, the potentiostats are used for analytical chemistry, battery research, fundamental studies of electrode processes, synthesis of chemicals, fuel cells and corrosion research. In principle, they control and measure a voltage or a current between three electrodes. Figure 10b shows a basic diagram of a potentiostat/-galvanostat. The most widely used potentiostats are assembled from integrated-circuits operational amplifiers and other digital modules. A three-electrode system is normally used in voltammetry for currents in rage of microamperes to milliamperes. In most cases the reference electrode is placed as close as possible to the working electrode (WE) and in some cases, to avoid contamination, it can be placed in a separate compartment.

Reference electrode: provides a stable, reproducible electrochemical potential which does not depend on temperature and does not vary in time.

Counter electrode: its role is to record/sustain a current, without limiting the measured cell response. Furthermore, it should have at least twice size of the WE.

Working electrode: consists of the sample to be examined and can have various geometric forms. Commonly used electrode materials are gold, platinum and glassy carbon.

Typically a potentiostat offers a voltage windows from −10 V to 10 V and can sustain a maximum current of 1 A. However, for FC applications, where high currents are required, an amplifier is necessary to extend the voltage/current range.

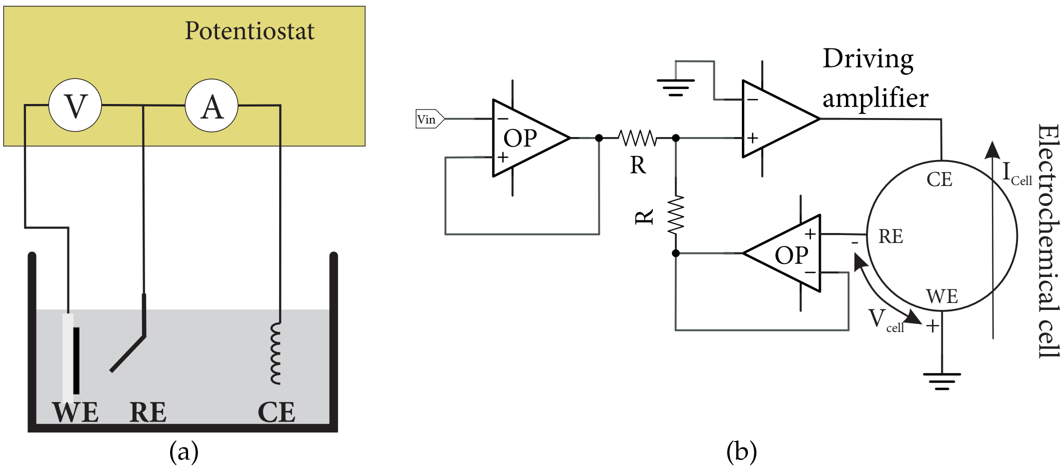

Figure 10: (a) A three-electrode cell setup in an aqueous electrolyte and (b) a basic diagram of a potentiostat/galvanostat using a voltage buffer to isolate the driving amplifier and the reference electrode.

4.2 PEM FUEL CELL HOUSING MANUFACTURE

A decisive factor on the FC testing is the homogeneous reactants distribution at the anode and the cathode. A good flow field design avoid the condensed water accumulation in the cell and conserve the reactants humidity, particularly on the cathode side [122]. Along the design, the used materials and the special processing tools plays an important role.

An system which permits the FC examination in an efficient and flexible way is constructed during PhD thesis, with the help of Dipl. -Ing. Rudolf Richter and the mechanics from mechanical workshop. Figure 11 exposes the structure of a single

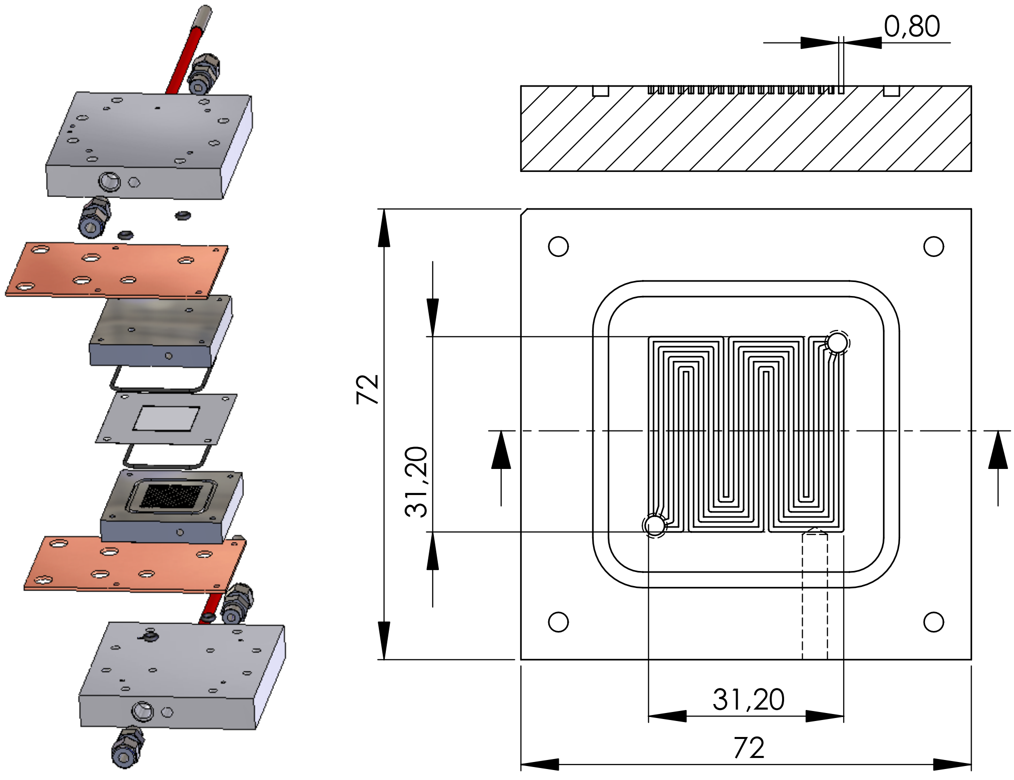

Figure 11: (a) Elements of the PEMFC housing and (b) structure of an graphite flow field.

fuel cell housing, with an active surface area of 10 cm^2. It is constructed symmetrically, with end-plates, current collectors and bipolar plates. The entire assembly assures, besides gas distribution, the heat and the electric current extraction. The end-plates are made of aluminium and guaranteed the gas connection and a good thermal conductivity. Moreover, they are used as support for the heating cartridge. In this way, the cell can reach very fast the working temperature of $60-80$ °C and maintain a constant temperature over the test period.
Also, on the flow field design some improvements are performed (Figure 11b). A four parallel serpentine system with a channel width and height of 0.8 mm are milled on Sigracet BBP4 plates, from Eisenhuth GmbH & Co. KG (Osterode am Harz, Germany) (Eisenhuth). In this arrangement, the gas found always a path to output and moreover, the water blockages are cleared [14]. In order to minimize the voltage losses, each current collector is coated with 2 µm gold layer. The coating is performed by Drollinger Metalveredelungswerke GmbH (Birkenfeld, Germany) (Drollinger). To be able to perform measurements at pressure over atmospheric pressure, the cell is equipped with Viton gaskets from Freudenberg Simrit GmbH & Co. KG (Weinheim, Germany) (Simrit). Due to the great success with this small cell, the cell design is extended to an active surface of 50 cm^2. To assure a tight gas connection, fittings from Swagelok with a diameter of 6 mm are used.
Due to its small size, the necessary GDE and PEM on the MEA can be saved. Moreover, due to its improved serpentine design, an optimum gas flow distribution is reached. Also the 50 cm^2 fuel cell housing makes possible the test of bigger MEAs without impediments.

4.3 FUEL CELL TEST BENCH SETUP

Typically FCs are tested in a fuel cell station which measures the FC components performances at distinct working parameters. The FC test stations are able to control the cell temperature, the inlet gas humidity and to measure the FC electrochemical proprieties. Moreover, these devices facilitate the FC evaluation at distinct pressures (from atmospheric pressure up to elevated pressures). Typically, the maximum pressure that can be applied on a FC is limited by the electrolyte, due to its thickness. One of the most used membranes in the PEMFC is the Nafion™ 212 which has a thickness of 50 μm and can be used up to 3 bar [123, 52]. At higher pressures, the membrane tend to get perforated and the fuel can be mixed with the oxidant, a fact that could end with tragic accidents. Therefore, in a FC test bench many safety measures are required, specially for the gas pressure control and temperature management systems.

Considering the fundamental requirements for PEMFC testing, in collaboration with the company Gamec Analysentechnik (Illingen, Germany) (Gamec) three different testing platforms are produced, one of them is commercialized.

4.3.1 *Test station safety strategy*

Most of the nowadays used devices are digitally controlled by a central microprocessor which can be easily disturbed or destroyed by high voltages or other electrical interferences. Therefore, the data acquisition and the control of the sensors, in a test station should act as standalone and should be independent from the rest of the system in emergency cases. One of the most dangerous situation in a FC test bench is represented by H_2 and O_2 leakage. In most of the laboratories researchers use high purity gases, which can produce disastrous damages. Thus, high sensitive gases sensors, which detects in an appropriate time an eventual gas leakage and a method to immediately turn off the gases are necessary. A solution to limit the leak danger is to combine mechanical valves in series with magnetic one. Mechanical valves can be manually switched while magnetic valves are controlled by the micro-controller. When a gas leak occurs or the micro-controller is destroyed, the magnetic valves switches to its initial state (typically close). Generally the magnetic valves are placed in the FC test bench housing, but they can be places as well in the gas cabinet, close to the gas source. In this way a further gas leak is avoided and the entire laboratory staff is protected.

In a report published by DLR in 2005 they draw attention on the explosion risks on the automotive drives by FCs. They have proposed three methods to stop the H_2 flow in case of leakage [124]:

- a detector which records the H_2 concentration and stops the flow when it is over 40 % of the lower explosion limit,
- sensors which log the FC pressure and temperature and after they exceed a critical value, gases and heat are closed,
- finally a manual switch that turn off the entire system.

The same rules should be applied on the FC test stations, although the entire measurements are made in laboratory and here multiple safety rules are already presented. The incorporation of extra sensors is still necessary to protect the operators against explosion or fire.

4.3.2 *Hardware system*

Before FC test bench development and assembly, a scheme and a list with necessary components is required. Most of them can be purchased from different produces, but there are a multitude of small components that should be particularly fabricated. Figure 12 presents a simplified test station model which is suitable for the characterization of single FC and small stacks (2-3 cells). This test bench configuration is optimum for our self-developed cells with a total area of $10\,\mathrm{cm}^2$ and $50\,\mathrm{cm}^2$ (see Section 4.2).

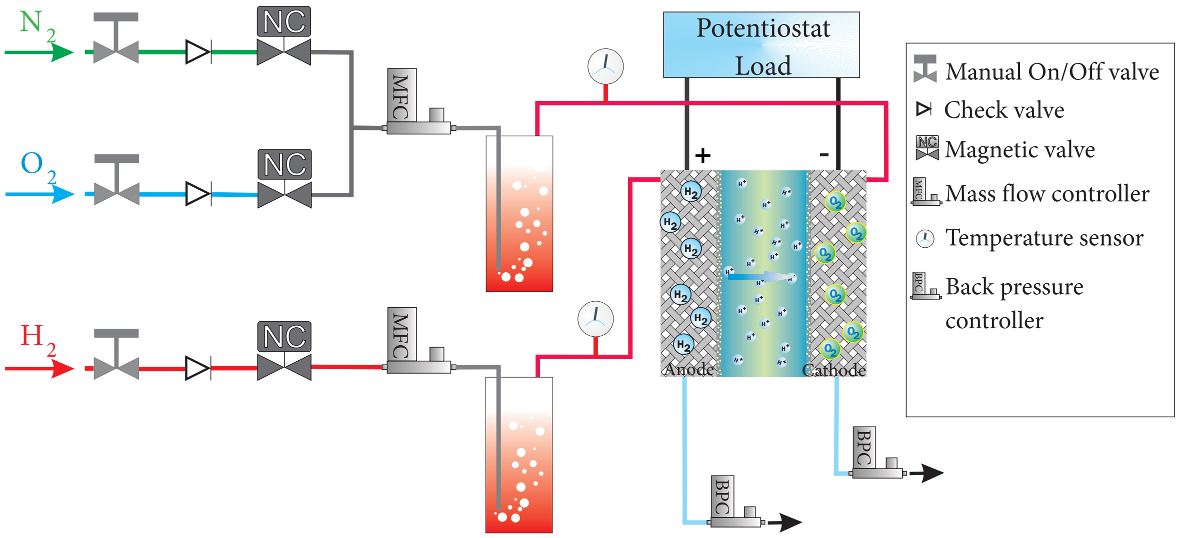

Figure 12: Scheme of FC test station containing two gas mass flow controllers, bubble humidifiers for each gas and the back pressure controllers.

The presented test bench can operate with three different gases (H_2, O_2 and N_2). All gases before to enter in the FC test station are controlled by manual and magnetic valves. The magnetic valves are normally closed and operated by the microprocessor unit. So, the FC can be tested with two different gases at cathode side, without any change on the physical connection. The gas flow control is assured by two mass flow controllers (MFCs) purchased from Brooks Instrument (Hatfield, USA (Brooks Instrument). The maximum flow is $2.6\,\mathrm{l\,min^{-1}}$ and $7.2\,\mathrm{l\,min^{-1}}$ for anode, respectively cathode. Moreover, the used MFCs support a multitude of gases that can be changed using the digital connection, a fact that is very helpful for long time FCs tests.

In order to not compromise the FC measurements when the gas pressure falls down (e. g. gas bottle is empty), for each gas check valves were purchased from PKP Prozessmesstechnik GmbH (Wiesbaden, Germany) (PKP) and installed before the magnetic valves. It contains a mechanical switch which turns off the measurement when the pressure drops down below $1-2\,\mathrm{bar}$. Thus, the withdraw current or voltage can not damage the catalyst or the membrane when one of the gases is missing. To assure a good proton conductivity in PEMFC, the electrolyte humidity should be high [125, 126]. Therefore, the employed gases should carry enough water molecules to humidify the membrane. Some general methods used for gas humidification and the chosen option for the self-developed test bench are described in subsection 4.3.3.

Figure 13: Test station system built during PhD duration. It contains on the front side all necessary connections to link a single PEMFC or a small stack.

A main part of the test system is represented by the potentiostat, which is responsible for FC current flow and the potential control. Furthermore, it has the ability to measure the response of the fuel cell at different frequencies. On actual fuel cell test station a booster from Bio-Logic SAS (Claix, France) (Bio – Logic) with a maximum current of ± 80 A and a voltage windows of ± 3 V is utilized. Although, this device can provide positive and negative current, for fuel cell test station it is used just to dissipate the FC current, acting therefore as a load. Control and data acquisition of the potentiostat is done using the supplied EC-Lab® development package V5.37 for LabVIEW (LV). The entire driver is incorporated in the self-developed program, which controls also the temperatures, gas flows and pressures (see Subsection 4.4). For better handling, all components were assemblies in an aluminium case (Figure 13). So, the laboratory staff is protected against possible explosions or fires that can take place in a so complex device.

4.3.3 *Humidification system*

The performance of a PEMFC depends strongly on the electrolyte proton conductivity [14]. Moreover, the water management is a key in improving the performance and durability of PEMFC [127]. In an ideal cell, the water produced at the cathode electrode keeps the electrolyte at the right hydration level. Furthermore, for a thin PEM ($\leqslant 50\,\mu m$) the water diffuses from cathode to anode side and thus the whole electrolyte benefits from a suitable state of hydration, without any external support. But, as in each real system, some problems exist. In this case, during the cell operation the H^+ ions, by its diffusion from the anode to the cathode, drag water molecules with them and can cause membrane dry out. This process is called electro-osmotic drag [43].

Moreover, the problem is more serious at high current densities, when the entire water can be removed from the anode, causing an abrupt loss in FC performance [15]. For each proton passing through the membrane up to five water molecules are dragged [128]. Studies have shown that at temperatures $\geqslant 60\,°C$, the air dries out faster than the water is produced in the FC by the H_2/O_2 reaction. One common way to solve this problem is to add water in the system by humidifying the reactants before they enter the FC. But, in the case that to much water is injected, flooding of the electrode can occur and so the gases does not reach any more the electrocatalyst [22]. Typically, the inlet gas humidity level is held above 80 % to prevent excess drying. Although it seems that employing gases humidification solves all problems, it is necessary to understand that the flow field design plays also an important role in the FC water management and a combination of both will exhibit the best cell performance. It is mandatory to control precisely the gas humidity used in a PEMFCs, in order to increase the FC performance.
Up to now no standards exist for FC humidification, each producer is experimenting with different methods. FCs are not the first systems where a gas has to be humidified, technologies used elsewhere can be adapted for FC applications. In laboratory FC test systems the reactant gases are humidified by bubbling them through water, whose temperature is controlled. The bubbling vessels can have different shapes and are made commonly of stainless steel. The water volume depends on the gas flow which should be humidified. It contains at least a gas input and output, but many other connections can be attached for thermocouples, water level and RH sensors. This kind of systems can be used with pressures over 10 bar and an autofilling system can be attached. During the humidification process it is assumed that the dew point (DP) of the gas is the same as the water temperature. The bubbling system is good for experimental work, but rarely is used on practical applications.
One of the easiest way to humidify a gas is the direct injection of water, as a spray. This method involves the use of a pump for water pressurization and a solenoid to control the water flow. Although the price of such systems is quite high, they own some advantages as the gas cooling (in case of reformate gases) and a very fast switch to different humidities.
Instead to humidify the gases it exists the possibility to inject water directly in the cell. Although it can induce cell flooding, this technique is combined with a special

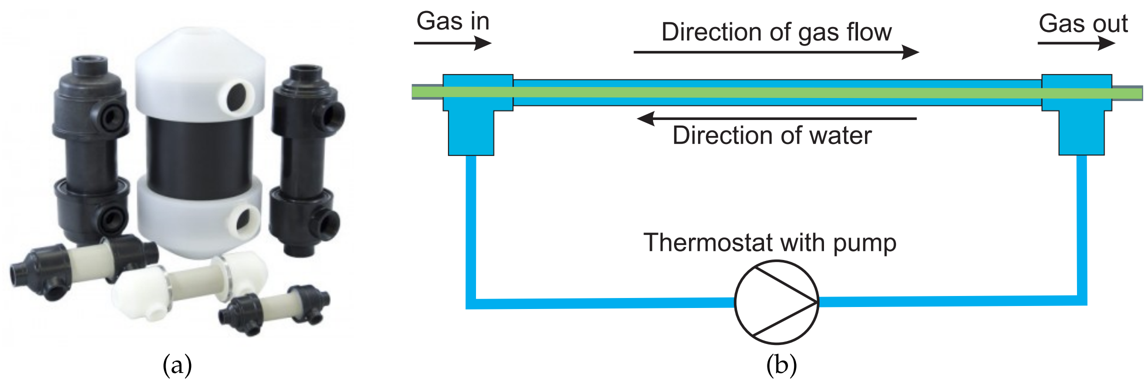

Figure 14: (a) Compact humidifier for portable systems produced by PermaPure [3] (b) Schematic draw of water to gas humidification principle.

flow field design, that forces the reactant gases to blow the water through the cell and over the electrode.

In the last years a cheap and efficient method to humidify gases was developed that uses the selective water transport properties through a series of micro-pores. In comparison with other humidification methods, this one has no power consumption [126]. Simultaneously, this type of humidifier has a long operation live time, is compact, has low weight and can be used as water to gas or gas to gas humidifier. Moreover, the gas humidification does not depend on the gas flow rate. This new technology contains a tubular membrane which is immersed in thermostated water (Figure 14). One single tube is enough to humidify a gas flow up to $1500\,\mathrm{ml\,min^{-1}}$, but for application where a higher flow is required (e. g. stacks) many tubes can be connected in parallel. Along to the thermostat or a pump with a heated vessel no other auxiliary components are necessary. Besides, this humidifier can be connected directly to PEMFC cathode output. So, the humidifier uses the water produced at the cathode, holds the pressure in the system in equilibrium and consumes no energy, likewise the PEMFC efficiency increases.

In the actual developed test station two humidifiers with a single Nafion™ tube (1.2 mm) are utilized (purchased from Perma Pure LLC (Lakewood, USA) (Perma Pure)) and assembled in the fuel cell test station. Two thermostats from Julabo GmbH (Seelbach, Germany) (Julabo) are used to control the DP temperature and implicitly the gases RH. In order to check the humidifiers' accuracy, both are calibrated using a chilled mirror hygrometer from Michell Instruments Ltd. (Cambridgeshire, United Kingdom) (Michell). This one uses an optical method to measure the formation of condensed water on the mirror surface. As the amount of reflected light decreases the Peltier element starts to heat the plate, until the mirror temperature reaches the DP. A high precision resistance temperature sensor (RTD) placed under the mirror is used to measure and maintain the temperature at the established DP (Figure 15a).

Figure 15b shows the calibration curves for different gas flows at a defined DP of 50 °C. As can be observed this type of humidifiers achieve a very good gas humidification. For different gas flows rate a deviation $\leqslant 1\,°\mathrm{C}$ from the selected DP is observed. Due to the small flow rate ($50\,\mathrm{ml\,min^{-1}}$) the transported moisture is not stable and the sensor records a higher value. This fact can be as well attributed to the long path which should be covered by gases up to the cell (over 1.5 m).

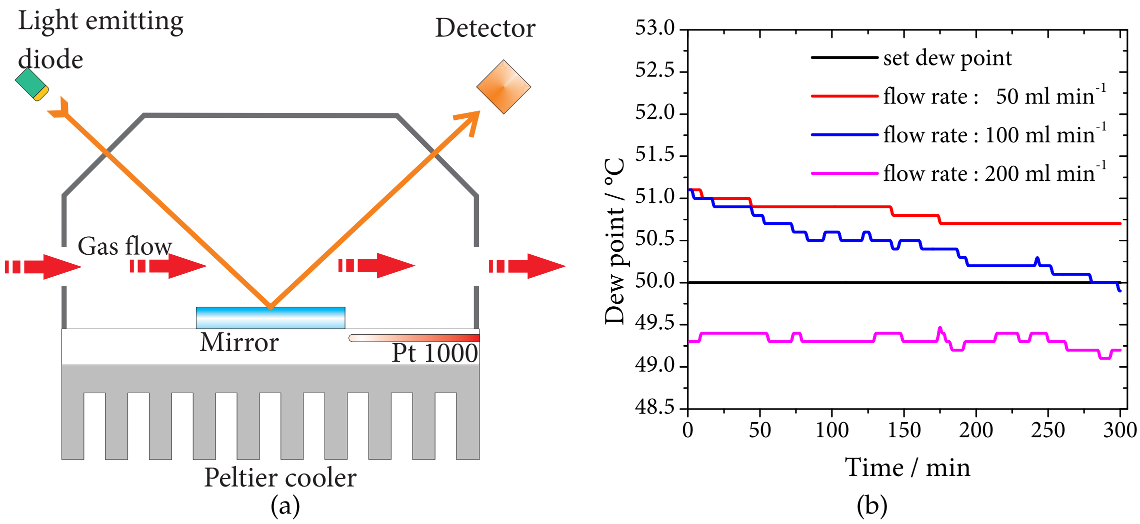

Figure 15: (b) Calibration curves an membrane humidifier used in actual test station and (a) a schematic representation of a chilled mirror used to determine the dew point.

Considering that during cell characterization, the applied current imply a gas flow variation, the DP during this period is a mix of the presented humidity results. It is know that at low current densities not enough water is produced to sustain the membrane humidification, therefore, in order to hold the cell humidification at optimum values the minimum gas flow is limited at $50\,\mathrm{ml\,min^{-1}}$. At higher flows, although the DP is under selected value, it does not influence the electrolyte humidity because enough water is produced at the cathode at currents exceeding $1\,\mathrm{A\,cm^{-2}}$, to humidify entire membrane.

A further positive fact of these humidifiers is the small water volume that is necessary to fully humidify the PEMFC. In the test station the thermostats have presented a volume of $5\,\mathrm{l}$ water, a fact that makes possible to reach a new DP in a few minutes. Also, smaller volumes can be used. Of course this method can not compete with the spray method with regard to the humidity feedback. Nevertheless, this procedure is very cheap and can be adopted for a variety of PEMFCs systems and applications.

4.3.4 *Controlling board*

The use of commercial products to control temperature, gas flow or other parameters is often problematic in the case that the number of used devices increases. Most of problems arise from different communication protocols used for each device. For an efficient control of all sensors and additional devices used in the presented FC test station, a controlling board is produced offering more than 20 input and output possibilities (Figure 16). The controlling board connects not only the hardware components but manages also the temperatures, pressures and gases flows rates. The central piece of the controlling board is the ATmega2560 micro-controller, produced by Atmel Corporate (San Jose, USA) (Atmel). Since it contains about 100 pins and the soldering process is complicated, it is bought already soldered on a Arduino Mega 2560 plate which is plugged in the developed board.

The ATmega2560 is equipped with 256 kilobits of programmable flash, 4 kilobytes EEPROM, 8 kilobytes SRAM, four USARTs, 54/86 general purpose I/O lines and many others features. The necessary firmware to control the outputs and to record the inputs values is written in C++ using the libraries provided by Arduino (Italy) (Arduino) (see Subsection 4.3.7).

Apart from the micro-controller, the controlling board contains diverse adaptors and the connections for all sensors and heating elements. In this way, all cables are connected to fixed position in the fuel cell test station. In order to facilitate

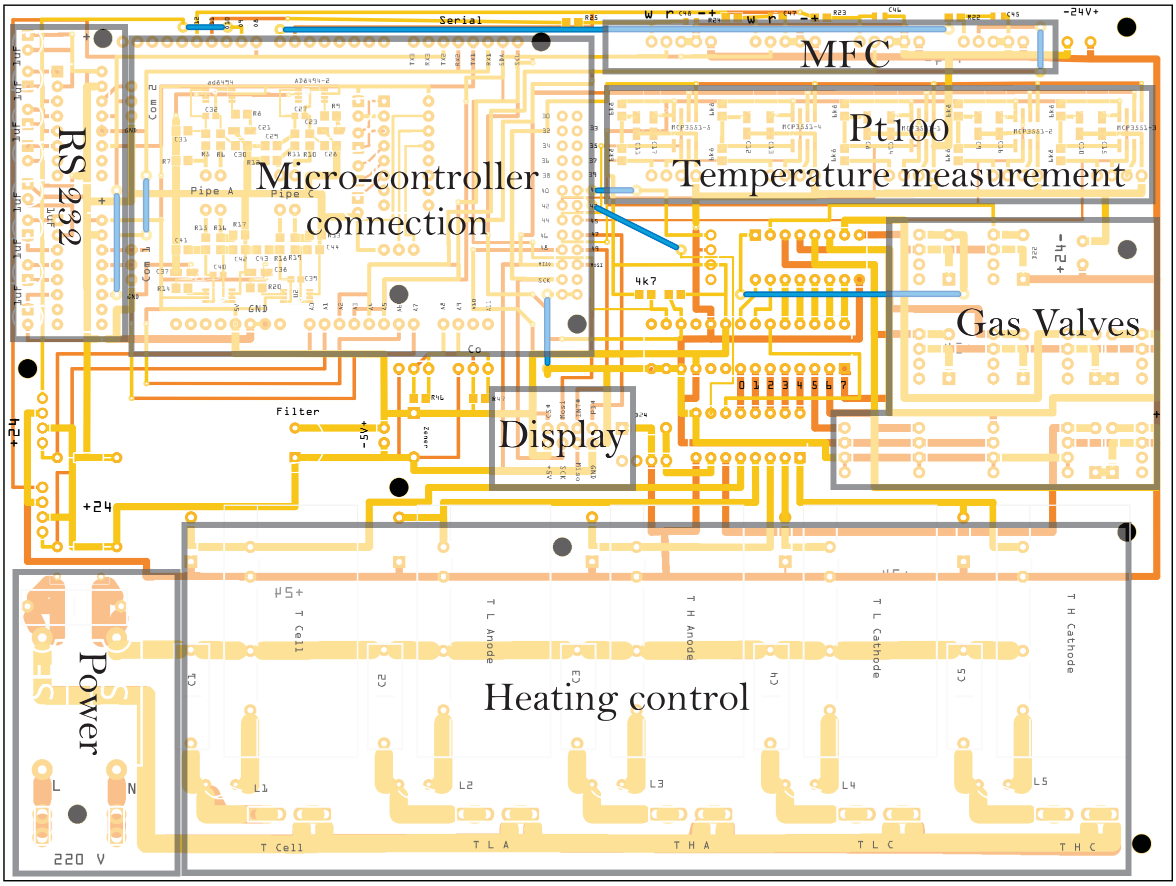

Figure 16: Controlling board schematic and the available connections. The board facilitates the connection of multiple temperature sensors, mass flow controllers, thermostats and magnetic valves.

a better overview and control over parameters, an VM800B touch screen display from Future Technology Devices International Limited (Glasgow, United Kingdom) (FTDI) is connected to the developed board. In this way the operator is able to modify parameters without connecting the test bench to a computer. For advanced experiments the user should use a PC which is equipped with an ethernet port and have installed the controlling software (see Section 4.4).

4.3.5 *External device control*

As already specified in subsection 4.3.3, two thermostats from Julabo are utilized to control the DP of the inlet gases. To communicate with the test bench it is necessary to develop a new driver using the commands provided in the operating manual and to include them in the firmware. Also the physically connection should be adapted, since the thermostats contain RS232 connections and the controlling board a USART connection. A MAX232x from Texas Instruments Incorporated (Dallas, USA) (TI) is used for each channel and integrated in the control board (Figure 16). The same problem arises for the mass flow controllers, where a new adaptor was constructed to convert the USART signal to RS485. Of course, commercial adapters exist, but each one is intended to be plugged on an computer USB port. This impedes the management of the current used by each adaptor and physical connection. Also the system lose its compact design and therefore its mobility decreases.

4.3.6 *Temperature management*

For a precise temperature reading Pt100 thermometers are used to measure the pipe and cell temperatures. Pt100 are RTDs sensors which uses platinum resistance/temperature relationship. So, by applying a small current the voltage drop over the resistance is measured and the temperature is calculated. Typically, these thermometers show a resistance of 100 Ω at $0\,°C$ and a linear behaviour. The circuit used to record the temperatures contains a high precision analog to a digital converter (MCP3551 with 22 bit, 4194304 distinct values) from Microchip Technology Inc. (Chandler,USA) (Microchip) and two $6.8\,k\Omega$ resistances to control the current flow. Together with the micro-controller these represents a viable and cheap method for accurate temperature recording.
In order to switch the current required for pipe and cell heating, solid state relays (SSRs) from Conrad are used (Figure 16). They are activated according to the proportional integral derivative (PID) output implemented in the firmware. The PID controller calculates the difference between the desired set point and the measured temperature and tends to minimize the difference over time by switching the relays (Figure 17). The change time value is determined by a weighted sum:

$$\mathrm{Output} = K_P\, e(t) + K_I \int e(dt) + K_D \frac{d}{dt} e(t) \tag{19}$$

where K_P, K_I and K_D are the coefficients for proportional, integral and derivative gain terms, $e(t)$ is the set point value at time t.

The integration of a PID controller in the firmware makes the implementation of safety rules significantly easier and the use of test station more secure. For example, in the case that the cell temperature exceeds the maximum limit ($120\,°C$), the micro-controller stops the heating for all other processes and brings the test station in a safety state (no gas flow and no heating).

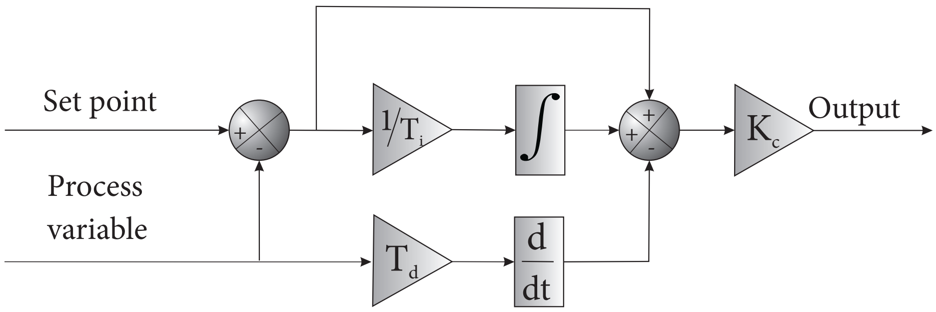

Figure 17: Block diagram of the PID control algorithm implemented in the firmware.

4.3.7 *Micro-controller firmware*

The firmware is a type of software that provides control, data monitoring and the data manipulation of the containing sensors and external devices. It is saved in a non-volatile memory device such as ROM or flash memory (on ATmega2560 256 kilobits are available). The source code is written in C++ and contains distinct functions to manage the gases flow rates, as well as the cell an pipes temperatures and DPs. Not at least, it enables the presentation of the read data on the integrated touch screen display. In addition, it is responsible to send and process commands and data to/from computer. The developed firmware was compiled and uploaded on micro-controller using Arduino IDE.

With the initialization phase the program reads default parameters from EEPROM and initializes all variables. Along these variables, the most important are the temperature limits, which can bring the test station in a critical state in the case that they are wrong. Therefore, a extra check is performed after the read and the values are compared with the ROM saved value. This check assures that all the variables are read correct from the memory.
Furthermore, the connection establishment with external devices belong to the initialization step. Distinct tests are performed to assures that the specified devices are physically connected and a complete initialization is performed. When no error appears during this stage, the program goes to the main loop. If errors occur, the execution stops and the user should start the debugging procedure depending on the message retuned on the main screen (Figure 18). Typically, errors appear due to non-appropriate connections, oxidized contacts or user mistakes.

Typically, in C++ the program execution is performed in a serial way. The necessary time to compute some functions can hinder the execution of meaningful functions. For example, in the case that the data display takes longer time compared to the readout of parameters or to the check some sensors, important information are missed. Therefore, task timing and classification are imperative for a long and error free operation. Thus, the tasks are divided in three distinct ones:

1. contains the sensor readout, computes the PID output and monitors the station status (each 300 ms),
2. checks the data that received at the Ethernet port and check the communication (each 5 ms),
3. displays the read data on the screen (each 900 ms).

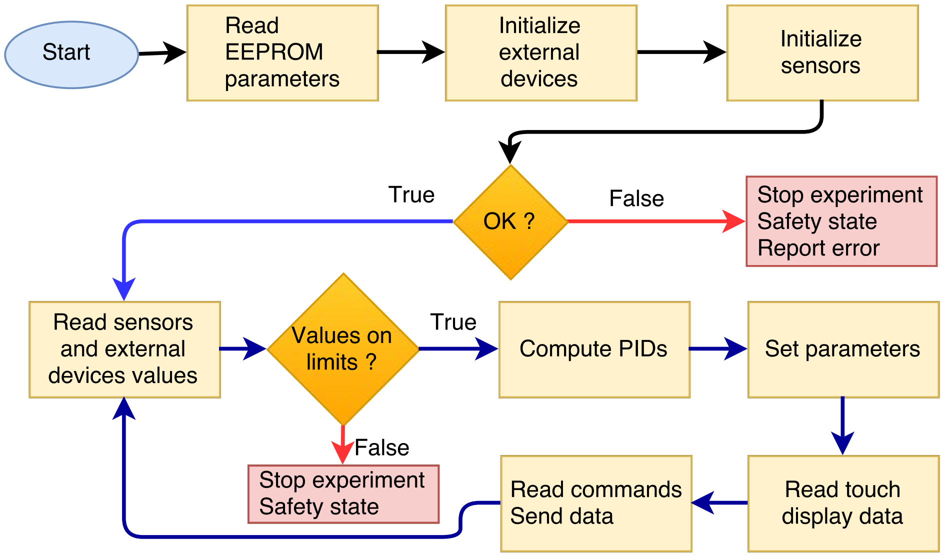

Figure 18: A simple representation of the firmware algorithm. After initialisation the program executes the main loop endlessly. Just a record value which is outside the limits can stop the program.

In this way no delay occurs due to the execution of additional functions, the processes are computed in real time and the microprocessor time is used efficiently. The structure of the entire firmware is represented as a flowchart in Figure 18.
In the case that a sensor records a value, which does not fit in the predefined limits, the operation of the entire test station is halted and a message is displayed on the screen. In addition, the user can abort at any time the operation and can bring the device in a safety state by pressing the emergency button situated on the housing front side (Figure 13). As a consequence, the firmware turns off the magnetic valves for each gas and modifies all temperature set points to a lower value. Another function of the developed firmware is the efficient communication with the computer. Thus, it uses the Ethernet technology to send and receive data. In this context, a binary format is chosen for data package. Thus many information can be efficiently send in the same package. To be sure that the data is received completely a simple check sum is implemented, summing the binary values of the contained package.
With all its features, the developed firmware provides a complete control of each test station component.

4.4 CONTROLLING SOFTWARE DEVELOPMENT

In order to be successful, a scientific instrument should not only be based on a good hardware infrastructure, but also a correct control software needs to be attached. Furthermore, the program needs to allow an efficient code modification for new hardware parts and to ensure absolute control of the device. Likewise, the user may have the possibility to modify all device parameters and to store them for similar measurements in the future. Essential for this type of applications is the user interface, which permits the modification of machine settings and the visualization of recorded data. Also the modularity should be presented at this level for code reusability and flexibility.

To attain the presented requirements, a new software is developed using the development environment LV. LabVIEW is a mature development tool with over 30 years improvement behind, that makes the automation a pleasure. First time it was released in 1986 for Apple Macintosh, by NI and after few years LabVIEW has imposed on the scientific and engineering world as a simple method for data acquisition, instrument control and industrial automation. It is actually supported by a variety of operating systems (Microsoft Windows, UNIX, Linux and Mac OS). LabVIEW, which stands for Laboratory Virtual Instrument Engineering Workbench, is programmed using a graphical language known as G, which is a data flow programming language [129]. Execution is determined by the structure of a graphical block diagram (the LV-source code) on which the programmer connects different function nodes by drawing wires [129]. The graphical system design takes out the complexity of other programming languages (C, C++, Java, etc.) and focuses the user just on the software development. With his graphical representation and intuitive design notation, LV reduces the learning process which is typically involved for other languages.
LabVIEW programs are called virtual instruments (VIs), because their appearance and operation imitates physical instruments. Furthermore, LV contains a comprehensive set of tools for acquiring, analysing, displaying and storing data, as well as tools to help on code troubleshooting [130]. The graphical approach allows non-programmers to build simple programs by dragging and dropping virtual representations of lab equipment. In order to produce more complex algorithms or large-scale code, it is important that the programmers possess an extensive knowledge of the special LV syntax and the topology of its memory management. Furthermore, advanced developers have the possibility to build stand-alone applications.

The developed software contains advanced programming techniques which are used to communicate with the FC test platform and to manage the amount of data that is recorded during the experiment. It is essential to separate the user interactions from the instrument-computer communication when such applications are designed .
If this simple criterion is not reached it can occur that during user events the data transfer is interrupted and the entire experiment is compromised. A preferable way to achieve this is to use a producer-consumer structure, where the code is splitted on three different levels:

(i) top level, deals with the user input and major execution,

(ii) bottom level, enables the transfer of data between the personal computer (PC) and hardware components,

(iii) data processing and saving.

In order to record the user events an event structure is used. It make possible to transfer the operation between levels and permit the integration of pre-built intelligence between. However, such architecture does not allow the execution of independent parallel processes. Many of the actions inside the program shall be

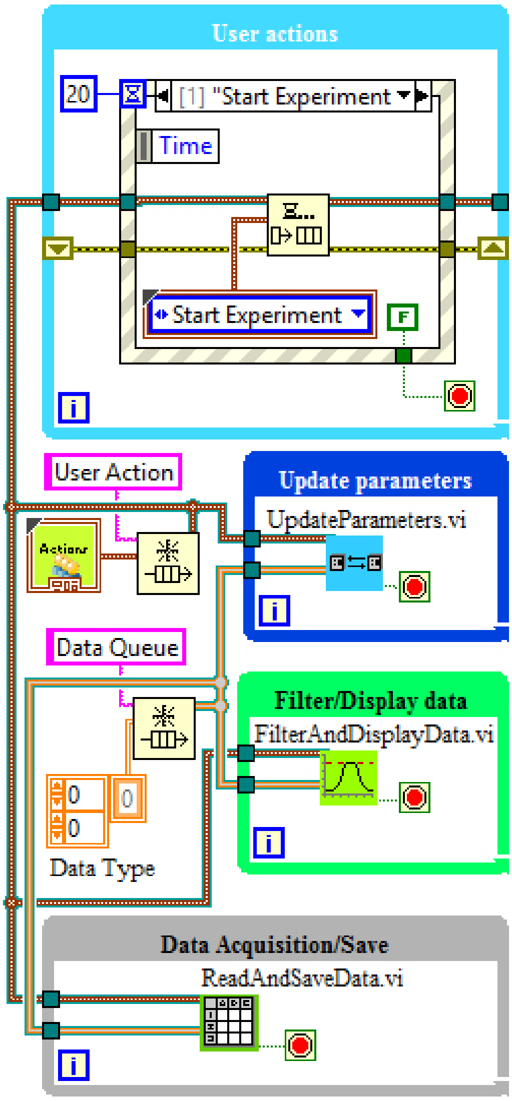

Figure 19: Producer-consumer design implemented in LabVIEW. The user actions are recorded and forwarded to the procesing loops.

executed on the same time (e.g. data reading and user input). In order to avoid this problem, an extended producer/consumer was created, where parallel processes are performed simultaneously in separate structures (Figure 19).
As can be observed, the data produced in the user actions loop is transferred further, using a queue system, to other loops. The packed message is open by the addressed consumer, who performs an action depending on the message content. For example, when the user starts the experiment, a message is distributed to all loops. On loop update parameters the necessary parameters are transmitted to the device and data acquisition /save loop start the data recording (Figure 19). So, the useraction loop remain free to record next user event.

Along the communication with the developed board, a new graphical user interface (GUI) is designed. It helps the user to define the experiment setting in an easier way (Figure 20). The GUI provides a multitude of functions necessary for each scientific program.

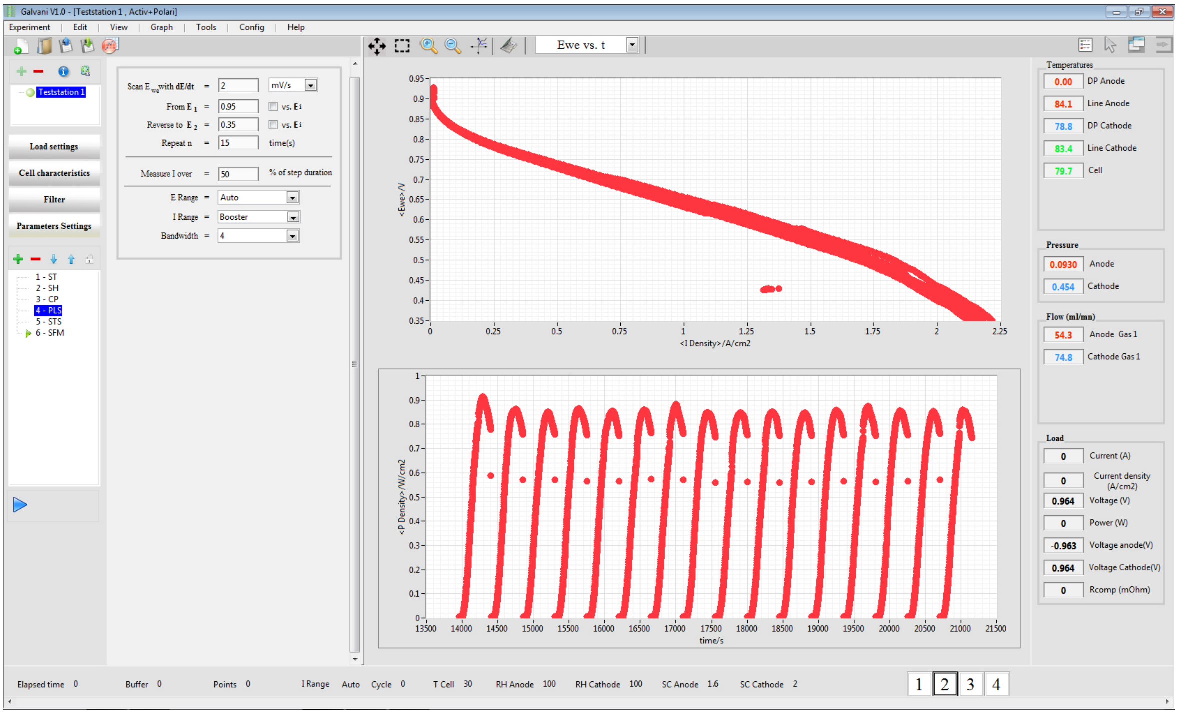

Figure 20: Screenshot of the graphical user interface of the developed software. According to the introduced parameters, the program controls the PEMFC test platform.

The GUI windows is divided in four sections, which contain lists, graphs and numeric indicators. The left side screen include the device list and the technique list. The technique list contains the procedures used during the experiment. Up to 40 techniques can be defined for a single investigation. The exemplified method are performed from top to bottom. Moreover, the user can choose from a multitude of techniques (Figure 21a) the appropriated one for his experiment. Along the typical electrochemical methods, in order to control the temperature, pressure and the cell current/voltage new procedures are defined. For each defined technique, the parameters can be individually specified making the use of the developed device more flexible (second screen region). On the screen middle, the graphs present the measured data. As can be noticed the user can choose different representations for each graph. Additionally, up to 15 graphs can be defined and particularized with an individual representation and style.
Typically, a complete FC characterization can take up to two days, during which time more that 10 parameters need to be read and saved. Thus, in order to make more clear the results collected from multiple techniques over long time period, a data filtering system is implemented as can be observed in Figure 21a.

Additionally, the filter can be applied individually for each graph depending on the technique, cycle, step, loop, etc. On the right side, the user can identify in real time, the most important test station parameters. These contains the FC temperature, pressure, flow rates and electrical values. Along this visualisation, the GUI contain on the bottom side some indicators, which shows the elapsed time, buffer size or the set point for DP and cell temperature.
With his simple graph representation and included tools, the developed software complete the created fuel cell test station.

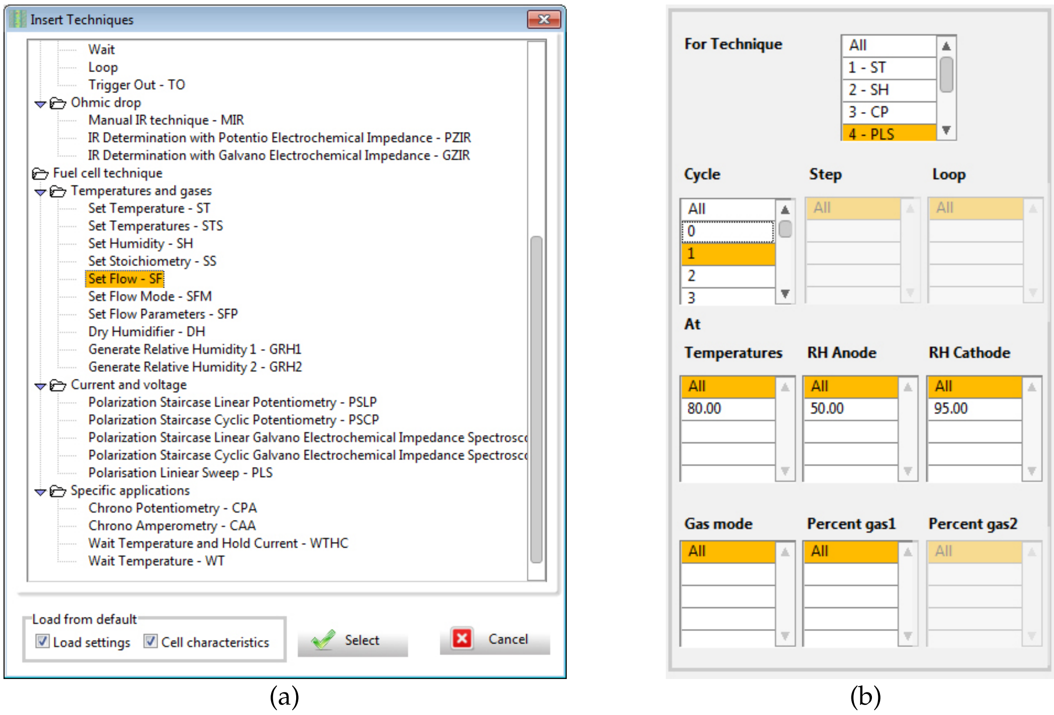

Figure 21: Screenshots of: (a) insert technique dialogue and (b) filter implemented for each technique defined in experiment.

4.5 SUMMARY

A short description of most used techniques on PEMFC testing (CV, polarization curves and EIS) is presented. For each technique, the necessary limits and parameters are defined. Along them, the design of a new fuel cell housing with an active surface of $10\,\text{cm}^2$ is introduced. Due to the employed sealing system the cell is completely tight for different MEAs thicknesses. For a better reactant distribution it contains four channels, each one with a width of $0.8\,\text{mm}$ and a length of $17.5\,\text{mm}$. To avoid the water accumulation, the proposed flow field design present four bends. Due to successful tests, the $10\,\text{cm}^2$ cell architecture is up-scaled to $50\,\text{cm}^2$. During the PhD period, over ten cells with distinct sizes are produced, all of them offering precisely and valuable data.

In this chapter, along to the testing methods and developed hardware parts, the producing steps of an completely new PEMFC test station are presented. The developed testing device contains standard components as thermostats and mass flow controllers, but also the self developed sensors and algorithms. One of the big issue on the PEMFC testing is the precisely temperature and humidity control. Therefore, a complex circuit is build to read and control the temperature with a resolution of $0.015\,°\text{C}$. Along that, new modules to manipulate the thermostats and the MFCs are manufactured. All electronic components are fixed to a self planned controlling board, which provides the possibility to connect over 20 inputs and outputs. For safety reasons the board contain a micro-controller, which computes in real time the sensors input.

For a precise humidity control, a Nafion^{TM} tube system is adopted. With its help relative humidities up to 100 % can be achieved with accurate control. Moreover, the developed device can be used for PEMFC with different sizes and can perform current measurements up to 80 A.

To manage easier the experiments, a powerful software is developed. It contains the already defined FC characterisation techniques and many useful one, as temperature and pressure control. Using an intuitive GUI, it permits the customization of each testing parameter. Additionally, it gives the possibility to present the recorded data in individual styled graphs. The implemented filter give the opportunity to refine the visible data over ten criteria. Along the numerous facilities, the developed software makes possible the FC measurements in a semi-automated way. So, when the experiment start, the system necessitate no user interaction and can operate for weeks without any external interventions. An advantage of this new system is its size, a fact that makes it more flexible and easy to transport. Due to its unique characteristics, in collaboration with the company Gamec one of them is commercialized.

The manufactured fuel cell housings and the test station represents the base for further research. These two elements are used to investigate the samples created on the further chapters and to improve the PEMFC performances.

5 EXPLOIT THE SPRAY AND ELECTRODEPOSITION TECHNIQUES FOR GDE PREPARATION

Since an inexpensive replacement for platinum has not yet been found, most of the researchers and engineers are focused on the electrode development with an as low as possible platinum loading. Along that, the prepared electrodes should maintain at least the same performance compared to those with a standard platinum loading. For this propose, various techniques have been developed to optimize the platinum utilisation and to improve the catalyst activity.

5.1 CATALYST PREPARATION METHODS

Chemical vapour deposition and sputtering [99] have been successfully used to obtain platinum loadings below $0.1\,\mathrm{mg\,cm^{-2}}$. However, the strict vacuum atmosphere required by these methods make them relatively expensive and hard adaptable for bulk production [80]. Methods such as electrospray or electrohydrodynamic atomization have been developed in the last years [111, 131]. Compared to other deposition methods, this technique requires no vacuum, is easy scalable and has a simple experimental setup. Moreover, the catalyst particles created with this approach are very well dispersed in the CL and the interaction with the ionomer is improved [131]. Nevertheless, some problems exist on the loading reproducibility and therefore further research is necessary.
Catalyst layer structures can be obtained by alternative coating techniques such as spraying, screen printing, brushing and decal methods [67]. Sambandam et al. have applied the spraying method to produce GDEs with an active area of $5\,\mathrm{cm^2}$ [59]. Typically, this procedure is used to spray solutions, which contain a catalyst ink, dispersed with an ionomer in H_2O or isopropyl alcohol (IPA), over an MPL. To create this layer Scott et al. have mixed Teflon and carbon black in IPA and then brushed it on a Toray carbon paper support [132].

Most of the commercial techniques manipulates an already prepared catalyst, which is sprayed over a GDL to constitute the CL. Unfortunately, the catalyst position in the CL structure cannot be very well controlled, causing a decrease on the triple phase boundary (TPB) density. Methods such as electrospray or galvanostatic deposition were used for in-situ catalyst production, but they require either high voltages (kV range) or involve a toxic plating bath. Furthermore, the large scale implementation is difficult, expensive and suffer low reproducibility.
Metal electrodeposition is one of the popular synthesis technique, which is applied in a variety of domains including electronics, nanotechnology and nanobiotechnology [133]. This method provides a precise composition and crystallinity control of the deposited material and can be applied onto surfaces of electrical conducting materials with various shapes and sizes. This method has found application in the

FC field, where it is used to coat the BP with different metals or to create the catalyst particles. Typically, in PEMFC the catalyst is represented by platinum or its alloys [134], which are easily deposited from different precursors. Most of the electrodeposition processes takes place in electrochemical baths containing platinum in divalent or tetravalent state [107]. This method provides a low energy consumption and a strict control of the platinum loading [48]. In order to increase the active surface, the researchers use carbon black as support. Miyake et al. have described a simple potentiostatic electrodeposition to prepare carbon supported platinum catalyst. Using the commercially available carbon black, Ketjen Black EC, as support they have deposited platinum particles by reduction of chloroplatinic acid at room temperature. The created catalyst particles offer diameters in range of $4.7 - 7.6\,\mathrm{nm}$ and a crystallite size of $8\,\mathrm{nm}$. They have observed that for potentials below $-0.7\,\mathrm{V}$ a strong H_2 evolution takes place at the WE, a fact that prevents the platinum deposition [48]. This influences also the deposition efficiency, which in this case amounted $85 - 97\,\%$ for acid solutions and $40 - 55\,\%$ for alkaline solutions.

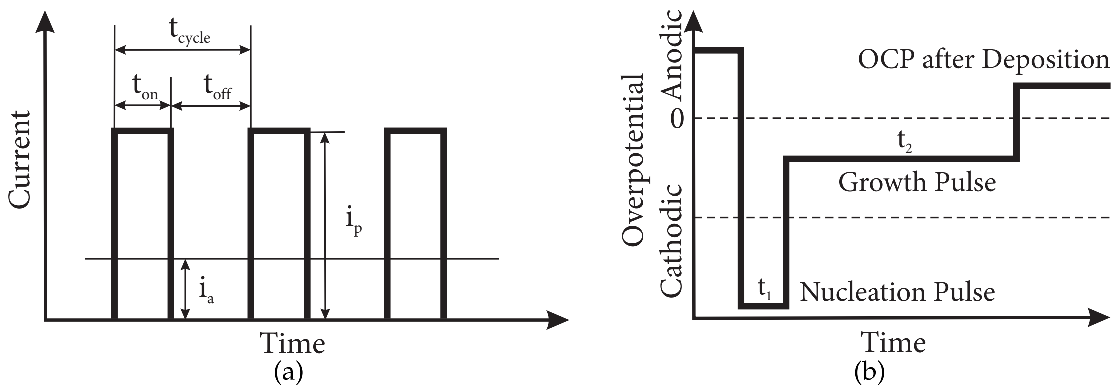

Figure 22: (a) A general concept of the pulse-current technique and (b) the double pulse sequence used to create and grow the catalyst particles.

For a better particle morphology control, Choi et al. have proposed a pulsed galvanostatic deposition method. In comparison to the direct current (DC) electrodeposition this method has many advantages such as stronger adhesion, uniform deposition, selectivity of hydrogen, reduction of internal stress, etc. . Moreover, it offers three variables that can be changed during the deposition, namely, t_{on} (on-time), t_{off} (off-time) and i_p (peak current) (Figure 22a). Here i_a represents the average current density and is equal to i_{DC}, because it determines the surface concentration of deposited metal ions [106]. In their case the best parameters were $10\,\mathrm{mA\,cm^{-2}}$ to $50\,\mathrm{mA\,cm^{-2}}$ for the current density and on, off-time, of $10\,\mathrm{ms}$ and $100\,\mathrm{ms}$, respectively. As result, the electrochemical active surface area (ECSA) of prepared catalyst was $25\,\%$ better than the DC deposited one [106]. Instead to use current pulses, Ueda et al. have prepared metallic nanoparticles by using a potentiostatic double pulse technique. This method is based on an extremely short nucleation pulse of high cathodic polarization followed by a much longer growth pulse at low cathodic overvoltage [135]. The first pulse, more negative than the potential where the reduction occurs, is used to initiate the nuclei formation. The second pulse, positively but more negatively than the reversible potential, is used to control the nuclei formed during the previous pulse and to handle the particle size.

All presented techniques were applied on small electrode surfaces and mostly the glassy carbon was employed as support. To adopt the electrochemical deposition technique in FC application it is necessary to increase the electrode surface and to assure an homogeneous particle distribution over the entire CL. Apart from that, many electrochemical processes need to be considered and engineering challenges must be countered.

5.2 POTENTIOSTATIC ELECTRODEPOSITION

It is know that when conventional methods are used to produce the CL, multiple inactive sites are present [106]. This is induced in most of the cases due to the poor contact between the ionomer and the electrocatalyst or catalyst and the reactant phase. In an ideal case, the catalyst has a permanent contact with the protons, the electron conductors and reactants at the so-called triple phase boundary (TPB). In practice, using traditional preparation methods, part of the catalyst is embedded in the polymer and the reactant cannot reach it any more. Another common problem is the MPL local flooding, a fact that reduces the FC performance.

In order to avoid these problems, Mitzel et al. [90] have demonstrated the principle of creating catalyst particles at the TPB using as template a self prepared GDL. They have deposited platinum nanoparticles directly on the MPL surface by applying a current/potential profile. The prepared samples exhibit a surface of $50\,\mathrm{cm}^2$ and a platinum loading of $0.4\,\mathrm{mg\,cm^{-2}}$. The FC tests have revealed that the use of a potentiostatic method improves the FC performance, in comparison to the galvanostatic deposition [136].
For a precisely in-situ catalyst layer construction, the same technique is adopted in the present work. The electrodeposition assembly contains a well know structure from the PEMFC, where the electrodes are pressed together with a membrane to form the MEA. In analogy with a PEMFC, here the MEA is replaced by an half-MEA, containing one GDE, at the anode side and a membrane. In the actual work the prepared half-MEA contains a Nafion™ 115 membrane from E.I. du Pont de Nemours and Company (Wilmington, USA) which is pressed at 125 °C for 6 min with a commercial GDE from Johnson Matthey (London, United Kingdom) ELE062 ($0.4\,\mathrm{mg\,cm^{-2}}$). The so-prepared MEA is then mounted in the electrodeposition cell, so that the commercial GDE acts as an reference and counter electrode. The setup ends by adding at the cathode the GDL, which integrates the precursor. This annexation method facilitates an easy GDE extraction after the electrodeposition process. During the deposition, the produced electrons at the reference electrode goes through the external circuit to the cathode where the precursor reduction occur. Simultaneously, the created protons pass through the electrolyte to the WE and are consumed in the reaction. Thus the counter electrode remain as a hydrogen depolarized anode (HDA). The supplementary reaction products from the cathode are evacuated with an inert gas (Figure 23).
Along to the desired reduction reaction, at the cathode the hydrogen protons can be reduced to H_2, so that the chemical reduction of the precursor occurs. In order

to avoid these disadvantageous reaction, the WE potential needs to remain positive. According to the $PtCl_6^{2-}$ reduction reaction, a potential higher that $+0.744\,V$ is required to reduce the platinum ions to platinum (Equation 20).

$$\begin{array}{lll} RE + CE: & H_2(g) \rightarrow 2H^+ + 2e^- & E^\circ = 0\,V \\ WE: & PtCl_6^{2-} + 2e^- \rightarrow PtCl_4^{2-} + 2Cl^- & E^\circ = +0.726\,V \\ & PtCl_4^{2-} + 2e^- \rightarrow Pt + 4Cl^- & E^\circ = +0.758\,V \end{array} \tag{20}$$

where E° is the standard potential.
However, when the potential exceed $1.23\,V$ the water oxidation emerge as a secondary reaction. At this point, due to high water oxidation overpotential in comparison to the H_2 evolution reaction, it is absolutely impossible to avoid the hydrogen evolution at the working electrode. Therefore, to reduce the risks of hydrogen evolution the potential should not exceed $1\,V$.
According to the setup scheme presented in Figure 23, the protons needs to cross through the membrane. Therefore, to enhance their mobility the electrolyte humidity is increased by humidifying the reference gas (H_2). In the same time, the ohmic losses due to the membrane are minimized. So, the hydrogen is purged with a constant flow rate of $150\,ml\,min^{-1}$. It should be considered that for a minimum membrane swelling and a good proton conductivity, the RH should not exceed 90 % [137]. In addition, at this humidity the mechanical properties of the membrane are improved [138]. To be sure that the electrolyte is completely humidified, prior to the electrodeposition process, the cell is purged for at least 5 h with the humidified gas.
For all samples presented in the actual work, hexachloroplatinic acid purchased from Umicore AG & Co. KG (Hanau, Germany) (Umicore) is used. The precursor reduction at the working electrode is accomplished by applying a double pulse profile (Figure 22b). First one creates small platinum nuclei, by gathering few $PtCl_6^{2-}$ at the carbon surface. In the same time the Cl^- ions together with the protons from the anode react to HCl. During the second pulse, additional $PtCl_6^{2-}$ are attached to the constituted nuclei and nanoparticles are created. Depending on the growing time the particles size can be controlled. It is essential during these two steps to remove the HCl due to its poisoning effect [101].
The imposed pulses are controlled by a VMP3 potentiostat connected to a $10\,A$ booster, manufactured by Bio-Logic SAS (Claix, France) (Bio − Logic). Therefore, for the nucleation pulse a potential of $-1000\,mV$ vs. HDA is hold for $1\,ms$ followed by a growth pulse of $100\,ms$ at a potential of $50\,mV$ vs. HDA. The entire process is repeated until the current through the cell remains constant, according to the cell resistance. In order to remove the reaction products (HCl) a constant nitrogen gas flow ($500\,ml\,min^{-1}$) is applied at the working electrode side (Figure 23). After the electrodeposition process, the not reduced $PtCl_6^{2-}$ are washed with distilled water. So, a large platinum amount can be collected and reused for future GDE preparation. The electrodeposition procedure ends with a drying process at $80\,°C$ for $20\,min$.

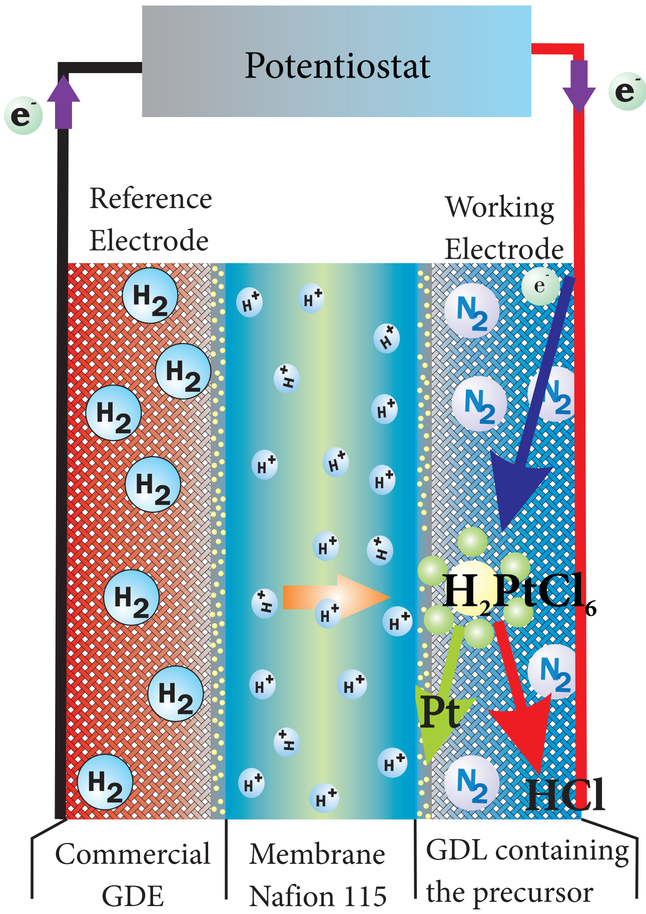

Figure 23: Electrodeposition principle with a hydrogen reference electrode

5.3 DEPOSITION CELL CONSTRUCTION

Although the electrodeposition seems to work on a classical PEMFC housing, some details related to the cell construction should be regarded. In the PhD thesis of Dr. Mitzel [136] a very simple electrodeposition setup is introduced. It contains a typical PEMFC housing with an active electrode area of $50\,\text{cm}^2$, connected to a bubble humidifier. This system presents some disadvantages, for example in the case that GDLs with different thicknesses are used. In addition, due to the adopted sealing system, the GDE thickness should be fixed. A change of this configuration can cause an inappropriate contact between the GDE and the electrolyte. Moreover, the cell is not any more tight. Therefore, a larger force need to be applied, which can cause the GDE support destruction. Commonly, the GDL penetrates in the flow field channels and thus cannot be used any more as GDE for further applications. Another important disadvantage is the membrane swelling that appears at high humidity and makes the electrolyte utilization for further electrodepositions process almost impossible. It should be noted that in the setup proposed by Dr. Mitzel, the electrolyte is humidified at room temperature and a precise RH control cannot be achieved.

Using the variety of mechanical processing features located in the university workshop, a new cell is developed. Before production all cell components are simulated on a computer-aided design program. Thus, a new cell with an electrode surface of 50 cm^2 as in Figure 24a is constructed. It contains a graphite flow field as reference electrode similar to the old setup. Compared to the previous design the top side is replaced by a graphite felt and a cooper plate. This assembly presses uniform the working electrode on the electrolyte surface independent from the GDE thickness. Due to the graphite felt compressibility, an uniform force distribution is assured. Furthermore, it ensures the electron conduction and is porous enough for an efficient product removal. This arrangement is similar to a vanadium/air redox flow battery system [139]. In the actual configuration instead of air and vanadium we are using hydrogen and nitrogen.

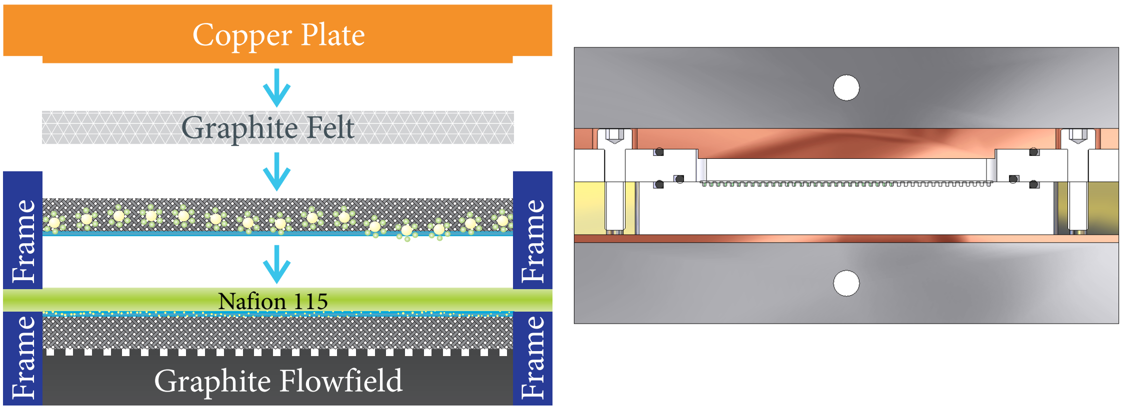

(a) (b)

Figure 24: (a) Electrodeposition cell with graphite felt as force 'buffer' and (b) schematic cross section of the entire deposition cell.

Another progress on the cell development is represented by the frame construction, which stretches the membrane and avoids its swelling. The frame provides an ideal membrane stability by holding it straight even at high humidities. Moreover, the frame enables the membrane utilisation for many deposition processes (Figure 24a, 24b) while assuring cell tightness. Also, due to the fixed frame height, the applied screw force is not important any more, the cell is tight by applying few N m. This is considered as an advantage when untrained people use the deposition cell or when no torque key is available.

Considering the above specified improvements on the electrodeposition cell and examining the application of the deposition method for bigger GDE, a new cell with a size of 225 cm^2 is constructed (Figure 25). This cell is not only bigger than the precedent cell, it is constructed from different materials and contains a better design.

Instead to use a graphite plate as flow field and a current collector for electrical connection, both functions are transferred in the end plate. For typical PEMFC housings, the end plates are made from aluminium, but due to its weak mechanical properties and fast oxidation, it is replaced by a stainless steal plate. Also the flow field pattern are modified. The flow field design contains parallel channels with a width of 1 mm, which connect the hydrogen input and output (Figure 26). Along that, it distributes the humidified gas on the GDL, assuring a good electrical contact and heat transfer.

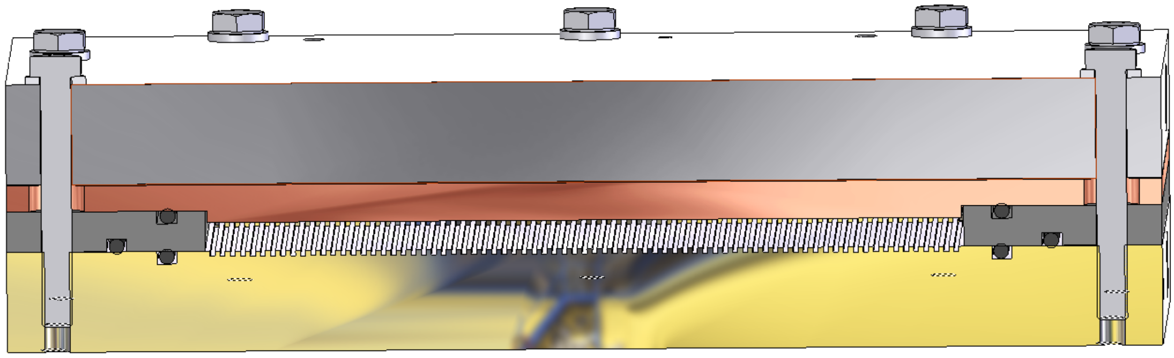

Figure 25: Structure of the up-scaled electrodeposition cell with an area of 225 cm^2. On the bottom side it contain a stainless steel flow field with parallel channels.

A disadvantage of the constructed cell is its weight, which in this case is over 10 kg. It must be specified that the top end plate is made from aluminium and not from stainless steal. Due to the high surface and the hard drill in stainless steal, unfortunately a heating cartridge cannot be used. Thus, two silicone heaters with a size of 150 x 200 mm are purchased from RS Components GmbH (Mörfelden-Walldorf, Germany) (RS) and bounded on the end plates. The cell temperature is controlled by two PID controllers purchased from Invensys Eurotherm (Ashburn, USA) (Eurotherm).

5.4 ELECTRODEPOSITION SETUP

The electrodeposition setup contains apart the cell and the potentiostat, systems for gas flow control, gas humidification and temperature management. Therefore, two mass flow controllers purchased from Bronkhorst High-Tech B.V. (AK Ruurlo, Netherlands) (Bronkhorst) are used for hydrogen and nitrogen. Each one has a maximum flow rate of 2000 ml min^{-1} and can be remotely controlled. Furthermore, a gas humidifier from Perma Pure, containing a single Nafion™ tube is used. A complete description of the working mode is presented in section 4.3.3. In the actual setup a thermostat produced by Neslab Instruments Inc. (New Hampshire, USA) (Neslab) is used to control the DP. The electrodeposition cell temperature is managed by two heating cartridges produced by Horst GmbH (Lorsch, Germany) (Horst) plugged on a PID controller manufactured by Jumo GmbH & Co. KG (Fulda, Germany) (Jumo). Figure 27 shows the developed electrodeposition setup.

5.5 FABRICATION METHODS FOR THE PRECURSOR-IONOMER LAYER

Before the platinum electrodeposition is performed with the method described in Section 5.2, the GDL needs to contain already the catalyst precursor and the ionomer, required to conduct the protons. One of the simplest methods to introduce both ingredients in the MPL is to dip the GDE in a solution which contains the necessary components. Due to the small GDE thickness ($200-300\,\mu m$) and the desired CL height $\leqslant 10\,\mu m$, the liquid level should not exceed $10-20\,\mu m$. In the case that the bath level surpasses these limits, the electrochemical reduction of the precursor

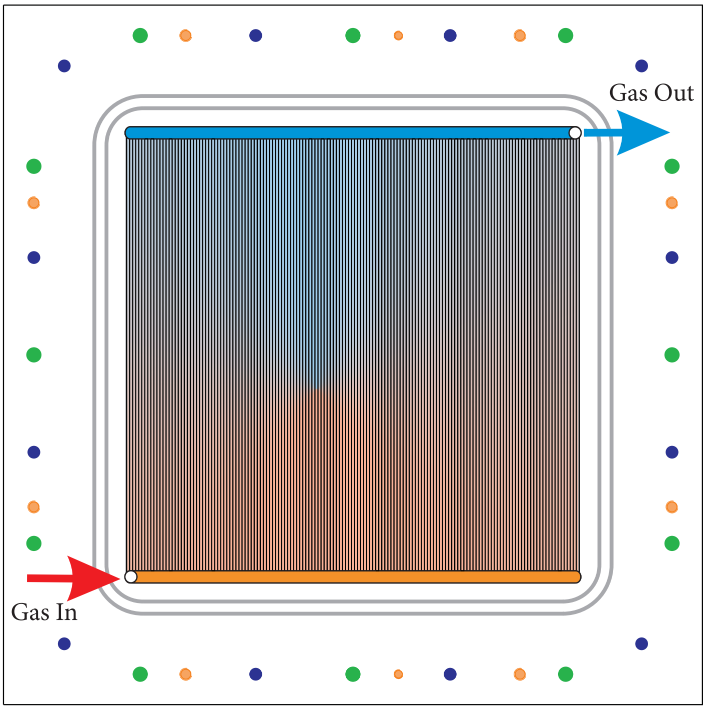

Figure 26: The flow field and the end-plate of an 225 cm^2 deposition cell. For an optimum humidity and gas flow, the flow field contains parallel channels.

cannot be realised. Finally, the not reduced metal ions and the formed hydrochloric acid are removed by washing the GDE in a water bath.

Both Mitzel and Arena have described in their PhD thesis a simple impregnation process [140, 136]. An hexachloroplatinic acid dispersed in IPA is poured in a Teflon form with a size of 50 cm^2. The GDL is introduced over the prepared solution, so that the MPL is impregnated (Figure 28a). In order to obtain an anhydrous precursor, a vacuum pump is used to extract the solvent. Both authors have used self-prepared GDL with a low hydrophobic grade. For commercial electrodes which are high hydrophobic, the precursor/ionomer mixture cannot penetrate deep enough in the MPL. So, during this process most of the ionomer sticks on the GDE surface and on the Teflon form. Thus, during the GDE extraction, large MPL parts remains attached on the Teflon form, making the GDE usage for further applications almost impossible. This problem is related to the ionomer quantity used for impregnation and the electrode properties (porosity and hydrophobicity). Also, due to the low bath level, the ionomer distribution over the GDE surface causes a different local loading, even when the form is balanced.

Other procedures used to apply diverse dispersions over the GDL or to create the MPL are the spraying and the brushing method. These are the most widely used methods in the laboratory scale since these do not require sophisticated apparatus and procedures [67]. In the present work, an airbrush BD − 142 with a 0.2 mm nozzle purchased from Conrad Electronic SE (Hirschau, Germany) (Conrad), is used to spray a precursor-Nafion™ solution, dispersed in 2 ml IPA. In order to evaporate the solvent and to avoid the precursor blowing, the GDL is heated at 80 °C. Theoretically, by controlling the distance to the substrate and the hot plate temperature, different CL thicknesses can be achieved (Figure 28b). However, in practice due to

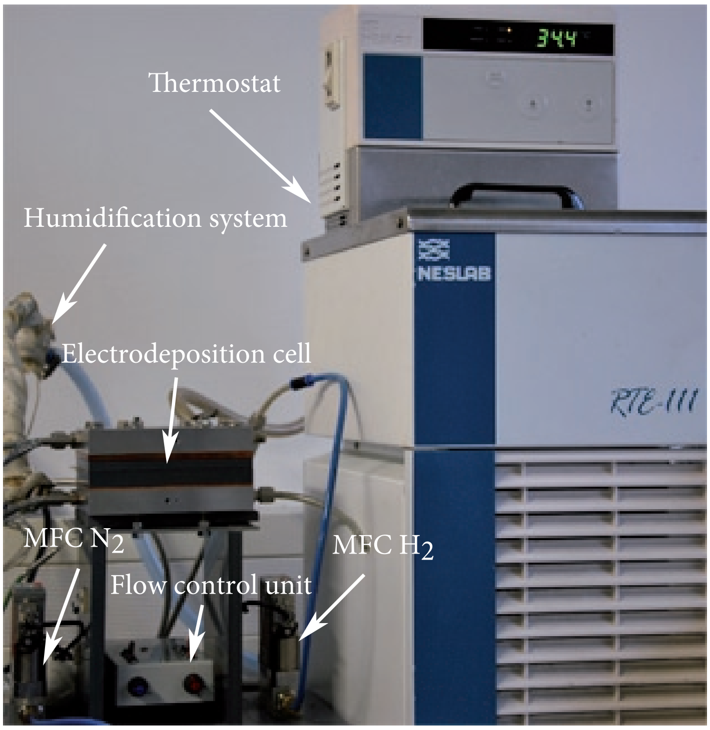

Figure 27: Electrodeposition setup consisting of the cell, two MFCs and the humidification system. Below the deposition cell the flow control unit used to manage the gas flow rates can be seen.

the hand movement, it is very difficult to maintain a constant distance between the nozzle and the GDE. Furthermore, after few spraying layers it is delicate to see an optical difference on the electrode surface. So different catalyst and ionomer loadings are obtained along the GDL surface. According to the achieved results, we have decided to improve this technique, by precise distance and moving speed control.

5.6 DEVELOPMENT OF THE AUTOMATIC SPRAYING DEVICE

In the last years, the amount of innovations observed on the 3D printing industry has outdone all the innovations within the industry in the prior 20 years [141]. As the price started to decrease, thousands of people were driven to the technology and tried to apply it on different fields.

The first step on 3D printing is the modelling and the simulation of the desired piece. Then, a special software slices the piece in different layers and computes the necessary coordinates for the moving pattern. A microprocessor processes the commands and sends electrical signals to the stepper motors, which assure the XYZ move. Apart the moving controller, in a 3D printer the printing head allows the material dosing, necessary for a printing step. Typically, the material is a thermoplastic polymer which melts directly before printing. Some 3D printer manufacturers are designing their printer for compatibility with other function heads such as milling or laser cutting.

In order to apply the 3D printing technology on the FCs electrodes production some modifications are required:

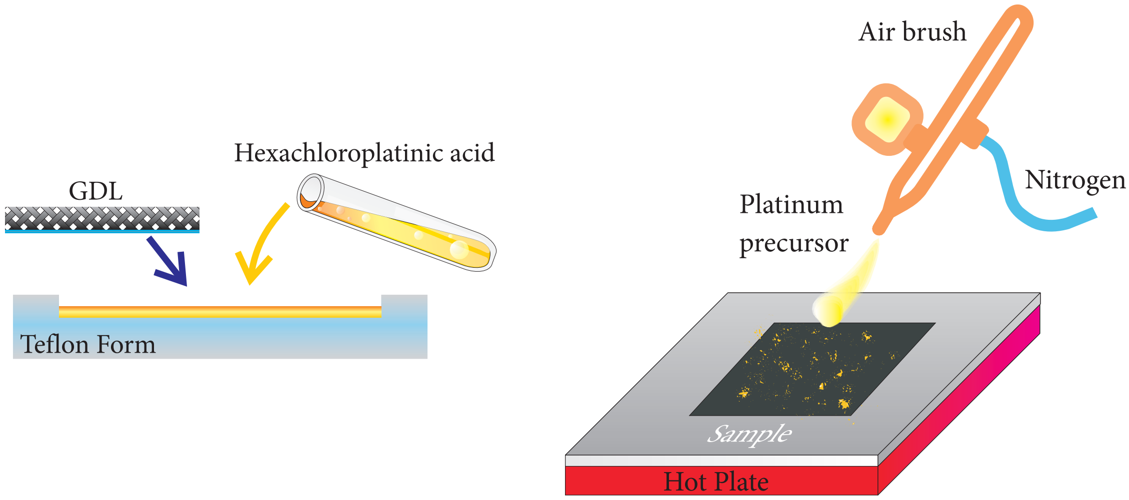

(a) (b)

Figure 28: (a) Schematic representation of the impregnation process for a GDL and a platinum precursor (b) manual spraying method used to attain the precursor on the MPL surface.

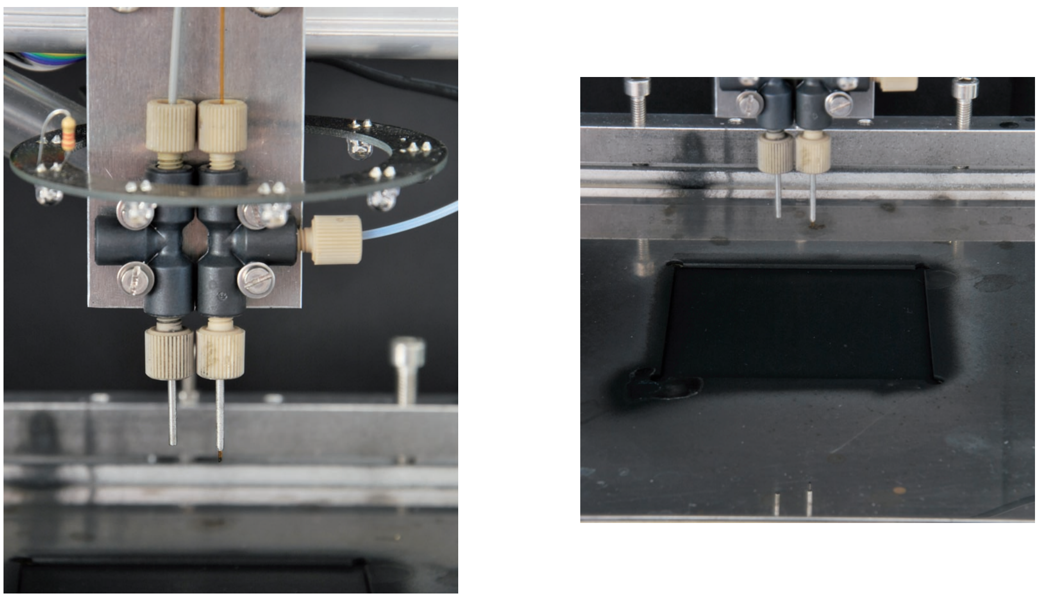

(a) (b)

Figure 29: (a) Airbrush system mounted on the 3D printer containing two spray heads and (b) the GDE fixing system used to mask a part of it and to assure a good contact with the hot plate.

- the printing head needs to be replaced by a spray or brushing device. This must assure a highly precise and controllable liquid flow rate. In addition, the extra peripheral needs to provide a high corrosion resistance against the chlorine.
- the heat plate must be replaced by a more powerful, which is able to hold the temperature constant even at high moving speed or high gas flows.

In the actual work, the necessary modifications are applied to a Velleman nv (Gavere, Belgien) (Velleman) K8200 printer, purchased from Conrad.

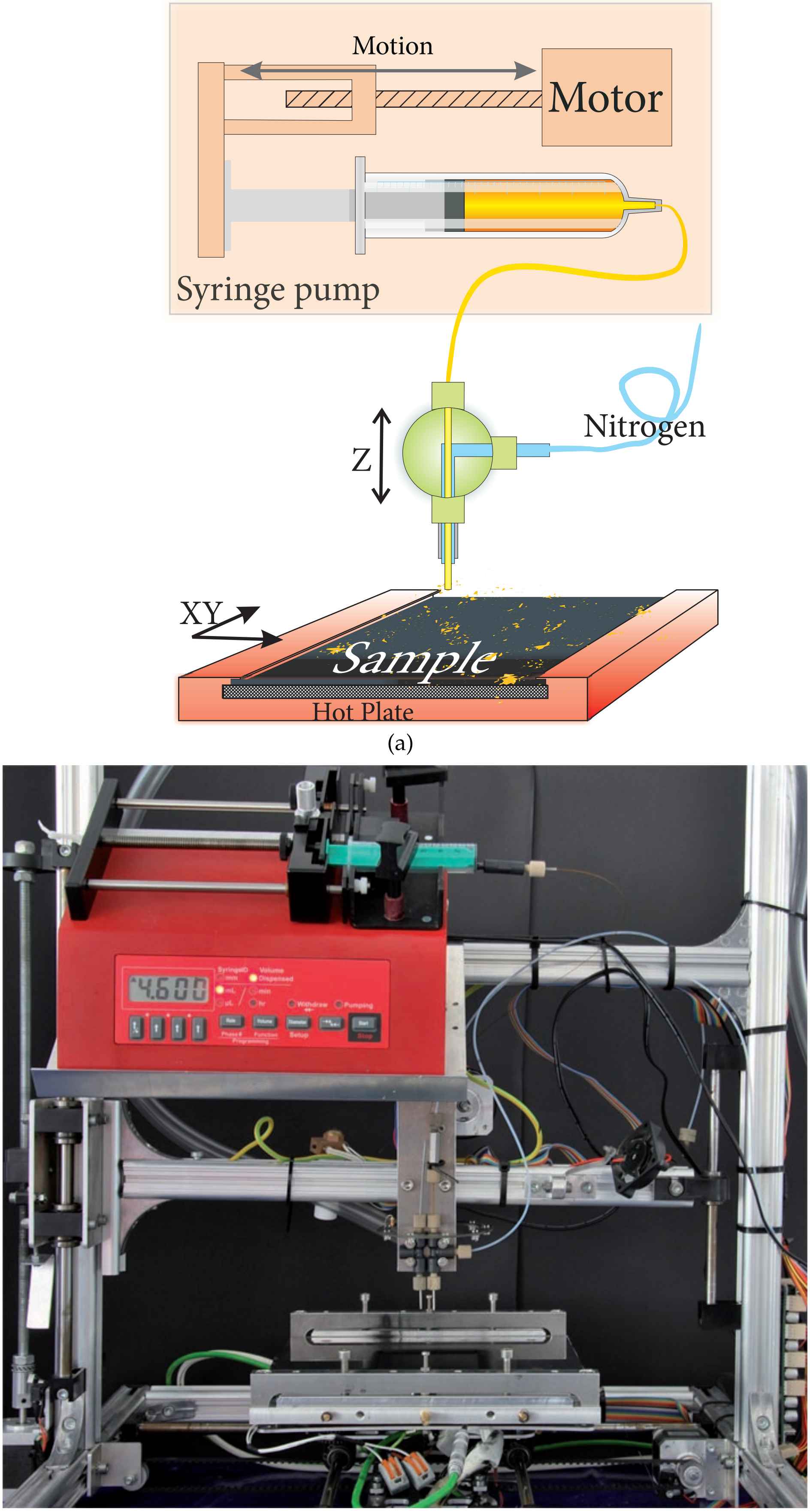

(a)

(b)

Figure 30: (a) Principle of the modified 3D printer, containing the syringe pump and the heating plate; (b) Photography of the developed spray device. During the printing processes, the nozzle is shifted in the Z axis direction and the sample performs a movement in the XY plane.

A self-made spraying system, containing a silica capillary with an inner diameter of 200 µm is connected with a gas pipe to a T union piece. In this way, the gas and the liquid phase are isolated one of each other (Figure 29a). When a fluid reaches the capillary output, it is directly separated by the gas flow in droplets. The created liquid droplets reaches the MPL surface and creates a homogeneous layer. Due to the plate temperature($\geqslant 80\,°C$), the solvent evaporates. So the ionomer together with the precursor remains bounded in the MPL structure. As shows in Figure 29a the developed system contains two spraying heads. This feature makes the use of capillaries with different diameters and higher pump rates possible. Apart from that, this configuration is quite useful in the case that big GDL surfaces need to be sprayed.

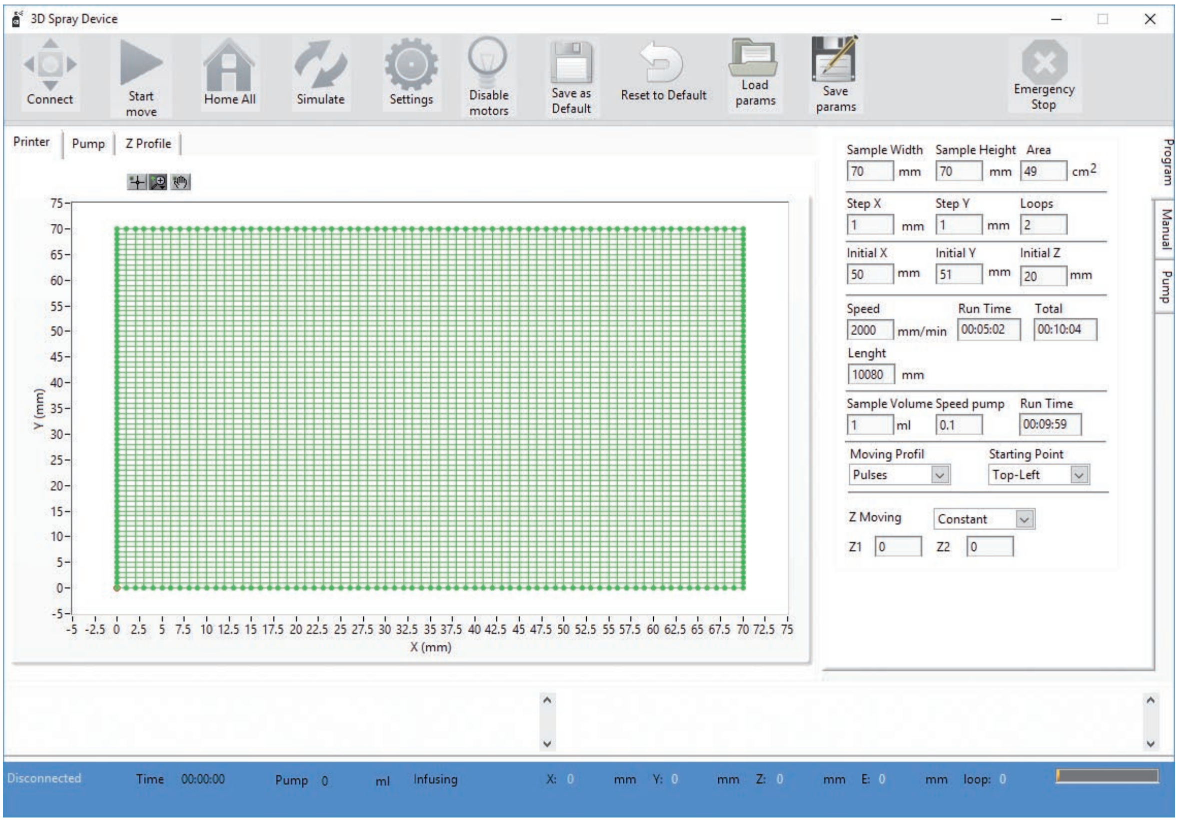

Figure 31: GUI of the 3D printer control software developed on LabVIEW. Here the user can visualize and modify the moving parameters. Along that, the user can control the pump volume, syringe diameter and many other useful parameters.

In order to assure an uniform temperature distribution over the entire GDE surface, a good contact with the hot plate is required. Therefore, a stainless steel mask with a frame size of 70x70 mm is constructed (Figure 29b). In this way $\sim$ 1 mm from the sample is used for fixing, a fact that should be considered on MEA manufacturing. Another parameter which affects the spraying quality is the liquid flow rate. For high liquid rates, the gas cannot split the solution perfectly into droplets. Thus, this leads to the formation of big flakes on the MPL surface. For a precise control a syringe pump produced by Landgraf Laborsysteme HLL GmbH (Langenhagen, Germany) (Landgraf) is used. It can manage two syringes in the same time, at a very low pump rates (few $\mu\,min^{-1}$). A complete view of the assembly is represented in Figure 30. Due to the capillary length ($\geqslant 30\,cm$) a small volume ($\sim 50\,\mu l$) remains in the silica capillary and is considered as dead volume. So, to obtain a well defined catalyst loading for each spraying process, an additional quantity of precursor needs to be added.

Apart from the hardware components, a new GUI is developed, which controls the sample movements and the pump flow rates (Figure 31). For a systematic MPL coating, the printer movements are firstly simulated on the self-developed LV software and then transferred via the serial port to the 3D printer controller. Before the spray procedure begins, the user can modify parameters such as the sample size, moving speed or the moving profile type. The program calculates automatically the moving path according to the inserted parameters. On a XY graph, situated in the middle of the screen, the entire moving points are plotted. The same software incorporates the syringe pump control. This one allows the user to adjust the volume and pump speed. Furthermore, the developed software contains an algorithm which is able to compute the time required to pump a known amount of solution (Figure 31). In order to synchronize both systems, the user can modify the moving speed or the loop number. In addition to the automatic mode, the developed software offers a manual mode, where the user can insert the move position for each axis. Apart from a precise movement control and multiple move profiles, the developed software offers the possibility to save the entire parameters to an external data file. This option is very useful when the user uses samples with different sizes.

5.7 SUMMARY

The theoretical and experimental details of an electrochemical deposition method are presented. The described technique is used to produce the electrocatalyst for PEMFC electrodes. One advantage of this technique is the accurate electrocatalyst positioning, at the triple phase boundary. In addition, due to the rigorous electrodeposition profile the morphology of the created electrocatalyst can be precisely controlled. In detail, during the first step a negative potential for few ms is applied. This induces the precursor ions reduction and the formation of small nuclei. In the next phase, a growing pulse lets the already created nuclei grow. According to the growth time, the cores grow by collecting more precursor ions, until a nanoparticle is created. To obtain a high active catalyst, hexachloroplatinic acid is used as precursor.

An extra attention has been given to the electrodeposition cell design. In comparison to a PEMFC housing, this one contains an improved sealing and membrane stretching system. It provides a better contact between the GDL and the electrolyte. Moreover, new facilities as accurate temperature and relative humidity control are implemented.

The developed cell can be used not only for platinum electrodeposition, but also for other metals precursors in an anhydrous form. In addition, the cell cathodic side is reshaped, so that the sample is uniformly pressed on the electrolyte. A big advantage of the new compression system is the possibility to use the same electrodeposition cell to deposit metals on GDLs with distinct thicknesses. As result of the significantly improved FC performances, the deposition cell is extended from

50 cm^2 to 225 cm^2. On the big cell, for a better gas and humidity distribution the anodic flow field is combined with the end plate. Along to the new flow field design, a frame is developed to keep the membrane straight on the electrodeposition cell. This makes the use of the electrolyte over many electrodeposition processes possible. Additionally, this feature makes possible the further cell up-scaling. The only limitation is represented by the membrane durability.

Before the electrodeposition process, the GDL should contain the precursor in an anhydrous state. Therefore, two different methods to apply the ionomer and the precursor on the GDL surface are tested: impregnation and spraying. It was found that due to the small GDL thickness, the necessary volume for impregnation is limited to few μl, affecting the precursor distribution on the MPL structure. The other tested technique can be utilized for large surfaces and bulk production. The spraying method is suitable to achieve thin CL thickness by holding a constant temperature and distance to the substrate.

For a precise control and high reproducibility an airbrush system is developed and attached to a 3D printer. For a accurate spray control, the liquid flow rate is managed by a syringe pump. A further improvement on the constructed device is the heat plate replacement. So, a constant temperature can be held during the spraying process, even at high gas flows. Using the developed system, samples with an area up to 400 cm^2 can be sprayed in a semi-automatic way. Along that, the system can spray different solution without corrosion risks.

To enhance the printer utilisation a new controlling software is developed. Thus, multiple moving profiles can be simulated and implemented. Moreover, the software controls the syringe pump parameters. So, both devices can be perfectly synchronised.

6 EVALUATION OF PREPARATION PARAMETERS FOR PEMFC ANODES

The main tasks of the MPL in a PEMFC electrode are to support the electrocatalyst and to manage the water and the heat produced during the PEMFC operation. In addition, the MPL should be porous enough to minimize the reactant barriers, expand the electrochemical surface area per unit of electrocatalyst mass and not at least, to dissipate the heat efficiently. According to Chen and Hwang, the number of catalyst active sites is linked to the employed MPL preparation method [73, 67]. During the last years some papers have revealed that the MPL composition influence the FC performance [142, 65].
Typically, a MPL architecture contains carbon black particles which are held together and bounded to the GDL surface with Teflon. In practice, it is very challenging to find an optimum balance between these two components and to create an electrode with a good electrical and thermal conductivity [143, 64]. However, an optimum Teflon loading, makes not only the FC operation at high RH possible, but in the same time it reduces the MPL porosity [66]. Especially at the cathode, where in addition to the gas paths, sufficient passages are necessary to remove the produced water. One frequently used method in practice is the application of different carbon black species, with distinct sizes and shapes. This technique improves not only the MPL porosity, but enhances the electrical conductivity of the created layer [47, 144]. Another technique approached by other authors is the implementation of so-called pore forming agents [145, 146, 147]. Commonly, they are carbonates compounds as $Na_2CO_3, (NH_4)_2CO_3, NH_4HCO_3$ [148, 149, 150], glycerol [68] and sulfate as $(NH_4)_2SO_4$ [151]. This chemicals are integrated in the prepared ink and transferred to the GDL surface through various methods.

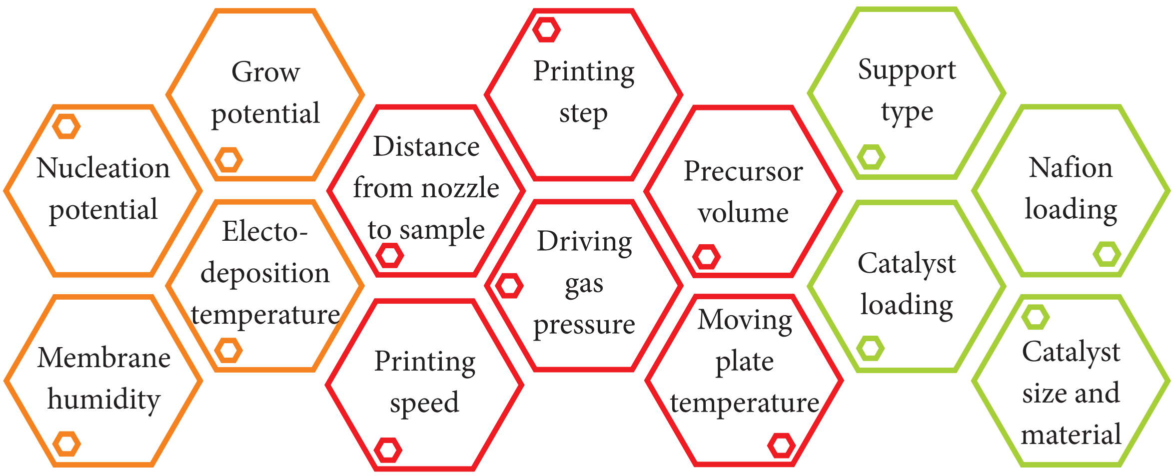

Figure 32: Diagram containing the parameters with a dominant impact on the CL proprieties. It is splitted in three regions, specific for each preparation step: electrodeposition, spraying and materials.

Producers such as Freudenberg FCCT KG (Weinheim, Germany) (Freudenberg) or Carbon SE (Wiesbaden, Germany) (SGL) are fabricating GDLs since many years with various proprieties. They have developed multiple versions of this GDLs and catalogued them for specific applications conform to the working temperature (e. g. GDL for FC operating at low or high temperatures). Apart from the high electrical conductivity, this GDLs offer an improved hydrophobicity. El-Kharouf already studied the physical proprieties of most available commercial GDL during his PhD. His studies revealed that the GDL properties affect significantly the MEA mass transport properties [65]. In addition, he showed that an increase of the Teflon loading in the GDL decreases the porosity and the conductivity. In the same time it increases the tortuosity, the permeability and the hydrophobicity. Without Teflon, even the best electrocatalyst and the catalyst support can be deactivated, especially at the cathode, where flooding can occur [152, 153]. The Teflon introduction in the MPL structure facilitates no only the removal of the product waste from the GDL, but also hinders the water based noble metal precursor to penetrate deeply in the GDL architecture. Even if the above specified barrier is crossed, a multitude of parameters need to be considered for a full working GDE. As we specified in Chapter 5.5, to include the catalyst precursor in a commercial GDL in order to obtain the best results, a spray technique should be selected. In addition, a multitude of physical parameters affecting the electrocatalyst distribution and morphology exist. In order to obtain a high valuable GDE, a systematic evaluation of each parameter is necessary. Figure 32 suggests few criteria that should be considered.

In the following sections the influence of each parameter is briefly discussed. The spraying process optimization is executed using the modified 3D printer (see Section 5.6). The prepared GDEs are examined as anode on a PEMFC. Nafion^{TM} 212 is adopted as electrolyte and as cathode a GDE from JM with a platinum loading of $0.4\,\mathrm{mg\,cm^{-2}}$ is applied. The FC evaluation is carried out at 80 °C, at 95 % RH and ambient pressure.

6.1 UTILIZATION OF COMMERCIAL GDL AS CATALYST SUPPORT

On the electrodeposition process, the possibility exists to use commercial coated GDL with different grades of hydrophobicity. Thanks to the close collaboration with the FEM on ISCED project (see Chapter 1) multiple GDL types are exchanged and proposed to be an ideal candidate for the in-situ electrochemical deposition. After some test we have concluded that the H23C8 produced by Freudenberg can be the searched catalyst support. It demonstrates a high hydrophobicity level, is ideal for automotive application and presents a very smooth MPL surface (Figure 33) [154]. The present investigations, using this GDL, are concentrated on the precursor impregnation. Therefore the H23C8 is impregnated in $2\,\mathrm{ml}$ IPA solution containing a platinum precursor and the ionomer. The chosen catalyst and ionomer quantity are equivalent to a loading of $0.4\,\mathrm{mg\,cm^{-2}}$, respectively $0.2\,\mathrm{mg\,cm^{-2}}$. The preliminary measurements as anode show a poor performance with a current density of $0.26\,\mathrm{A\,cm^{-2}}$ at $650\,\mathrm{mV}$ (Figure 36). A subsequent TEM measurement indicates that the particles exhibit a size of $19 \pm 6\,\mathrm{nm}$ (Figure 35a). This excessive particle size can be attributed to an agglomeration effect, due to the poor ionomer penetration.

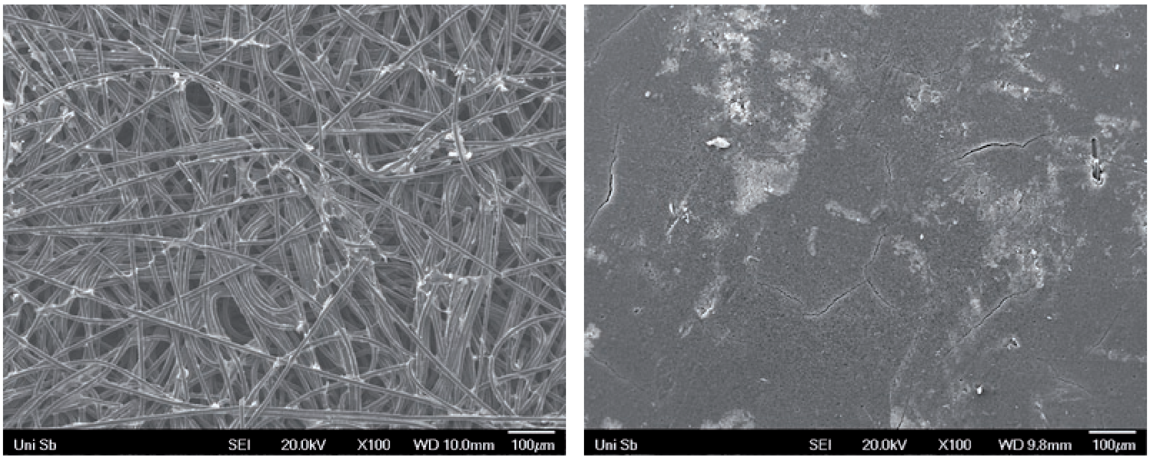

(a) (b)

Figure 33: SEM images of Freudenberg H23C8. (a) the bottom side of H23C8 with a "spaghetti" structure and a high porosity. The carbon fibres present a light carbon coating as result of preparation method. (b) the MPL structure shows a well defined surface with few cracks caused by handling method. The white points represent the Teflon sites.

Therefore, during the electrodeposition process the platinum ions agglomerate at the GDE surface. In order to verify if this GDL prevents the creation of well dispersed particles with a smaller diameter, the H23C8 is coated with a mixture of carbon particles (Ensaco 350 G purchased from Timcal Graphite & Carbon Ltd. (Bodio, Switzerland) (Timcal)), Teflon (E.I. du Pont de Nemours and Company (Wilmington, USA) (DuPont)) and ionomer (Nafion™D2021 from DuPont). Prior to the coating, all components are mixed for 45 min. To obtain a homogeneous ink, the components are mixed by applying simultaneously two different blend techniques:

1. mechanical homogenizer from IKA Werke GmbH & Co. KG (Staufen, Germany), model T25 with a power of 500 W. Its head, which contains a rotating knife is centered, so that its reach the bottom of the vessel. Due to its high rotation speed (over 18000 rotations per minute), the agglomerates are separated and an homogenized ink is obtained.
2. ultrasound bath from Badelin electronic GmbH & Co. KG (Berlin, Germany) with a power of 480 W sustains the mechanical blender (Figure 34a). It use ultrasound waves to agitate the suspension. In this way the uniformity and stability of the prepared solution are improved.

The processed ink is transferred to the commercial GDL by using a doctor blade. The substrate, is fixed on the glass plate of a Coatmaster 509C (Erichsen GmbH & Co. KG (Hemer, Germany)) (Figure 34b). The coating is performed with a spiral blade (220 mm width and 200 μm wet layer thickness) at a constant speed of $5\,\mathrm{mm\,s^{-1}}$. Subsequent to the coating process, the solvent and the residuals need to be removed from the MPL structure. An improper drying process affects the proprieties of the created MPL and thus the catalyst coating process. Therefore, for a complete residual removal the GDE is dried for 1 h hour at room temperature and then for 12 h at 80 °C. Figure 35b displays the catalyst particles which decorate the Ensaco 350 G carbon particles. The nanoparticles diameter analysis reveals a value of 4 ± 0.6 nm.

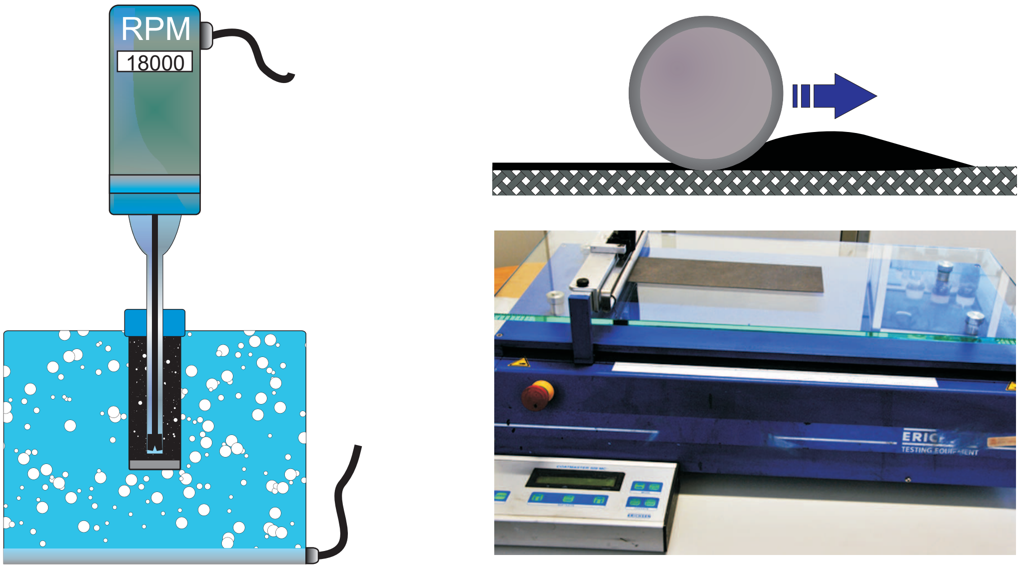

(a) (b)

Figure 34: (a) Ink mixing process using an ultrasound bath and a mechanical blender and (b) doctor blade technique used to create an uniform layer on the GDL surface.

By coating the H23C8, named further H23C8 c + i, a significant improvement is observed on the PEMFC performance. The additional layer improves the GDE performances with over 65 % at a working voltage of 650 mV. In addition, due to the efficient hydrophobic layer, at high current densities ($\geqslant 1\,\mathrm{A\,cm^{-2}}$) no mass transport limitations are observed.

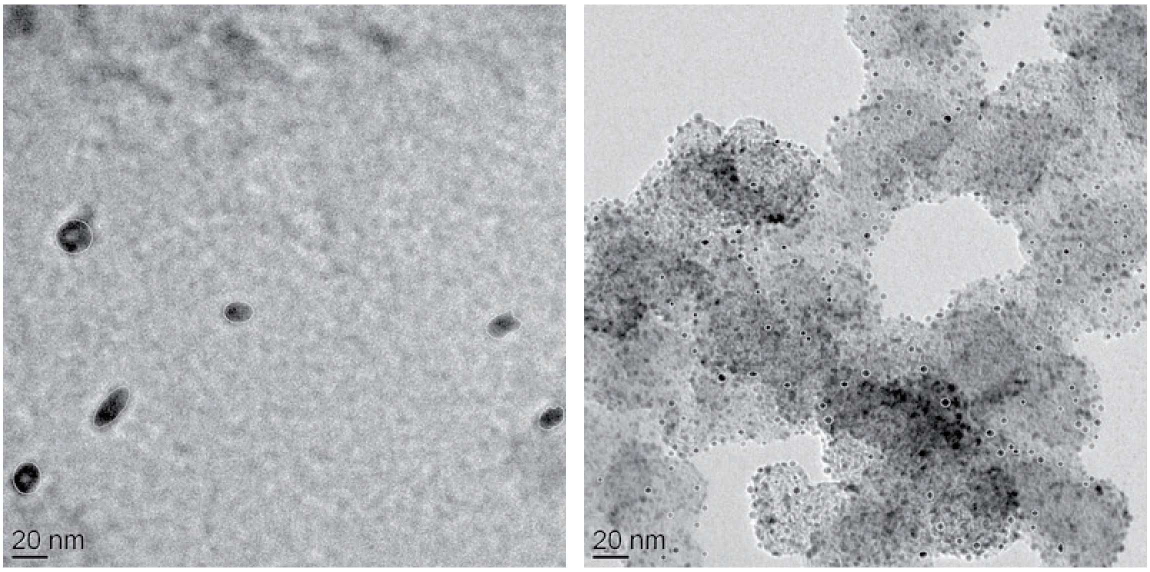

(a) (b)

Figure 35: TEM images of catalyst nanoparticles created after impregnation of (a) H23C8 without any coating (b) H23C8 c + i coated with Ensaco 350 G and carbon nanofibers.

This can be the main factor which contributes to the weak quality of the platinum deposition on the first attempt, without any extra layer. To assure a better distribution of the precursor and ionomer over the MPL surface, a second method is tested.

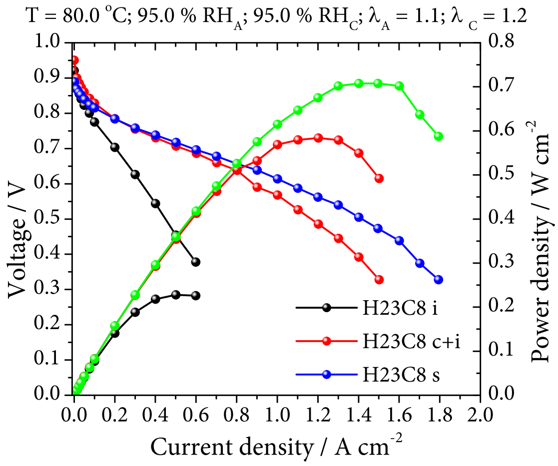

Figure 36: Performances of GDEs obtained utilizing impregnation (H23C8 i) and spraying (H23C8 s) methods. Along that, the behaviour of the coated H23c8 c + i is presented. Using an impregnation technique the precursor and the ionomer are introduced in the GDL.

Instead to impregnate the entire GDL in the precursor solution, it is sprayed utilizing the hand-spray technique, described in Section 5.5. By using this method the FC current/power density at 650 mV is improved by 70 % versus the impregnated electrode and 10 % compared to the coated one.

6.2 SPRAYING PROCESS OPTIMIZATION

Similar to each new system, which needs to be optimized, some initial parameters should be chosen. Therefore, some preliminary tests of the syringe pump and the 3D printer are made, to fix moving speed, pump rate, distances, etc. Also, the new spray nozzle should to be examined and calibrated. In this context, a pump rate of $0.5\,\mathrm{ml\,min^{-1}}$ combined with $2\,\mathrm{bar}$ pressure of the driving gas is found to be advantageous for the atomization of the fluid. According to the precursor volume (in this case $2\,\mathrm{ml}$) the speed of the moving table and the number of layers are selected. The already developed calculator, which is included in the controlling software, computes these values automatically. Another critical parameter is the distance between the spray nozzle and the sample. Initial tests show that a distance of $1.5 - 2.5\,\mathrm{mm}$ provides the best results. In order to evaporate the solvent of the sprayed solution, the moving plate is operated at a constant temperature of 120 °C. For initial tests an electrocatalyst loading of $0.4\,\mathrm{mg\,cm^{-2}}$ and $0.3\,\mathrm{mg\,cm^{-2}}$ dry ionomer is preferred.

6.2.1 *Spraying layers*

The spray method, in comparison to the impregnation technique, allows the segmentation of the catalyst layer on the spraying phase (Figure 37b). This provides countless combinations to introduce the catalyst precursor and the ionomer in the MPL structure. This architecture is chosen to improve the contact between precursor, ionomer and carbon sites. So, the $PtCl_6^{2-}$ ions can move freely across the electrolyte and organize in nanoparticles at the TPB. For preliminary tests six combinations, noted as E1 to E6, are selected (Table 2).

	Layer 1 $mg\,cm^{-2}$	Layer 2 $mg\,cm^{-2}$	Layer 3 $mg\,cm^{-2}$	Layer 4 $mg\,cm^{-2}$	j at 650 mV $A\,cm^{-2}$	Pt loading $mg\,cm^{-2}$	mean size nm
E1	Nafion™ 0.15	Platinum 0.4	Nafion™ 0.15	–	0.59	0.15	3.1 ± 0.4
E2	Platinum 0.4	Nafion™ 0.3	–	–	0.84	0.16	3.0 ± 0.3
E3	Nafion™ 0.3	Platinum 0.4	–	–	0.67	0.1	3.4 ± 0.6
E4	Nafion™ 0.3 + Platinum 0.4	–	–	–	0.94	0.11	2.9 ± 0.6
E5	Platinum 0.2	Nafion™ 0.3	Platinum 0.2	–	0.67	0.14	3.7 ± 0.5
E6	Nafion™ 0.15	Platinum 0.2	Nafion™ 0.15	Platinum 0.2	0.84	0.05	3.5 ± 0.5

Table 2: Layers composition obtained by interlacing the ionomer and the platinum precursor. Both components are sprayed up to 4 layers until the desired loading is achieved.

So, each layer contains one more components with a well defined quantity. e. g.E1 contain $0.15\,mg\,cm^{-2}$ Nafion™ in the first layer, in the second layer the entire platinum quantity ($0.4\,mg\,cm^{-2}$) and the third layer Nafion™. The same notation system is adopted for all other combinations, except E4, where the ionomer and the precursor are firstly mixed, in an ultrasound bath and then sprayed on the MPL surface.

In a next step the $PtCl_6^{2-}$ is electrochemically reduced as described in Section 5.2. The deposition process takes place at room temperature. To improve the electrolyte proton transport proprieties, this is humidified to 90 % RH.

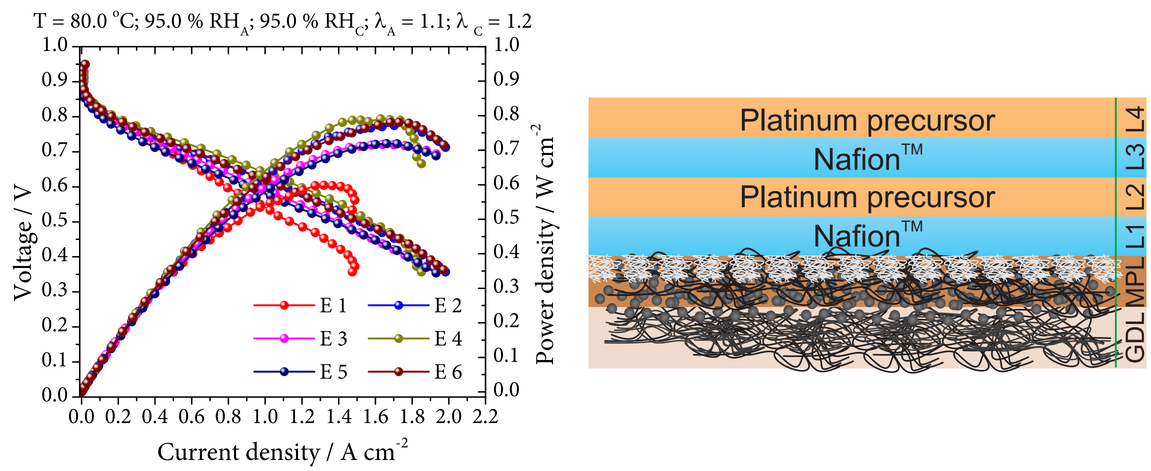

(a) (b)

Figure 37: (a) Performances of the GDE containing a layer catalyst-ionomer structure. The FC are tested at 80 °C and 95 % RH. (b) CL configured by spraying multiple layers containing the precursor and the ionomer. Each layer contains a well defined loading, defined in Table 2.

A summary of the GDE performances, obtained in the FC tests, is presented in Figure 37a. For all samples a good electrochemical activity, with current densities in the range $0.7 - 0.9\,\mathrm{A\,cm^{-2}}$ at $650\,\mathrm{mV}$, are found (see Table 2). Moreover, the performance of the E4 is increased by 10 % in comparison to the previous GDE, prepared by hand spraying. This improvement is achieved using a considerably lower catalyst loading for the new electrodes. Table 2 compares the recorded current density at $650\,\mathrm{mV}$ for all prepared GDE. It can be observed that in all cases when $\mathrm{Nafion}^{\mathrm{TM}}$ is applied as the first layer, the MEAs suffer a performance decrease. We suppose that the $\mathrm{Nafion}^{\mathrm{TM}}$ layer application obstructs the MPL pores. So, a direct contact between the $PtCl_6^{2-}$ and the carbon support is limited. This implies a decrease of the electrochemically reduced platinum quantity and implicitly a poor FC operation.

The carried out ICP – OES analysis confirms our theory. So, it can be noticed that for E2 a higher platinum quantity is deposited in comparison with the E3, just by inverting the spraying order (Figure 2). Thus the initially introduced $\mathrm{Nafion}^{\mathrm{TM}}$ decreases the deposited platinum loading by more than 60 %. This influences the FC performance, which is decreased by over 30 % at $650\,\mathrm{mV}$. When the sprayed $\mathrm{Nafion}^{\mathrm{TM}}$ quantity of the first layer is lower, no high discrepancy on the deposited electrocatalyst is observed. E1 exhibits quite the same loading as E5. Here no correlation can be done between the electrocatalyst loading and GDE performance. Although E5 contains 5 % less noble metal, it performs 15 % better compared to E1. A thin $\mathrm{Nafion}^{\mathrm{TM}}$ layer does not cover completely the pores and multiple attaching places remain available for the catalyst particle fixation. According to our theory, the $\mathrm{Nafion}^{\mathrm{TM}}$ sprayed on the fist layer influences in a negative way the fuel cell performance. However, it can be observed that E6 provides the same power density as E2, although its catalyst loading is $0.05\,\mathrm{mg\,cm^{-2}}$. This is a clear evidence that most of the deposited platinum particles are situated at TPB and have a high ECSA. According to the recorded polarization curves (Figure 37a) the best result is achieved with E4. In this case, by mixing the ionomer with the precursor before spraying, an almost ideal interlaced structure is obtained. So, a current density of $0.94\,\mathrm{A\,cm^{-2}}$ at $650\,\mathrm{mV}$ is achieved.

The TEM images (Figure 38) indicate a homogeneous catalyst distribution along the carbon support. The particle size analysis reveals a nanoparticle diameter between $2.9 - 3.7\,\mathrm{nm}$ (Table 2). In the case of E1 and E2 the optical investigation indicates particles agglomerations comparing to the other GDE. This is in good agreement with the ICP – OES measurements. Similar behaviour is observed for E5. To create a multilayer CL structure the precursor ions need to be in the vicinity of a support carbon particle. Thus, new nuclei are created which can be further grown to particles. Due to the low binding energy of the created particles, the free $PtCl_6^{2-}$ ions attaches to the already formed particles. This involves a further nanoparticle growth, which ends with particle agglomerates observed on TEM images. Thus, the ECSA is decreased and implicitly the FC performance drop. In the case of E4 no agglomerates are visible and therefore the FC performance is superior to the other ones. Unfortunately, for all prepared electrodes, from the proposed $0.2\,\mathrm{mg\,cm^{-2}}$ platinum loading, only a maximum of 81 % is deposited (E2). The not reduced precursor is washed out according to the preparation method (see Section 5.2).

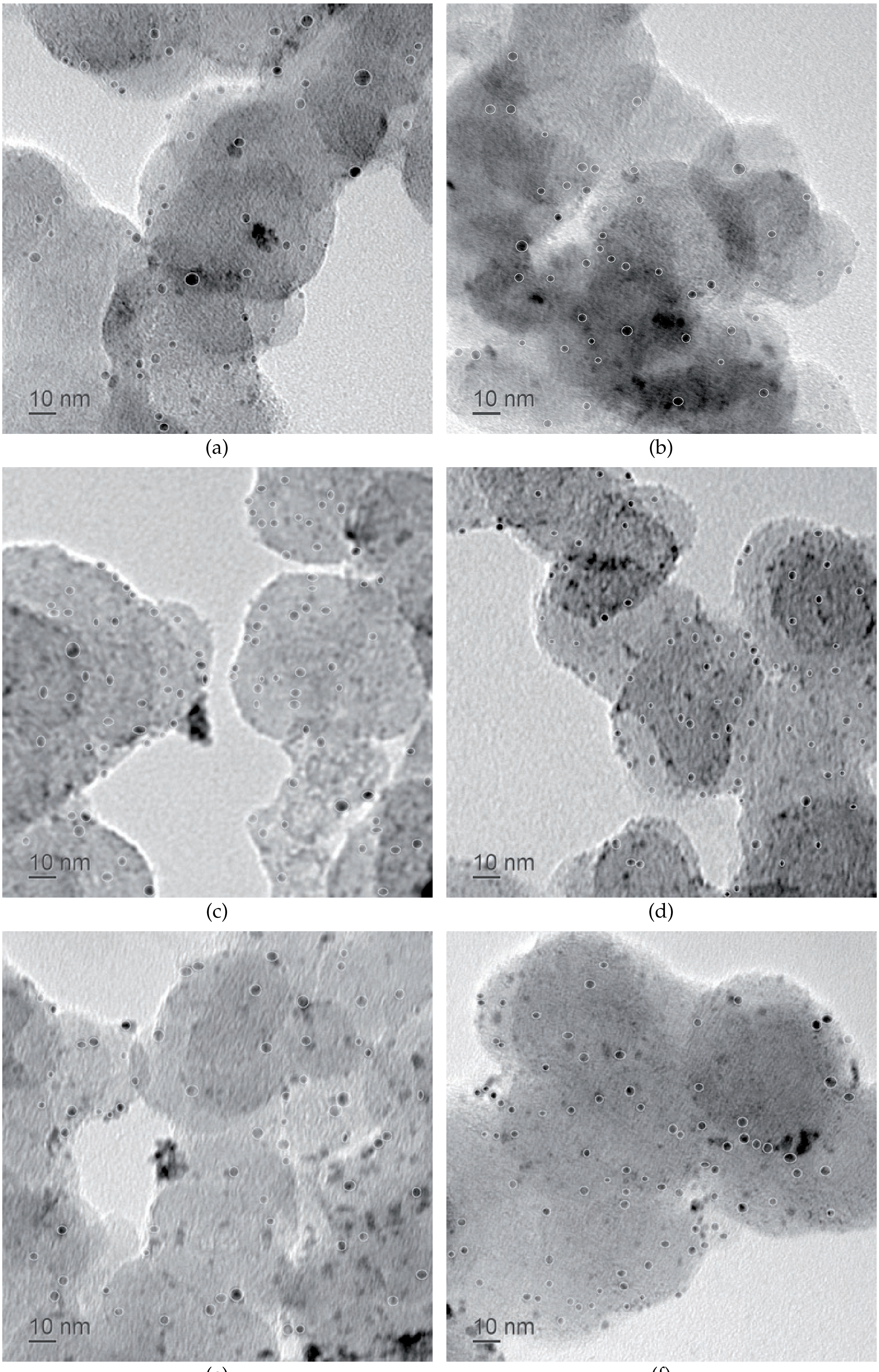

Figure 38: TEM images of the catalyst particles obtained by interlacing the ionomer with the precursor on Section 6.2.1. (a) E1, (b) E2, (c) E3, (d) E4, (e) E5 and (f) E6 GDE produced by a spraying method.

Therefore, in order to decrease platinum wasting, for the electrodes prepared in the future a maximum catalyst loading of $0.1\,\mathrm{mg\,cm^{-2}}$ is adopted. According to this optimization step, it is clear that the best result, in term of FC performance and catalyst distribution, is obtained for the prior mixed ionomer with the precursor (E4).

6.2.2 *Hot plate temperature*

During the spraying process, the moving table is carried along the X and Y axis, according to a pre-defined pattern. In order to obtain a homogeneous layer, the GDL temperature needs to be precisely controlled. Especially by the fact that the plate temperature, due to the high gas flow can locally significantly decrease, the plate heating system should be powerful enough to hold a constant temperature during the spraying process. Apart from that, a good contact between the sample and the moving plate is absolutely necessary. It is known that GDL has a very high heat conductivity and therefore we assume that the temperature is constant over the entire GDL [65]. If these rules are not satisfied, then the solvent remains in a liquid phase at the GDL surface. Thus, the fluid together with the air stream disperse the ionomer and the precursor over the MPL, so that an inhomogeneous layer is produced.
Therefore, the hot plate temperature plays an important role for the ionomer and precursor distribution in the MPL arrangement. In this way an optimum CL thickness of $10-20\,\mu\mathrm{m}$ can be achieved. When the plate temperature is under the solvent boiling point most of the mixture goes deep in the MPL structure. This happens for solvents such as IPA, ethanol, acetone, ether and chloroform which posses a small contact angle value. For the prepared GDE, IPA with a boiling point of 82 °C is used as solvent. It is essential to find an optimum plate temperature, at which the precursor penetrates deep enough in the MPL, maintaining a good accessibility for the protons. So, the TPB is increased and the noble material wasting is reduced.

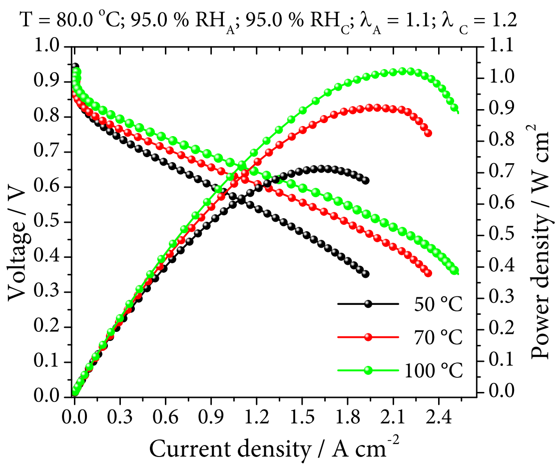

(a)

Figure 39: (a) PEMFC performances for the samples prepared using distinct temperatures of the 3D printer plate.

In order to investigate the hot plate temperature influence on the FC performances, three different temperatures are tested: 50 °C, 70 °C and 100 °C. The spraying and electrodeposition parameters are held at the same values as for the previous samples (see Subsection 6.2.1). Figure 39 presents the polarization curves of the prepared GDEs. It can be observed that, as the plate temperature is increased, the FC performance improves. This can be attributed to the fast solvent evaporation, which influences the ionomer drying. So, at 100 °C the solvent evaporates immediately and the ionomer has not enough time to fill up the MPL pores. At low temperatures (e. g. 50 °C), due to the slow solvent evaporation, the ionomer creates a film which hinders the precursor reduction and impacts the reactant/oxidant path.

Thus, by increasing the plate temperature from 50 °C to 100 °C the FC current density is boosted with over 35 % at 350 mV. In the same time, due to the optimum plate temperature power densities above 1 $W\,cm^{-2}$ are reached. For the next optimization steps a temperature of 100 °C is utilized.

6.2.3 *Driving gas pressure*

In the attempt to reduce the necessary noble metal amount in the PEMFC electrodes, the influences of further physical parameters implemented in the spraying process need to be examined. Apart the moving plate temperature, the driving gas pressure can have fundamental influence on the catalyst layer structure. In literature, many authors use, instead of the pressure, the gas flow rate, according to the specific gas mixtures [155]. Other authors are providing only information about the spraying temperature, without considering the gas pressure as an important parameter [73, 156, 148]. We consider that by spraying the precursor solution with an optimum pressure, in combination with an elevated plate temperature, a 3D CL architecture with few µm thickness can be produced. Simultaneously, the applied pulses during the electrodeposition process create nanoparticles with a well defined shape and an increased ECSA.

For the present study four distinct pressures are selected. A platinum precursor and ionomer loading of 0.1 $mg\,cm^{-2}$ are sprayed over a H23C8 GDE placed on the moving plate. During the entire process the plate temperature is maintained at 100 °C. According to the polarization curves, the best result is obtained for a spraying pressure of 2 bar (Figure 40a). This outcome can be attributed to the increased platinum loading, which according to the ICP – OES measurement is higher than for the other employed pressures. Nevertheless, the platinum difference between the electrodes prepared by 2 bar and 2.5 bar is to small to produce this significant difference (~ 0.24 $A\,cm^{-2}$ at 650 mV).

Quite interesting are the results for 1.5 bar and 2.5 bar which are rather identical. We believe that at low pressures the liquid cannot be completely splitted in droplets and an inhomogeneous layer is created, therefore a smaller loading is obtained. At higher pressures, the ionomer is introduced deeper in the MPL and fewer vacancies remain available for the catalyst support. In accordance to the ICP – OES results the noble metal quantity is increased, but it is not electrochemically active. We attribute this behaviour to the massive nanoparticles agglomerations inside the

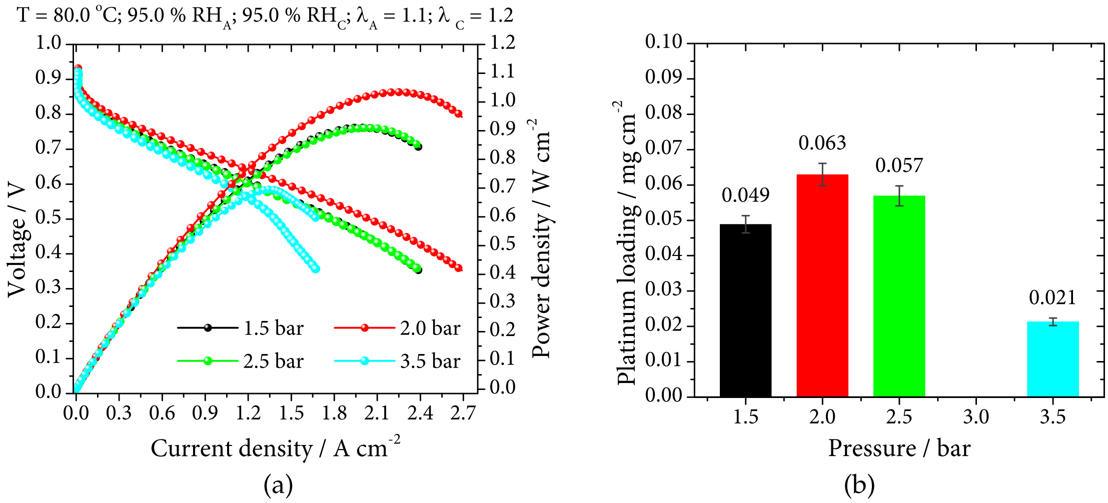

(a) (b)

Figure 40: (a) Polarization curves of the electrodes prepared at distinct spraying pressures. (b) Precise catalyst loading measured by ICP – OES. On both graphs the MEA containing the GDE sprayed at 2 bar displays the best performance.

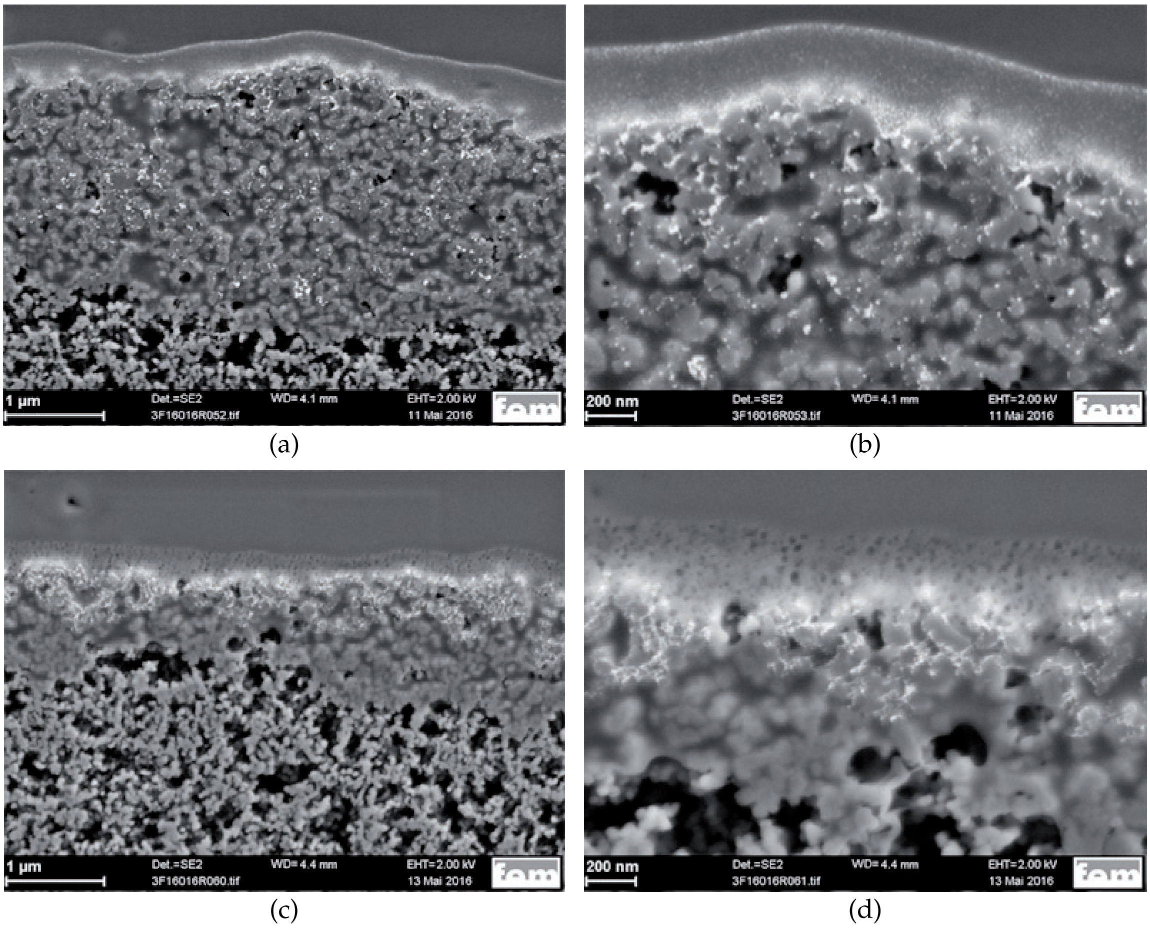

(a) (b) (c) (d)

Figure 41: SEM images obtained after a transversal cutting using an ion beam slope cutting technique for the GDE samples prepared at (a) 2 bar and (b) a zoom of the catalyst layer of the same sample. (c) The catalyst layer structure obtained for a spray pressure of 3.5 bar and (d) a zoom of the catalyst arrangement of the identical sample.

MPL. Rising the pressure to 3.5 bar the FC performance drastically decreases. At this pressure the gas flow is so high that the solvent is directly evaporated and only small precursor quantity reaches the GDL surface. Even the $PtCl_6^{2-}$ which achieves the GDL surface are intensively flushed by the high gas flow rate and many of them are pulled out from the structure. This justifies the low catalyst loading (20 % from the planned platinum loading) and implicitly the FC performance.

In order to understand the driving gas pressure influence on the GDE structure, highly sensitive analytical methods are recommended. In collaboration with colleagues from FEM, partners in the ISECD project, a transversal cut of the GDE is performed, utilizing an ion beam slope cutting technique. The sections are then analysed with a SEM device (Figure 41). We want to specify from the beginning that the blurred part from the picture does not represent the ionomer. This component exhibit the epoxy glue used to fix the GDL structure during the preparation process. Thanks to this method, the structure of the catalyst layer can be examined in detail. The presented pictures indicate a variable CL thickness for both electrodes. In the case of low pressure (2 bar) the CL present a thickness of ~2 µm. This is significantly higher than the measured CL thickness of the other electrode, prepared at 3.5 bar, which indicates a value of ~0.5 µm. Also, the displayed zooms illustrate a catalyst agglomeration at the MPL surface for both GDEs (Figure 41b and Figure 41d). However, the GDE prepared with a spraying pressure of 2 bar suggest a further catalyst expansion, deeper in the structure. Nevertheless, the total CL thickness does not exceed 2.2 µm. This value is far away from the suggested optimum CL thickness ($10-20$ µm). This kind of catalyst layer structures provides some benefits as direct contact with the electrolyte and increased TPB. Besides, due to its small thickness the water removal is problematic, here an additive hydrophobic element needs to be introduced.

6.2.4 *Solvent composition*

According to the Subsection 6.2.3 the sprayed mixture penetrates only 2 µm in the MPL. Therefore, for a better precursor/ionomer distribution another procedure is necessary. One possible solution is the use of different solvents mixtures. Thus, the temperature of the moving plate is held constant at 100 °C and the solvent boiling point is varied. In order to test our theory, multiple GDE are prepared by mixing the IPA with distilled water. So, the boiling point is gradually decreased from 100 °C for water to 82 °C for IPA.

Figure 42a displays the performances of the prepared samples. All MEAs indicates no transport problems at high current densities. As can be observed the power density increases with the IPA concentration until it reaches a maximum at 40 % IPA. Up to this value, the PEMFC performance starts to decrease until it reaches the initial value. Quite interesting are the catalyst loadings measured by ICP – OES (Figure 42b), which illustrates an inverse behaviour compared to the current density. On the first part, up to 40 % IPA, the graph indicates a slight increase at 10 % IPA and then the catalyst loading decreases until it reaches a value of 0.025 mg cm^{-2} for 40 % IPA. In the same time, the current density reaches a maximum of 1.23 A cm^{-2} at 650 mV. Then, by increasing the IPA concentration up to 50 %, the entire GDE

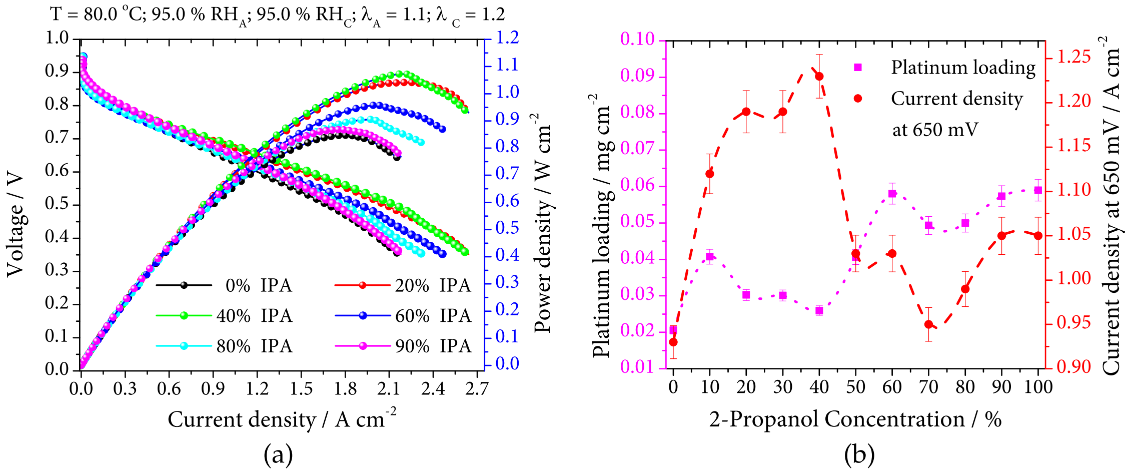

Figure 42: (a) Polarization curves show the influence of the solvent composition on the FC operation. (b) Current density at 650 mV and the platinum loading obtained from ICP – OES analysis plotted vs. IPA concentration.

properties are switching. So, from this concentration the deposited platinum catalyst quantity increases and the current density decreases. We can assume that IPA enhances the ionomer organisation so that the $PtCl_6^{2-}$ ions have a better mobility. However, in this step the electrocatalyst loading does not reach the target of $0.1\,mg\,cm^{-2}$, although the performances are significantly improved.

In order to visualize the water influence on the CL structure a transversal cut of the sample with 0 % IPA is performed (Figure 44). A first view indicates that the CL is situated on the MPL top side and has small thickness. An analysis of the zoomed picture (Figure 44b) indicates that the catalyst penetrates ~6 μm in the MPL. Furthermore, it varies along the surface, on many places the CL thickness is reduced to ~1.7 μm, indicating an inhomogeneous layer structure. This can be explained by the high boiling point and the large contact angle of water. During the spraying process the GDLs suffer from a local cooling, thus influencing the water evaporation time. So, temperature gradients are created and the water remains in the MPL surface. The precursor and the ionomer profits from this temperature decrease and permeate deeper in the structure, so that a connection with the following layers is provided. On the other hand, by adding IPA the solution the boiling point decreases and the ionomer with the catalyst can be better positioned on the MPL architecture with an improved connection. For an IPA concentration of 50 % we assume that the ionomer covers the porous structure and the $PtCl_6^{2-}$ ions cannot reach the carbon sites.

Therefore, above this concentration a slight variation of platinum loading and FC performance are observed, indicating a saturation limit. The TEM images presented on Figure 43 indicate well-dispersed platinum nanoparticles. The analysis reveals a diameter for the produced nanoparticles of $2.5 \pm 0.75\,nm$. In addition, a slight particle agglomeration is observed by increasing the IPA concentration. This suggests a well defined ionomer layer and implicitly a better $PtCl_6^{2-}$ ion mobility.

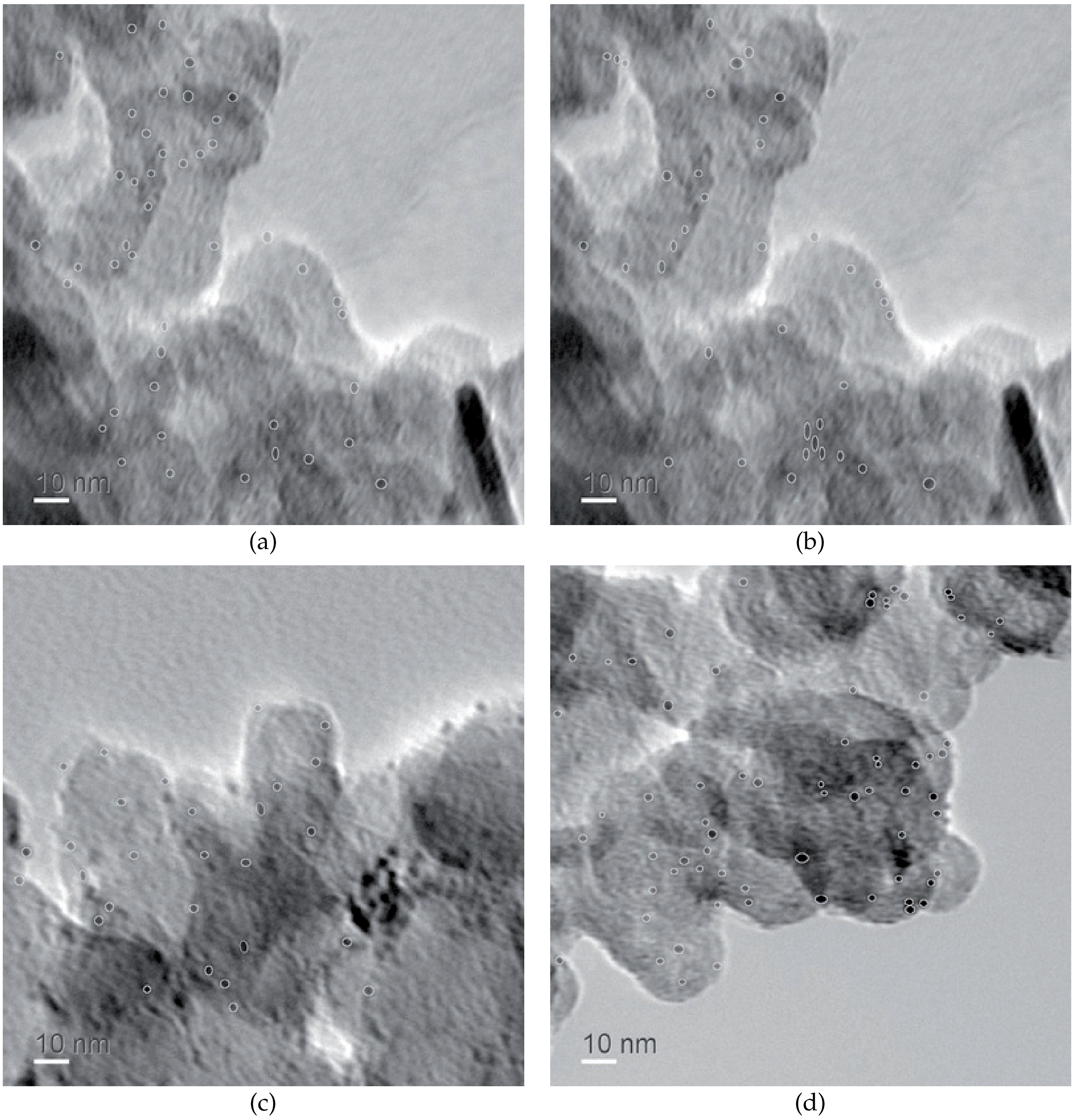

Figure 43: TEM images of the prepared electrodes using four different IPA concentrations (a) 0 %, (b) 40 %, (c) 60 % (d) 100 %.

6.3 IMPROVEMENTS OF ELECTRODEPOSITION METHOD

Apart from the spraying parameters, the electrodeposition process is essential for CL formation. With this technique, one of the most important component of a FC is produced, the electrocatalyst. While in the spraying process the position of the precursor and the ionomer are designated, through electrodeposition the morphological properties of the electrocatalyst are tuned. Therefore, a high attention needs to be given to all parameters which are involved in the catalyst production. Especially, to the pulse configuration that controls the particles size and composition. A significant consideration needs to be provided to the particular setup, developed during the PhD period for the electrodeposition process. Multiple problems can appear and a quick and precise debug procedure is required. Even the small varia-

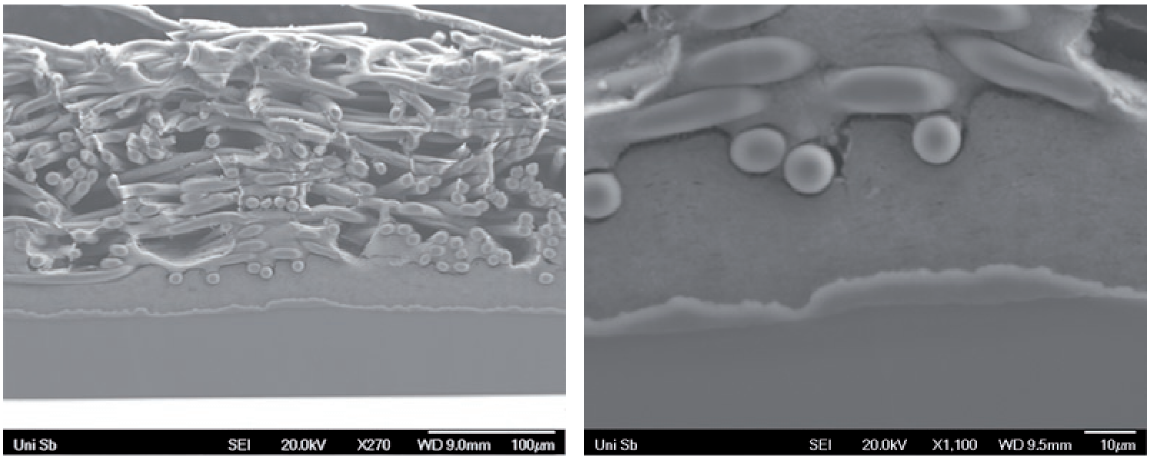

(a) (b)

Figure 44: (a) Transversal cut of the GDE containing 100 % water. (b) A zoom in for the same electrode indicates an inhomogeneous thickness of the coating layer.

tions on the gas flow or screw torque can influence in a negative way the catalyst on its future applications.

6.3.1 *Electrolyte humidification stage*

The electrolyte in the electrodeposition cell is represented by a Nafion^{TM} 115 membrane produced by DuPont. Through this the protons flow from the anode to the cathode, where together with the Cl^- ions hydrochloric acid is formed. As each membrane used up to now on PEMFC, for a better electrolytic conductivity it needs to be humidified. According to the electrodeposition setup this can be achieved by humidifying the gas used at the anode (see Section 5.2). Through the osmotic drag, also the ionomer contained in the MPL structure can be humidified. We suppose that the transferred water molecules improve the $PtCl_6^{2-}$ mobility, and so an enhanced catalyst architecture is constructed. In order to prove our assumption, four distinct relative humidities are investigated: 70 %, 80 %, 90 % and 100 % RH. A platinum loading of 0.4 $\mathrm{mg\,cm^{-2}}$ is suggested for this step.
The polarization curves and the corresponding power densities of the CCS prepared at different RH are presented in Figure 45a. The polarization curves show a slight mass transport loss within the measured current densities. By examining the polarization curves, we observe a dramatic increase with the RH. At the proposed working voltage of 650 mV the current densities of the GDEs at 70 %, 80 %, 90 % and 100 % are 0.62, 0.80, 0.84 and 0.95, respectively. The sample prepared at 80 % and 90 % RH shows quite the same behaviour. The maximum power density is also obtained by a relative humidity of 100 %, with a peak value of 0.92 $\mathrm{W\,cm^{-2}}$. This can be related to a significant decrease in the electronic resistivity upon water sorption on the MPL during the electrodeposition. Along that, the ICP – OES measurement indicates a platinum quantity increase through the RH (Figure 45b). At low relative humidities quite the same platinum quantity is deposited (0.07 $\mathrm{mg\,cm^{-2}}$).

To gain greater insight into the observed GDE performance, the TEM images of catalyst particles are shown in Figure 46. The TEM images indicate a catalyst size

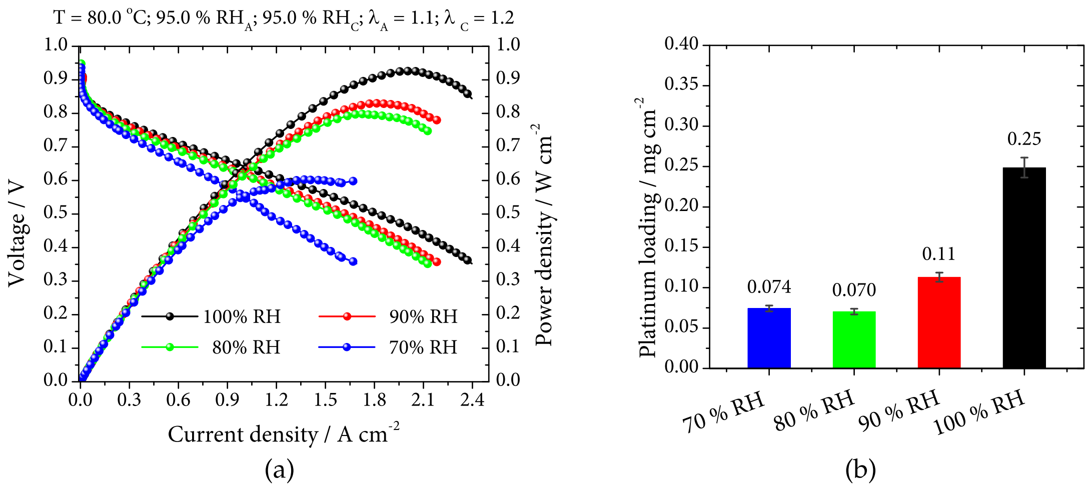

Figure 45: (a) Change of GDE performances prepared at distinct relative humidities from inlet gas stream. (b) ICP – OES results of the same samples.

of 4.0 ± 0.5 nm, 3.1 ± 0.5 nm, 1.8 ± 0.3 nm and 4.2 ± 0.7 nm for 70 %, 80 %, 90 % and 100 % RH, respectively. Especially, at low humidities the created particles are agglomerated and present a large particle size distribution. Moreover, at this RHs, the created catalyst particles are not well distributed around the carbon support. Furthermore, it is observed that as the humidity increases the particles exhibit a well defined form. An exception is the GDE prepared at 90 % RH, where the nanoparticles display a distributed size. We suspect that during electrodeposition the contact between the GDL and the electrolyte was not perfect. Anyway, the sample indicates the same dependence on the RH. Based on this results we can specify that the RH of the electrolyte improves the $PtCl_6^{2-}$ mobility and the nanoparticles structure.

6.3.2 *Deposition temperature*

According to the electrodeposition principle described on Section 5.2, the precursor reduction is accomplished by the electrons and protons flow provided from the anode. In order to improve the kinetics of these two elements, the electrodeposition cell temperature needs to be increased. Therefore, five distinct temperatures ranging from room temperature to 70 °C are investigated. In all cases a constant RH of 100 % is maintained.

Figure 47a displays the performances of the MEAs containing the GDE prepared at distinct temperatures. As can be observed, the electrode produced at 25 °C indicates a low catalyst activity, with a current density of 0.71 A cm^{-2} at 650 mV. By increasing the cell temperature a significant current density increase is achieved. So, at 50 °C and 70 °C a current density of 0.97 A cm^{-2} at 650 mV is recorded. Apart from that, for the same GDE the maximum power density is registered, with a peak at 0.95 W cm^{-2}. Nevertheless, by increasing the temperature over 50 °C no significant FC improvements are noticed. The deposition cell temperature influences also the deposited platinum quantity (Figure 47b). So, at 70 °C the catalyst loading is twice of the platinum quantity deposited at 25 °C.

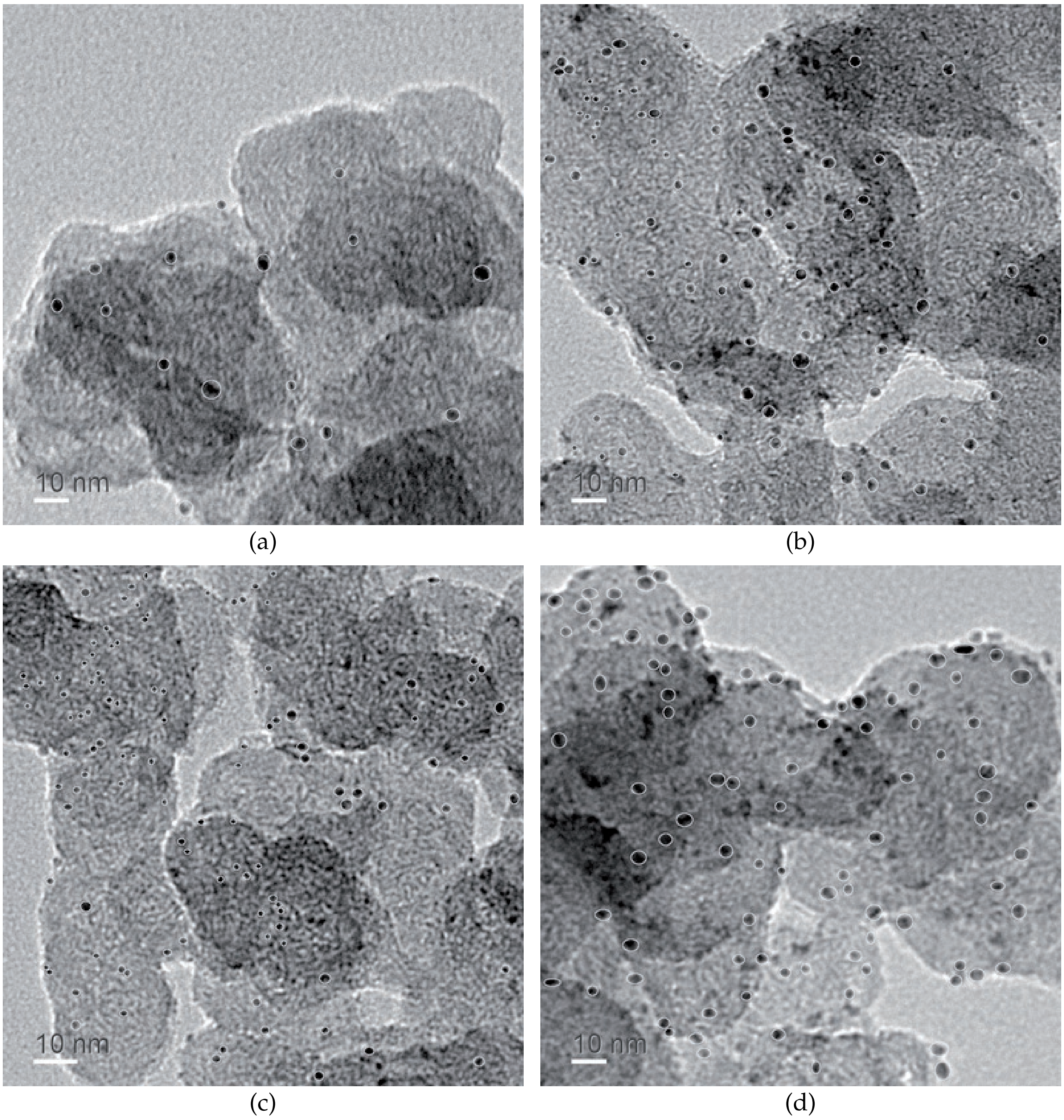

Figure 46: Platinum particles morphology obtained at separate electrolyte relative humidities: (a) 70 %, (b) 80 %, (c) 90 % and(d) 100 %.

The TEM images indicate the rise of the particle size with the temperature (Figure 48). A fundamental analysis reveals a particle size of $2.32 \pm 0.4\,\mathrm{nm}$, $3.03 \pm 0.5\,\mathrm{nm}$ and $3.34 \pm 0.4\,\mathrm{nm}$ for 25 °C, 50 °C and 70 °C, respectively. Due to the poor $PtCl_6^{2-}$ mobility the particles deposited at 25 °C present a higher nanoparticle density and a small size. At this RH the particles contain only the $PtCl_6^{2-}$ situated near to the nuclei, although the electrolyte humidity is 100 %, the multitude of nuclei cannot grow further. At higher temperatures the $PtCl_6^{2-}$ mobility is improved and the particles show a greater diameter. So, at 50 °C the particles decorate uniformly the carbon support and present an optimum size. Comparing the GDE performances prepared at 50 °C and 70 °C we can say that the deposition temperature influences significantly the catalyst layer properties.

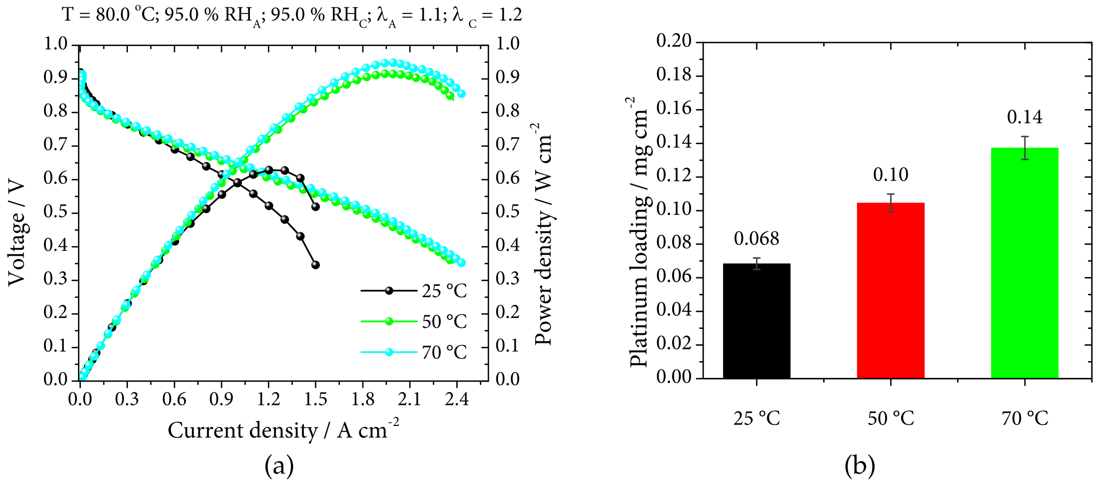

Figure 47: (a) Polarization curves showing the influence of the electrodeposition temperature on the PEMFC performances. (b) ICP – OES statistics of the electrodes prepared at distinct temperatures.

6.3.3 *Nucleation pulse*

Electrochemical deposition is one of the most utilized techniques to coat electrical conductive materials. One advantage of this method is its flexibility, a fact that makes it compatible for a wide range of applications [133]. Most of the electrodeposition processes take place in an liquid electrolyte, thus the employed deposition parameters need to provide an optimum structure and be energetically efficient [107]. According to the actually used deposition method, in order to obtain the best catalyst not only a good electrodeposition cell design is required (see Section 5.3) but also an accurately deposition profile (Figure 22b). This implies the tune up of the contained pulses: nucleation and grow pulse. Therefore, by holding the previously improved parameters at the optimized level, new samples are prepared using different nucleation potentials.

According to Kulp et al. the platinum is deposited at a potential under -0.042 mV [105]. Therefore, each applied potential under this value should reduce the $PtCl_6^{2-}$ to platinum. In order to see the effect of negative potentials on the catalyst morphology and on PEMFC performances eight different potentials are investigated. Thus, the nucleation potential is varied from -0.3 V to -1 V vs. DHE, with steps of -0.1 V.

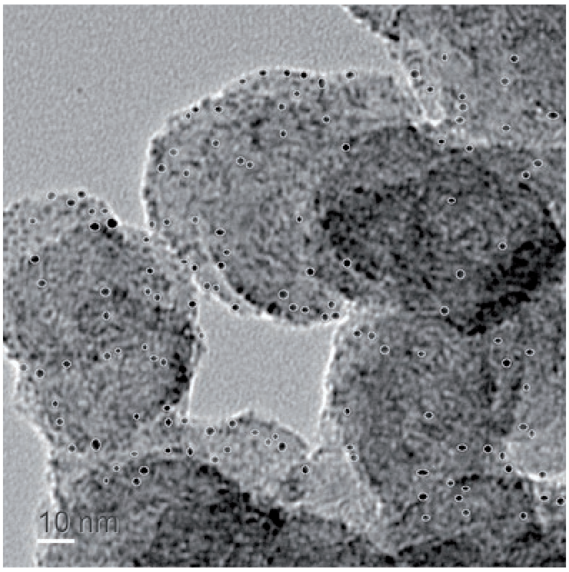

(a)

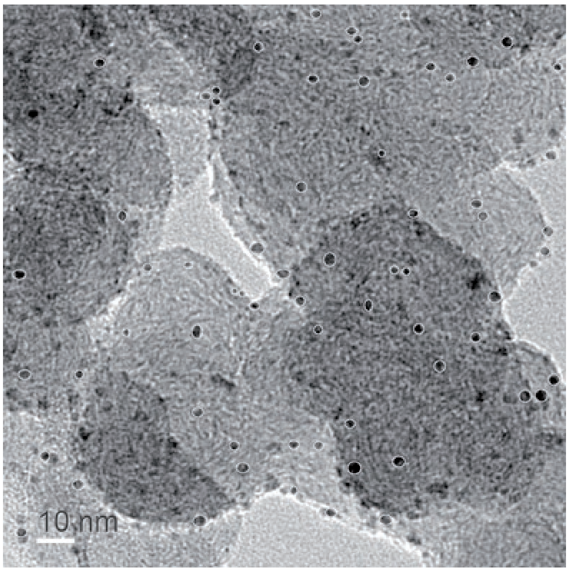

(b)

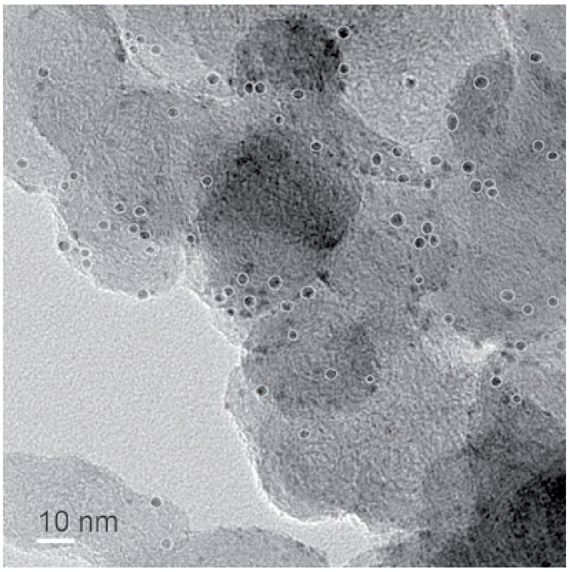

(c)

Figure 48: TEM pictures of the samples prepared at (a) 25 °C, (b) 50 °C and (c) 70 °C. At 25 °C the density of particles per cm^2 is increased.

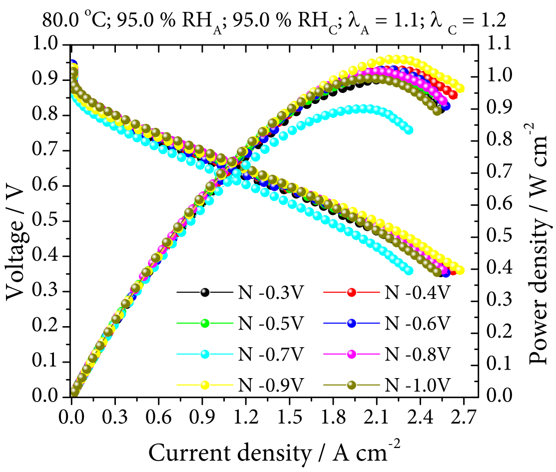

(a)

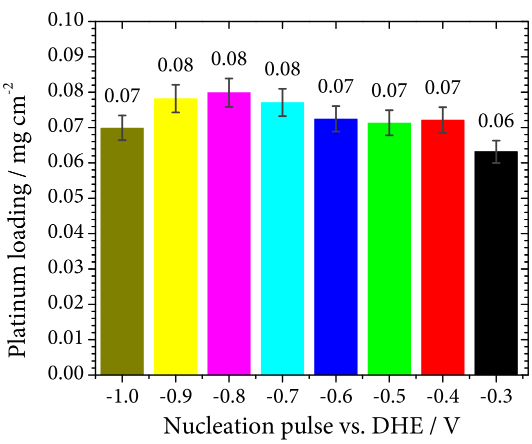

(b)

Figure 49: (a) Polarization curves and (b) catalyst loading of the GDE prepared by applying distinct nucleation potentials.

Figure 49a shows the GDEs performances prepared by applying distinct nucleation amplitudes. According to the measured curves, all samples shows the same behaviour. A small performance decrease is registered for the GDE prepared with a nucleation pulse of $-0.7\,V$ vs DHE. According to the ICP − OES measurements, displayed on Figure 49b, this electrode contains the same platinum loading as all others and a performance decrease is not justified. It can be observed that at a potential of $-0.3\,V$ the deposited platinum quantity is the lowest one. According to Whalen et al. at this potential the reduction of Pt(II) to Pt(0) is slower than for reduction of Pt(IV) to Pt(II) [157]. Nevertheless, it shows a very good performance in the FC operation, competitive with all others. When the potential is more negative, a slight catalyst loading increase is observed, until it reaches a maximum at $-0.8\,V$. Then, the platinum loading decrease to a value of $0.07\,mg\,cm^{-2}$.

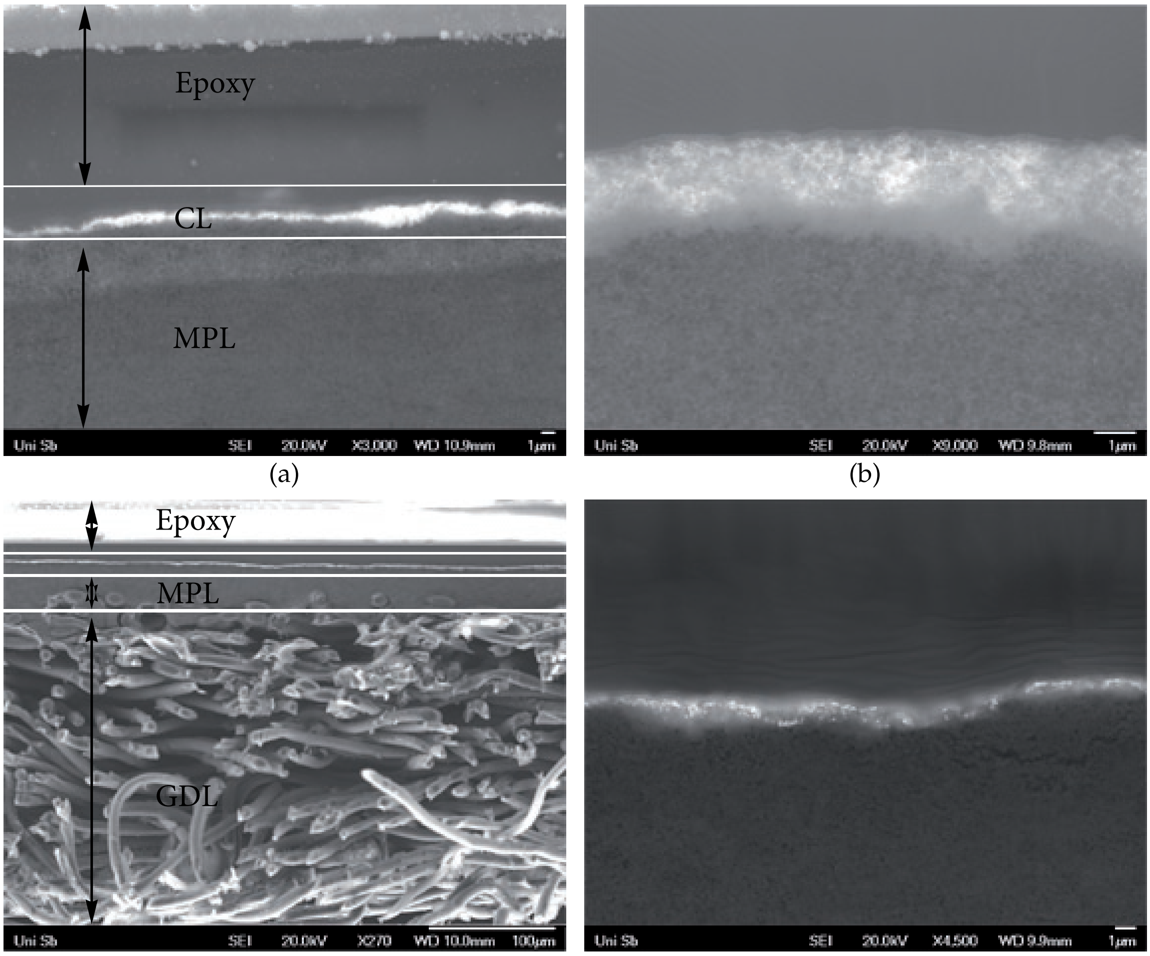

Figure 50: SEM images of the electrodes prepared by applying a nucleation pulse with an amplitude of (a) $-0.3\,V$, (b) $-0.9\,V$ and (c) $-1\,V$. (d) present a zoom of GDE prepared with a nucleation pulse of $-1\,V$.

In order to investigate the CL structure and to see the nucleation pulse influence, three GDE are cut with an ion beam and investigated by means of SEM (Figure 50). According to this images, the CL presents an average thickness of $1.0\,\mu m$, $2.7\,\mu m$ and $1.1\,\mu m$ for an applied pulse of $-0.3\,V$, $-0.9\,V$ and $-1\,V$, respectively. As can be observed the layer structures varies along the MPL surface. So, at −0.3 V the layer shows platinum agglomerates and a higher thickness on the right side of the picture. On the other side a significant thickness decrease is observed, with a small platinum quantity. The same result is obtained for a pulse with an amplitude of −1 V vs. DHE. Here the CL presents the same thickness, although it contains a significant higher platinum quantity. A complete view of the GDE surface indicates a good electrocatalyst dispersion with a constant thickness (Figure 50c). The sample prepared by −0.9 V vs. DHE, Figure 50b indicates the thickest CL from all produced electrodes. It can be observe that the catalyst layer is splitted in two regions. The first one is situated at the surface and contains particles with a bigger size. The second region, as a cloud, surrounds the other bigger particles and is situated deeper in the MPL structure. We think that during the electrodeposition process the MPL top side, situated in contact with the electrolyte, is better humidified and the $PtCl_6^{2-}$ have an improved mobility. In accordance to the second region the humidity is reduced and only nuclei are created. In accordance to the recorded data a potential $\leqslant -0.4$ V is optimal for the platinum electrochemical deposition.

6.4 SUMMARY

In order to obtain a high electrochemical active catalyst an electrodeposition method is adopted. Prior to deposition the metal precursor should be positioned in the MPL network. Therefore, two distinct methods are investigated. During the first one the ionomer with the precursor come in a Teflon vessel and the GDL is impregnated with the prepared solution. The GDL is positioned so that the MPL side comes in the contact with the liquid. The research has revealed that due to the high hydrophobicity and small pore size the impregnation method cannot be used for the commercial GDLs.

The second technique implies the spraying of the same components on the MPL surface using an airbrush. During the spraying process the substrate is heated, so that the solvent evaporates and the precursor remains in an anhydrous state. These techniques are applied on a commercial GDL (H23C8). The preliminary results have revealed that the spray technique improves with $\geqslant$70 % the GDE performance. Simultaneously, it is found that due to the high hydrophobic grade, during the impregnation process the ionomer does not permeate in the MPL architecture. Therefore, the GDL is re-coated with an ink containing Teflon, ionomer and carbon particles using the doctor blade technique. In this way the electrode surface is increased and the catalyst particles can be created at the TPB. TEM measurements confirm that the catalyst decorates the carbon particles and have a size of 4 ± 0.6 nm. Moreover, the FC performance at 80 °C and 95 % RH indicate an improvement of over 60 % compared to the non-coated GDLs.

Motivated by the results obtained for the sprayed GDE we have investigated the influence of the spraying parameters on the CL structure and FC performance. For a simple catalyst evaluation the prepared GDE are tested as anode in the self developed fuel cell housing. On the first test phase improvement on the spraying order should done. So, the ionomer and precursor layers are spread over multiple layers, until the necessary loading is achieved. We have found that by spraying the ionomer on the first layer the GDL pores are blocked and the precursor cannot penetrate deeper on the MPL structure. An optimum combination is found to be the mixture of the both components before the spraying process and sprayed together on the heated GDL. In this way a current density of $0.94\,\mathrm{A\,cm^{-2}}$ is achieved at a voltage of $650\,\mathrm{mV}$. A further step on the tune up process is the substrate temperature during the spraying process. Thus, it is found that the GDEs prepared at a temperature of $100\,°\mathrm{C}$ shows the best performance from all studied temperatures. Another inspected parameter is the effect of the driving gas pressure. The investigations have revealed that a pressure of $2\,\mathrm{bar}$ is optimum for the spraying process. When the pressure is too high, then the entire precursor is blown from the GDL surface and the catalyst loading decrease significantly. Intensive analyses are performed to increase the CL thickness, by modifying the solvent composition. We have established that the water addition improves the FC performance but in the same time decreases the electrodeposited catalyst quantity.

A great emphasis is laid on the catalyst morphology. Therefore, the electrodeposition parameters (electrolyte humidity, deposition temperature and pulse amplitude) are considered. We have observed that the deposited platinum quantity depends exponentially on relative humidity. Also, an optimum deposition temperature of $50\,°\mathrm{C}$ is established. According to the recorded polarization curves, the performance is boosted by over 35 %, comparing with the samples prepared at room temperature. Finally, the nucleation pulse variation indicates the possibility to reduce the $\mathrm{PtCl_6^{2-}}$ at a potential under $-0.3\,\mathrm{V}$ vs. DHE. A maximum on the catalyst loading is obtained at a potential of $-0.8\,\mathrm{V}$ vs. DHE.

Thus, the investigations have revealed the influence of the spraying and deposition parameters on the GDE microstructure and on the PEMFC performance.

7 THE IMPACT OF PREPARATION FRAMEWORK ON PEMFC CATHODES

Nowadays, the oxygen reduction reaction (ORR) is probably among the most important challenges in electrocatalysis. However, despite the intensive experimental and theoretical ORR research, up to now the exact ORR mechanism is not completely understood [158]. One of the most active and stable electrocatalyst used in PEMFCs is platinum, which due to its high price retards the FC marketing. Therefore, in order to extend the FC market, the platinum quantity needs to be reduced and optimum used.

The improved method presented in the actual thesis is a potential solution to this rigorous requirements. As introduced in Chapter 6, the tested electrodes as anode possesses a low catalyst loading and a high electrochemical activity. To verify the feasibility of this method, new investigations are required for the PEMFC cathode side. Therefore, GDEs containing distinct catalyst loadings and different GDLs are prepared. The spraying and electrodeposition parameters, optimized in Chapter 6 are used such as in Table 3. In addition, the developed GDEs are subjected to an ageing procedure. It consists in a CV sweep between $0.4 - 1.4\,\mathrm{V}$ vs. DHE for 500 times, followed by another CV scans from $0.05\,\mathrm{V}$ to $1.4\,\mathrm{V}$ vs. DHE for 500 times. During the ageing procedure, the cell is supplied with a constant H_2 flow at anode of $100\,\mathrm{ml\,min^{-1}}$ and at cathode with a N_2 flow of $200\,\mathrm{ml\,min^{-1}}$. The relative humidity of both gases is 95 % RH. The ageing losses in percent is calculated according to equation 21:

$$\mathrm{losses} = 100 \cdot \frac{\mathrm{ECSA_{initial}} - \mathrm{ECSA_{aged}}}{\mathrm{ECSA_{initial}}} \tag{21}$$

Along to the ageing process, the polarization curves, EIS response and the CV curves are recorded. The combination of multiple techniques retrieve fundamental informations regarding the catalyst and the GDLs proprieties.

7.1 MULTILAYERED CATALYST LAYER FRAMEWORK

Generally, the electrocatalyst in a GDE is uniformly distributed, with a constant loading over the entire active surface, so that the reaction is homogeneous. However, due to electrode nature and flow field shape, the oxygen concentration, RH and the amount of liquid water varies along the GDE [159]. One possibility to avoid this imbalanced system is to distribute the electrocatalyst over multiple layers in the MPL Z plane [160]. Through this arrangement the electrochemical active surface is increased, the catalyst is used efficiently and the ORR is improved. In an ideal GDE this kind of CL can also manage the MEA humidity, so that a humidification system is no longer required. Additionally, using a catalyst gradient the platinum loading can be reduced considerably, without important FC performance losses [161].

Parameter	Value
Spraying layers	Nafion™ and precursor mixed for 5 min
Moving plate temperature	100 °C
Driving gas pressure	2.0 bar
Solvent composition	70 % IPA and 30 % H_2O
Deposition RH	100 %
Depostion temperature	50 °C
Nucleation potential	−1 V vs. DHE for 1 ms
Growth potential	0.05 V vs. DHE for 200 ms
Substrate	H23C8 from Freudenberg

Table 3: Optimum spraying and electrodeposition parameters employed on GDE preparation.

The rotating disc electrode investigations conducted by Antoine et al. shows an improved catalyst utilisation on the gradient structures [162]. However, the only limitations for the implementation in PEMFC GDEs are induced by the preparation methods.

Typically, the prepared catalyst ink contains the carbon-supported catalyst powder, Nafion™ and IPA. In the literature most of the authors use a spraying method to distribute the ink containing diverse catalyst loading over the MPL surface [159, 161]. According to the method developed on the actual PhD thesis this kind of structures can be very easy created. In detail, after each sprayed step the precursor can be reduced using diverse nucleation and growth pulse shapes, so that the prepared structure has a multilayer form. In addition, for each sprayed layer a specific electrocatalyst loading can be used and the nanoparticles size can be precisely controlled.

In order to obtain a multilayer architecture we propose to distribute a catalyst and ionomer loading of 0.3 mg cm^{-2} over three distinct layers. Therefore, 0.125 mg hexachloroplatinic acid (equivalent of 0.1 mg cm^{-2} catalyst) is mixed with 24 µl Nafion™ D2021 (corresponding to 0.1 mg cm^{-2} ionomer) in 1 ml solvent. The entire solution is mixed for 5 min in a ultrasound bath. The spraying and the electrodeposition is made using the parameters displayed in Table 3. The entire procedure is repeated for three times until a catalyst and ionomer loading of 0.3 mg cm^{-2} is achieved. For MEAs preparation, along to the self prepared electrode, a Nafion™ 212 membrane and a commercial GDE from JM (ELE0162) are used. All three components are pressed by applying 0.5 kN cm^{-2} for 6 min. The process takes place at 125 °C. The tests are performed in the self-developed fuel cell housing with an active size of 10 cm^2 (see Section 4.2).

The investigations as anode illustrates a small transport limit at high currents (Figure 51a). In this case a current density of 1.05 A cm^{-2} is obtained at 650 mV. To examine the ORR, the MEA is reversed and measured as cathode. As can be observed in Figure 51a, the PEMFC performance decreases with over 50 % in comparison to the anode tests. However, no mass transport limitation is observed, indicating an enhanced GDE architecture. The significant performance drop can be justified by the lower catalyst loading which is measured as $0.067\,\mathrm{mg\,cm^{-2}}$. This value is far away from the target loading, but if we calculate the mass activity obtained for the used catalyst loading we achieve an unexpected result. The developed electrode shows twice of mass activity of the commercial GDE at a cell voltage of $650\,\mathrm{mV}$ (Table 4).

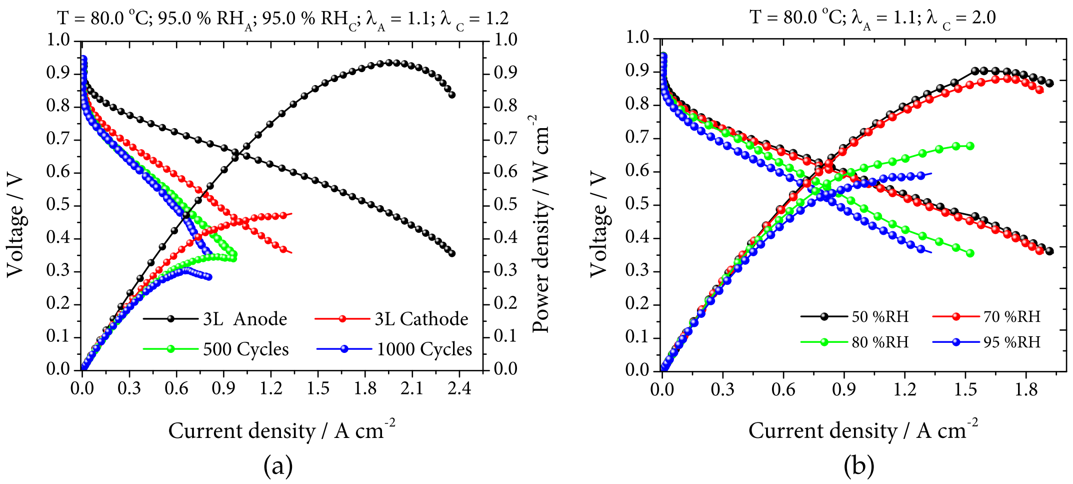

Figure 51: (a) Polarization of the three layer electrode tested as anode and cathode. During the cathodic test the prepared electrode is aged. (b) Present the polarization of the same GDE tested at cathode with different relative humidities. As the RH is decreasing the MEA performance is improving.

Moreover, the measurements at different RHs reveals that the performances of the developed electrodes are increasing by reducing the RH. Thus, the mass activity is rising until it reach a value of $10\,\mathrm{A\,mg^{-1}}$ at $650\,\mathrm{mV}$ and $50\,\%$ RH. This value is ~ 5 times higher than that obtained for the JM electrodes. This effect can be attributed to a lower overpotential of the oxygen reduction reaction (ORR) and an improved reactants path.

In the literature various dependencies of the ORR overpotential (η_{ORR}) are reported [39, 38, 163, 40]. Thus, in the absence of mass transfer losses, the overall cell voltage ($E(i)$) can be described as a summation of the various voltage terms and voltage losses in a PEMFC (see Section 3.2). Considering that the anode proton resistance and anode overpotential associated with the hydrogen oxidation reaction (HOR) are negligible under full humidified condition the iR-free cell voltage ($E_{iR-\mathrm{free}}$) can be written as [39]:

$$E_{iR-\mathrm{free}} = E(i) + i\,R_{\mathrm{ohmic}} + i\,R^{\mathrm{Cathode}}_{H^+,cl} = E_r - \eta_{\mathrm{ORR}} + \Delta\eta^{x\,\%RH}_{\mathrm{ORR}(a_{H_2O},\,a_{H^+})} \tag{22}$$

where $E(i)$ is the recorded cell voltage, i is the current density, R_{omic} is the RH-dependent cell resistance, $i\,R^{\mathrm{Cathode}}_{H^+,cl}$ is the RH-dependent proton resistance in the cathode CL, η_{ORR} is the cathode overpotential, $\Delta\eta^{x\,\%RH}_{\mathrm{ORR}(a_{H_2O},\,a_{H^+})}$ represent the changes in the ORR kinetics with RH due to the water and proton activity modification. E_r

	Relative humidity (%)	95	80	70	50
	j at 650 mV as anode	1.05	–	–	–
initial	j at 650 mV ELE0162	1.25	1.09	0.92	0.87
initial	A mg^{-1} at 650 mV ELE0162	3.1	2.72	2.30	2.17
initial	j at 650 mV as cathode	0.41	0.51	0.62	0.67
initial	A mg^{-1} at 650 mV as cathode	6.11	7.61	9.25	10
aged	j at 650 mV ELE0162	0.96	–	–	–
aged	A mg^{-1} at 650 mV ELE0162	2.4	–	–	–
aged	j at 650 mV as cathode	0.27	–	–	–
aged	A mg^{-1} at 650 mV as cathode	4.02	–	–	–
	R/ Ω at 0.5 A cm^{-2}	0.259	0.052	0.019	0.002

Table 4: Current density and mass activity of the three layer electrode evaluated at different relative humidities and ageing periods. Along that, the table indicates the performance of an commercial MEA, containing JM GDEs with 0.4 mg cm^{-2} platinum.

is the thermodynamic cell potential as a function of temperature, reactant partial pressure and water vapor activity (a_{H_2O}) [164]:

$$E_r = 1.23 - 0.9 \times 10^{-3}\,(T-298) + \frac{2.303\,RT}{4F}\log\left[\left(\frac{p_{H_2}}{p^*_{H_2}}\right)^2\left(\frac{p_{O_2}}{p^*_{O_2}}\right)\left(\frac{a^*_{H_2O}}{a_{H_2O}}\right)\right] \tag{23}$$

where R is the universal gas constant, F is the Faraday constant, $\frac{a_{H_2O}}{a^*_{H_2O}} = 1$ for RH$\geqslant$ 100 % and $\frac{a_{H_2O}}{a^*_{H_2O}} \equiv$ RH (given as fraction rather than in %) at saturated conditions.

Considering that the partial pressure of the hydrogen and oxygen are kept constant for all experiments (1.013 bar), the variation of $E_{iR-free}$ is attributed to the well described E_r (Equation 23) and the unknown RH-dependence of the ORR kinetics $\Delta\eta^{x\,\%RH}_{ORR(a_{H_2O},\,a_{H^+})}$. Moreover, the η_{ORR} remain constant and can be expressed as:

$$\eta_{ORR} = \frac{2.303\,RT}{\alpha_c F}\log\left[\frac{i+i_x}{10\,L_{Pt,cath}\cdot A_{Pt,el}\cdot i^*_{o,s}\left(\frac{p_{O_2}}{p^*_{O_2}}\right)^{\gamma}}\right] \tag{24}$$

where α_c is the cathodic transfer coefficient with a determined value of $\alpha_c = 1$ [38], i_x is the H_2 crossover current (A cm^{-2}), $L_{Pt,cath}$ is the platinum loading in mg cm^{-2}, $A_{Pt,el}$ is the catalyst ECSA ($m^2\,g^{-1}$), $i^*_{o,s}$ is the catalyst-specific exchange current density normalized to reference oxygen partial pressure ($p^*_{O_2}$) of 1.013 bar at the reference temperature (T^*) of 80 °C and $\gamma = 0.54$ [39] is the kinetic reaction order with respect to oxygen partial pressure. Thus, inserting the equations 23 and 24 into equation 22, $E_{iR-free}$ can be expressed as

$$E_{iR-free} = 1.23 - 0.9 \times 10^{-3}(T - 298) + \frac{2.303\,RT}{4F}\log\left[\left(\frac{p_{H_2}}{p^*_{H_2}}\right)^2\left(\frac{p_{O_2}}{p^*_{O_2}}\right)\left(\frac{a^*_{H_2O}}{a_{H_2O}}\right)\right]$$
$$- \frac{2.303\,RT}{\alpha_c F}\log\left[\frac{i + i_x}{10\,L_{Pt,cath}\cdot A_{Pt,el}\cdot i^*_{o,s}\left(\frac{p_{O_2}}{p^*_{O_2}}\right)^{\gamma}}\right] + \Delta\eta^{x\,\%RH}_{ORR(a_{H_2O},a_{H^+})} \tag{25}$$

Here, the only unknown variables are the $i^*_{o,s}$ and the possible additional RH-induced overpotential losses, $\Delta\eta^{x\,\%RH}_{ORR(a_{H_2O},a_{H^+})}$. By definition, the later term is zero under fully humidified condition and thus $i^*_{o,s}$ can be determined if all the ohmic losses are quantified adequately, to obtain $E_{iR-free}$ from the measured cell voltage. Considering an exchange current density $i^*_{o,s} = 1.7 \times 10^{-8}\,A\,cm^{-2}$, the Equation 25 allows now the calculation of the $iR-free$ voltages in the case that $\Delta\eta^{x\,\%RH}_{ORR(a_{H_2O},a_{H^+})}$ is assumed to be zero at any of the measured RH. Figure 52a shows the calculated $E_{iR-free}$ values with assumed RH-independent ORR kinetics together with the experimental determined $E_{iR-free}$ values (Equation 22).

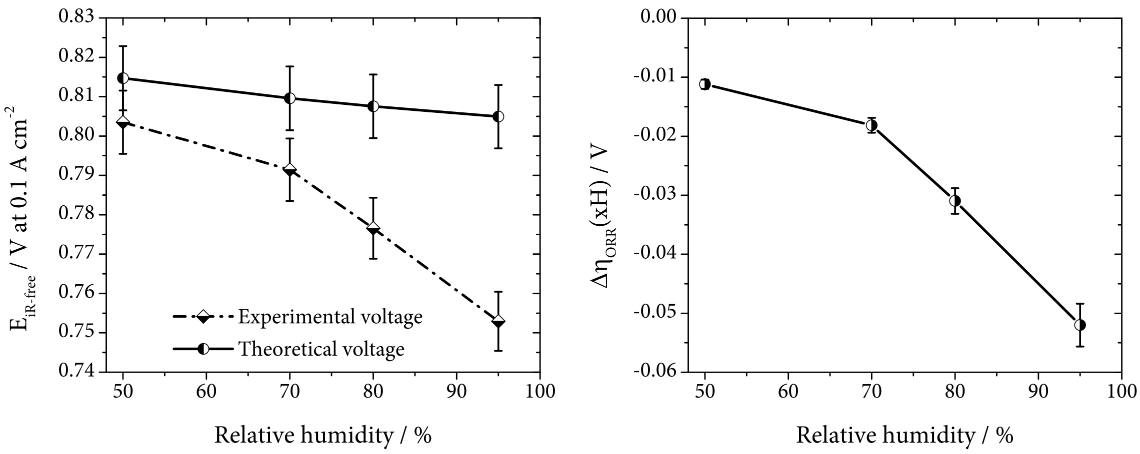

(a) (b)

Figure 52: (a) Comparison of $E_{iR-free}$ values calculated from equation 25 assuming $\Delta\eta^{x\,\%RH}_{ORR(a_{H_2O},a_{H^+})} = 0$ and experimental results from equation 22 at a current density of $0.1\,A\,cm^{-2}$. (b) RH-induced kinetic ORR overpotential losses $\Delta\eta^{x\,\%RH}_{ORR(a_{H_2O},a_{H^+})}$ increase as the relative humidity is reduced.

It should be noted that the experimental results obtained for $E_{iR-free}$ are evidently smaller than the theoretically ones and decrease by increasing the humidity. On the other side, the calculated $E_{iR-free}$ values indicates the same behaviour, announcing a significant $\Delta\eta^{x\,\%RH}_{ORR(a_{H_2O},a_{H^+})}$ increase at low RH. By plotting the voltage difference between the obtained results (Figure 52b), which correspond to

$\Delta\eta^{x\,\%RH}_{ORR(a_{H_2O},a_{H^+})}$, we can say that the introduced multilayer catalyst layer design reveal an improved ORR kinetics at low RH, with a loss of ~11 mV. Therefore, at lower RHs the inserted water quantity is lower and the reactant paths remain free. This proves that the in-situ produced water at the cathode its enough to sustain the necessary humidity.

The applied ageing process demonstrate that the prepared GDE has lost 34.1 % of its initial current density at 650 mV. This value is in accordance with the target proposed by the DOE in 2012 (the ECSA loss should be under 40 % [165]). In addition, the CV measurement reveal an initial ECSA of 43.28 $m^2\,g^{-1}$ and 37.75 $m^2\,g^{-1}$ after the ageing procedure (~ 12 % loss). Additionally, the mass activity remains significantly higher for the self prepared GDE in comparison to the commercial GDE. To understand better the cause of the high stability for the prepared catalyst a TEM analysis is performed. The picture evaluation reveals an average nanoparticle size of 5.1 ± 0.7 nm (Figure 53). Along that, the developed CL design indicates big particle agglomerates.
We suppose that during the nucleation and the growing phases the free $PtCl_6^{2-}$ ions, due to the particle low energy, are attaching to this ones. Furthermore, the not reduced $PtCl_6^{2-}$ and maybe some catalyst particles are washed between new spraying process (see Section 5.2). In this way the total catalyst amount in the MPL decrease. Nevertheless, the achieved catalyst loading is quite small for a PEMFC cathode. According to DOE, the catalyst loading purpose for the cathode is 0.2 $mg\,cm^{-2}$ [89].

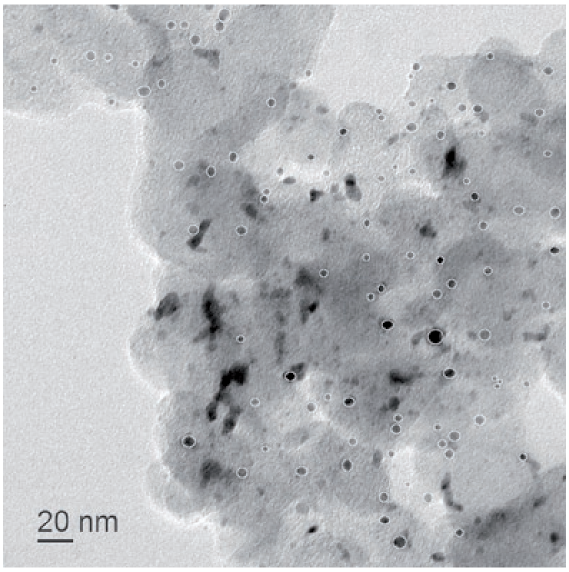

Figure 53: TEM image of the three layer GDE prepared by electrochemical deposition. A significant particles agglomeration can be observed.

Thus, we can sustain that using the studied method, a new CL architecture with improved proprieties can be produced. In the same time the catalyst loading can be reduced without a significant performance decrease.

7.2 CARBON SUPPORT TYPES FOR PEMFC CATHODE

As presented in Chapter 6, to obtain the maximum FC performance, the influence of spraying and electrodeposition parameters needs to be optimized. Up to now, the tuning procedure is accomplish on a single commercial GDL from Freudenberg (H23C8). According to the datasheet, this one has a smooth and high hydrophobic surface [154]. Our investigations have demonstrated that these two properties influence in a positive way the electrodeposition and the FC performance. Nevertheless, it is not clear if this type of GDL represents the best choice for the presented method.

In order to provide an comprehensive answer we have proposed to investigate five different GDLs from two producers. The first two comes from Carbon SE (Wiesbaden, Germany) (SGL) (SGL10BB and SGL30BC), each one with 5 % Teflon in its MPL structure. The only differences concern to the porosity and thicknesses. Therefore, SGL10BB has a thickness of 420 μm and a porosity of 84 %, while SGL35BC has a thickness of 325 μm and a porosity of 80 % [166, 167]. The other GDLs are procured from Freudenberg: H23C4, H23C6 and the already used, H23C8. A complete properties list is provided in citation [154]. In comparison to the other GDLs, H23C4 is the only one without a hydrophobic layer.
Along the presented GDL, a modified H23C8 GDL obtained during the ISECD project is tested. The colleagues from FEM have etched its surface with plasma, so that it presents a reduced hydrophobicity. For the next tests the treated GDL is named H23C8 + P.

The SEM pictures of the sprayed GDL indicate a different surface type. Thus, SGL30BC top side is very smooth and present few cracks (~ 20 ± 3 μm) (Figure 54a). On the other side, H23C4 from Freudenberg shows a porous architecture with multiple cracks. Due to non hydrophobic treatment, the MPL at each bending breaks off very easily. In this way cracks with a width $\leqslant 5$ μm are created (Figure 54b). We suppose that in a such structure, the sprayed precursor and ionomer can be deeper inserted. In the case of H23C8 its MPL is coated with a hydrophobic solution, so that the cracks and the porous network are not visible.
Moreover, the GDL from Freudenberg and SGL differ from each other through the support fibre structure. Thus, the support of SGL GDLs is a straight fibre paper while the other ones, from Freudenberg contain a felt fibres carbon paper substrate.

According to the recorded polarization curves, in comparison to the other prepared GDEs, H23C8 exhibits the best performance (Figure 55a). Also, the plasma treated H23C8 fallows the same direction, but without significant improvements. Both MEAs illustrates a current density of $0.85\,\mathrm{A\,cm^{-2}}$ at $650\,\mathrm{mV\,s^{-1}}$ (Table 5). In addition, the ECSA of the non-treated GDE is with 13 % higher than the plasma handled one, although the difference on platinum loading is $0.05\,\mathrm{mg\,cm^{-2}}$ (Figure 55b). We suppose that due to the low Teflon quantity at the surface of H23C8 + P, during the electrodeposition the $PtCl_6^{2-}$ mobility is enhanced and the created particles are larger. On the other side, the not treated GDL hinder the creation of larger nanoparticles, so that the particle are smaller and in a larger number. An quite unexpected result is registered for H23C4 GDL. Its behaviour illustrates no mass transport limitations although it contain no extra hydrophobic layer. The polariza-

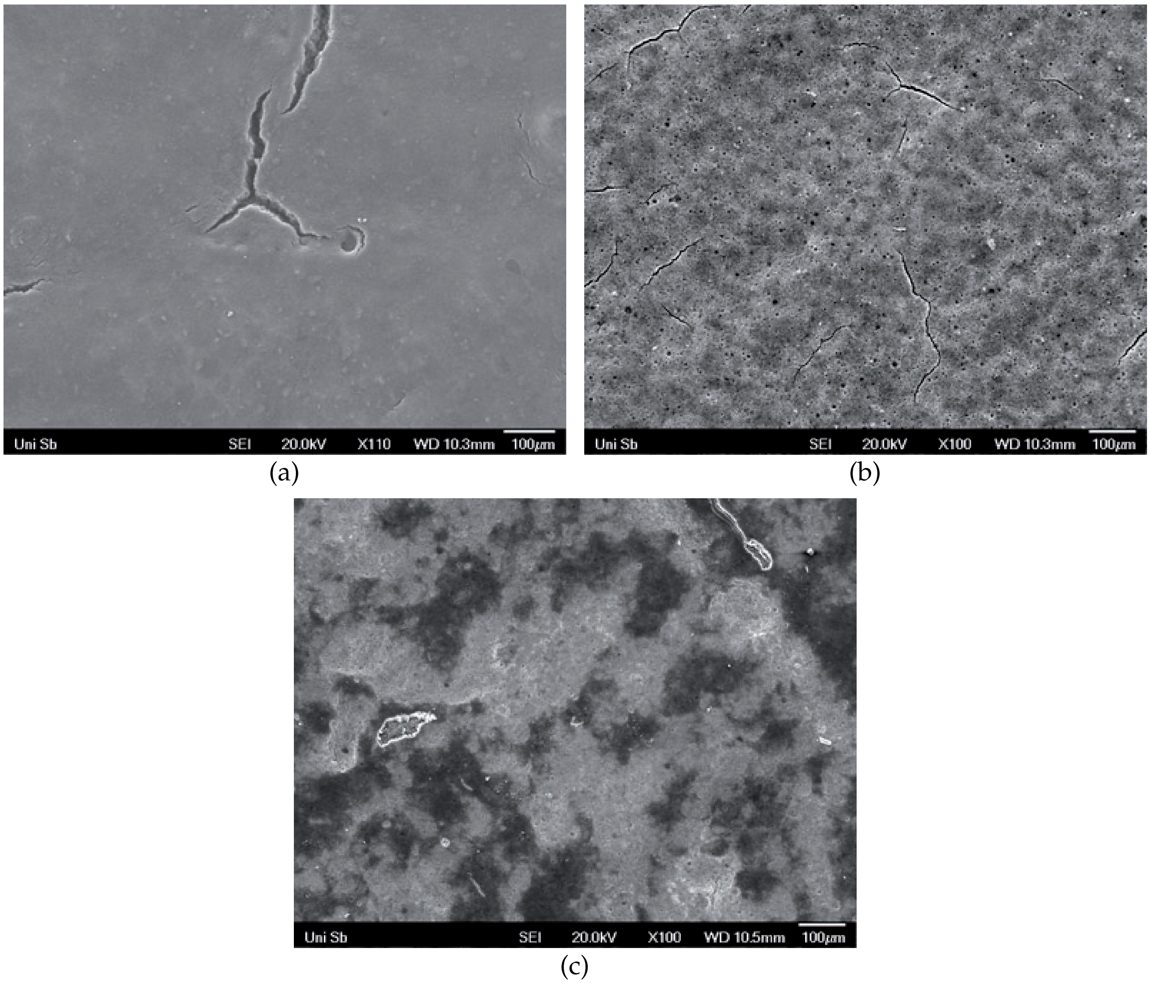

Figure 54: SEM pictures of (a) SGL35BC, (b) H23C4 and (c) H23C8. Each electrode present specific characteristics as porosity, hydrophobicity and cracks.

tion curves in Figure 55a indicate a linear course without mass transport limitations at high currents, for both GDL types. A view over the other GDE performances from SGL and Freudenberg indicates no substantial difference. Both GDLs types show a constant current-voltage characteristic with current densities over 2.1 $\mathrm{A\,cm^{-2}}$ at 350 mV. Moreover, in the case of the GDLs from SGL no notable difference on the ECSA and polarization curve is observed ($48 \pm 5\,\mathrm{m^2\,g^{-1}}$). From all prepared electrodes the SGL30BC shows the highest current density at 650 mV of 0.92 $\mathrm{A\,cm^{-2}}$.

As described at the beginning of the chapter, all prepared electrodes are subjected to an ageing procedure. As can be observed in Table 5, the FCs performances decrease significantly. According to Mecado et al. by polarizing the catalyst in acidic media the particle sintering occur [79]. In addition, through different mechanisms the platinum is dissolute and redeposited on other MPL places [168]. Thus, the highest current density loss at 650 mV is registered for H23C6 with over 27 % from the initial value. At the opposite side is the H23C8 which demonstrate a loss under 16 %. This small decrease in the performance can be attributed to a better contact between the ionomer and catalyst, but also to the efficient water management. Moreover, the losses can be associated with the small contact angle of H23C6, which is significantly smaller than H23C8 or H23C4 [65]. Our assumption is confirmed by

		SGL10BB	SGL30BC	H23C4	H23C6	H23C8	H23C8 + P
initial	ECSA ($m^2\,g^{-1}$)	44.84	46.96	50.11	48.89	53.38	46.74
	PS (nm)	4.37	4.17	3.91	4.00	3.65	4.19
	j at 650 mV	0.81	0.92	0.76	0.72	0.85	0.85
aged	ECSA ($m^2\,g^{-1}$)	37.65	40.17	37.18	33.89	41.40	36.14
	PS (nm)	6.29	4.87	5.27	5.78	4.73	5.42
	j at 650 mV	0.66	0.75	0.62	0.52	0.78	0.67
	j losses at 650 mV (%)	19.09	19.00	17.93	27.48	15.59	20.62
	ECSA losses (%)	16.04	14.45	25.80	30.68	22.73	22.67

Table 5: Summary of the FC performance for the electrodes prepared using distinct GDL. The developed GDE are tested as cathode in a PEMFC at 80 °C and 95 % RH.

the plasma treated GDL which indicates an accentuated performance loss of 20.6 %. Nevertheless, the H23C4 which contains no Teflon layer, shows a small current density loss at 650 mV, of ~18 %.

So, we conclude that the Teflon extra coating does not influence significantly the FC performance losses. The GDEs performances are influenced at most by the support hydrophobicity. This result is sustained by the SGL10BB and SGL30BC, which have the same structure and the same substrate hydrophobicity. The losses are similar (~19 %) for both GDEs. As reported by El-Kharouf the SGL MPLs presents a lower water contact angle than the substrate itself [65]. This interesting feature shows its influence in the ECSA after the electrochemical ageing. Thus, the SGL30BC suggest the smallest ECSA losses (~15 %) from all prepared GDEs. Close to this value is the ECSA of SGL10BB. Also the other MEAs indicate losses below 31 %, a fact that shows an improved stability. As expected, the H23C8 and the H23C8 + P reveal the same losses percentage of ~22 %. It can be also observed that the deposited platinum quantity does not depend on the substrate type (Figure 55b). It can be recognized that for H23C4 the deposited platinum quantity is lower as for others. A possible explanation could be that due to the low hydrophobicity a significant precursor quantity permeate through the MPL to an position where it cannot be electrochemically reduced.

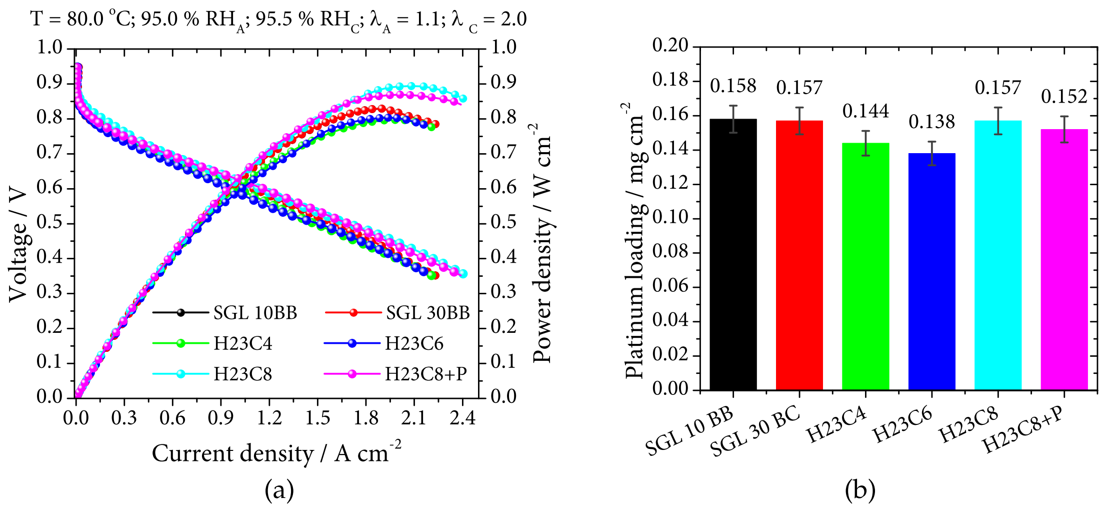

Figure 55: (a) Polarization curves of the electrodeposited electrodes tested as cathode and (b) catalyst loading obtained from the ICP – OES measurement for distinct substrates.

Therefore, the GDLs from SGL present an improved performance with an enhanced corrosion resistance. On the other side, the GDEs containing the Freudenberg GDLs exhibit a higher ECSA. Comparing the recorded results of all samples we can say that the GDL type does not influence the FC performance. Additionally we have proved that the electrochemical method can be applied on any GDL type.

7.3 CATALYST LOADING VARIATION

On the conventional GDE preparation methods, plenty catalyst sites are not electrochemically active. Therefore, to increase the TPB density we have optimised the method presented in Section 5.2. However, up to now the catalyst loading has varied so much, that an exact power to catalyst loading quantification cannot be done. Thus, we propose to study systematically the electrocatalyst loading influence on the PEMFC performance. In detail, four distinct platinum loadings are investigated: $0.05\,mg\,cm^{-2}$, $0.1\,mg\,cm^{-2}$, $0,2\,mg\,cm^{-2}$ and $0.4\,mg\,cm^{-2}$. During the electrodeposition and spraying process the parameters presented in Table 3 are used.
The polarization curves presented in Figure 56 indicate a high performance with current densities $\geqslant 2\,A\,cm^{-2}$ at $350\,mV$ for each prepared sample. Also, after the ageing procedure the catalyst remains stable and develops current densities above $1.5\,A\,cm^{-2}$ at $350\,mV$.
Table 6 present in details the performances of the developed electrodes. It can be observed that the highest ECSA is obtained for a loading of $0.05\,A\,cm^{-2}$. In addition, its noticed that the ECSA decrease by growing the catalyst loading. This can be attributed to the big particles created during the electrodeposition. This idea is sustained by the ageing procedure, which shows for the electrode containing $0.4\,mg\,cm^{-2}$ catalyst a loss of $15\,\%$ at $650\,mV$. Quite unexpected is the behaviour of the GDE with $0.05\,mg\,cm^{-2}$ loading. Its indicate the highest loss after the ageing process, but it still sustains the highest mass activity of all prepared samples ($13.28\,A\,mg^{-1}$).

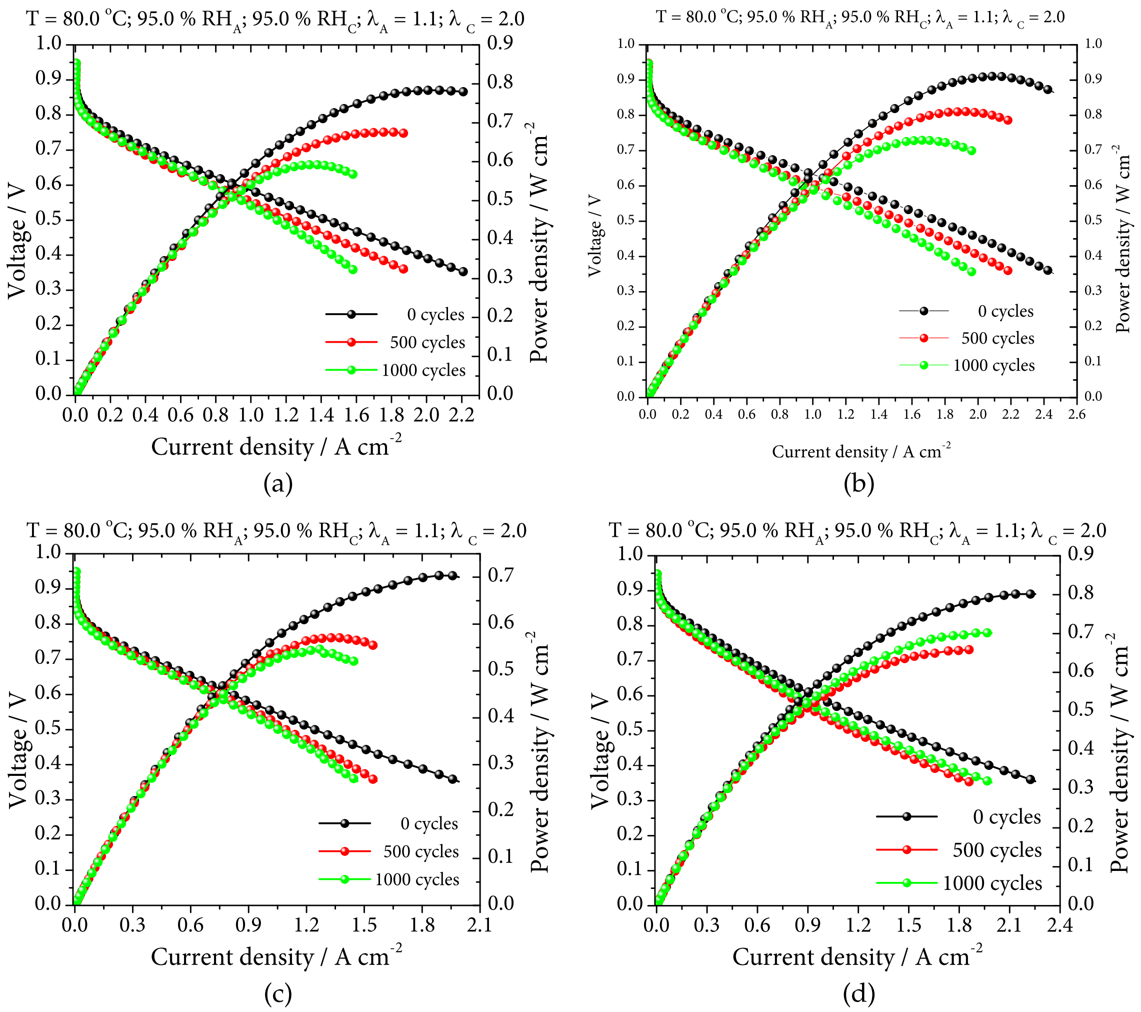

Figure 56: Polarization curves of the electrodes containing a catalyst loading of (a) 0.05 mg cm^{-2}, (b) 0.1 mg cm^{-2}, (c) 0.2 mg cm^{-2} and (d) 0.4 mg cm^{-2}. The investigation were made before and after an ageing procedure.

	Catalyst loading (mg cm^{-2})	0.05	0.1	0.2	0.4
initial	ECSA (m^2 g^{-1})	126.19	93.47	64.25	84.80
	j at 650 mV	0.66	0.89	0.61	0.73
	A mg^{-1} at 650 mV	13.28	8.91	3.03	1.83
	g kW^{-1} at 650 mV	0.12	0.17	0.51	0.84
aged	ECSA (m^2 g^{-1})	94.50	67.88	46.45	73.00
	j at 650 mV	0.50	0.70	0.52	0.62
	A mg^{-1} at 650 mV	10.02	7.01	2.62	1.54
	g kW^{-1} at 650 mV	0.15	0.22	0.59	1.00
	j losses at 650 mV	24.55	21.32	13.37	15.59

Table 6: MEAs performance analysis at 650 mV before and after ageing process. Each MEA contains at the cathode a GDE with a different catalyst loadings.

To understand better the kinetic and mass transport losses, the polarization curves are analysed using a semiempirical model [169]. The FC voltage E at the current density i is described by

$$E = E_0 - i R_{ohmic} - b \log(i) - m \exp(n i) \quad (26)$$

where

$$E_0 = E_r + b \log(i_0) \quad (27)$$

E_r is the reversible potential which is 1.18 V at 80 °C (see Equation 23), i_0 and b are the Tafel parameters for oxygen reduction and R_{ohmic} is the ohmic resistance. The predominant contribution to R_{ohmic} is the ohmic resistance of the electrolyte. The last term in Equation 26 is an empirical quantity that describes the high current overpotential that is associated with the mass transport [170]. This term can be expressed as a voltage difference (ΔE) between the expected value of E and the experimental value

$$\Delta E = m \exp(n i) \quad (28)$$

where m and n are constants and have the units of potential and current density, respectively.

	Catalyst loading ($mg\,cm^{-2}$)	0.05	0.1	0.2	0.4
	E_r (V)	1.18	1.18	1.18	1.18
initial	b ($mV\,dec^{-1}$)	50.33	44.33	52.18	48.56
initial	i_0	$5.1 \cdot 10^{-9}$	$1.4 \cdot 10^{-9}$	$1.1 \cdot 10^{-8}$	$2.1 \cdot 10^{-8}$
initial	R_{ohmic} ($\Omega\,cm^{-2}$)	0.17	0.15	0.20	0.19
initial	ΔE	$3.6 \cdot 10^{-16}$	$4.2 \cdot 10^{-4}$	$6.9 \cdot 10^{-3}$	$8.9 \cdot 10^{-3}$
aged	b ($mV\,dec^{-1}$)	53.15	61.91	54.35	48.63
aged	i_0	$9.1 \cdot 10^{-9}$	$9.9 \cdot 10^{-9}$	$1.2 \cdot 10^{-8}$	$1.3 \cdot 10^{-8}$
aged	R_{ohmic} ($\Omega\,cm^{-2}$)	0.19	0.15	0.21	0.22
aged	ΔE	0.015	0.001	0.019	0.046

Table 7: Fit results for the samples prepared with different catalyst loading using the equation 26.

As can be observed in Table 7 the ΔE on the initial state is very small, indicating no mass transport limitations. After ageing, the ΔE increase significantly for all prepared samples. The same behaviour is registered also for the Tafel slope. In comparison to the theoretical one ($2.303\,R\,T/\alpha\,n\,F = 70\,mV\,dec^{-1}$) the obtained values are under this value, illustrating a two electrode mechanism. Moreover, the cell resistance, R_{ohmic} grows by increasing the catalyst loading. In addition for each sample after the ageing step, the cell resistance increases, suggesting a catalyst shift in the MPL structure.

According to the obtained results we can say that the electrodeposition method is suitable to create CLs with well defined loadings and with a high electrochemically activity. We suggest the application of this method for platinum loadings up to $0.2\,\mathrm{mg\,cm^{-2}}$. A further increase in the loading induces particle agglomeration and a platinum waste.

7.4 UPSCALE THE GDE PRODUCTION

Along to the improvements on the spraying and electrodeposition parameters our objective is to prepare, using the electrochemical method GDEs with a size larger than $50\,\mathrm{cm^2}$. Therefore, as presented in Section 5.3 a new deposition cell with an active area of $225\,\mathrm{cm^2}$ is constructed. In addition, to study the effect of the upscaling a new fuel cell housing with an active area of $50\,\mathrm{cm^2}$ is tested (see Section 4.2). Thus, having all the necessary hardware components, GDEs with a catalyst loading of $0.2\,\mathrm{mg\,cm^{-2}}$ and $0.2\,\mathrm{mg\,cm^{-2}}$ ionomer are produced. As for the previously prepared GDE on this chapter, the parameters listed in Table 3 are applied.
In order to investigate the performances of the new prepared GDEs, MEAs containing the same components but with different sizes ($10\,\mathrm{cm^2}$ and $50\,\mathrm{cm^2}$) are investigated. This configuration is chosen to be sure that the deposited catalyst loading is uniform distributed along the GDE surface. Moreover, we want to examine the FC housing influence on the GDE operation. For both cell configuration the prepared GDE are tested as cathode.

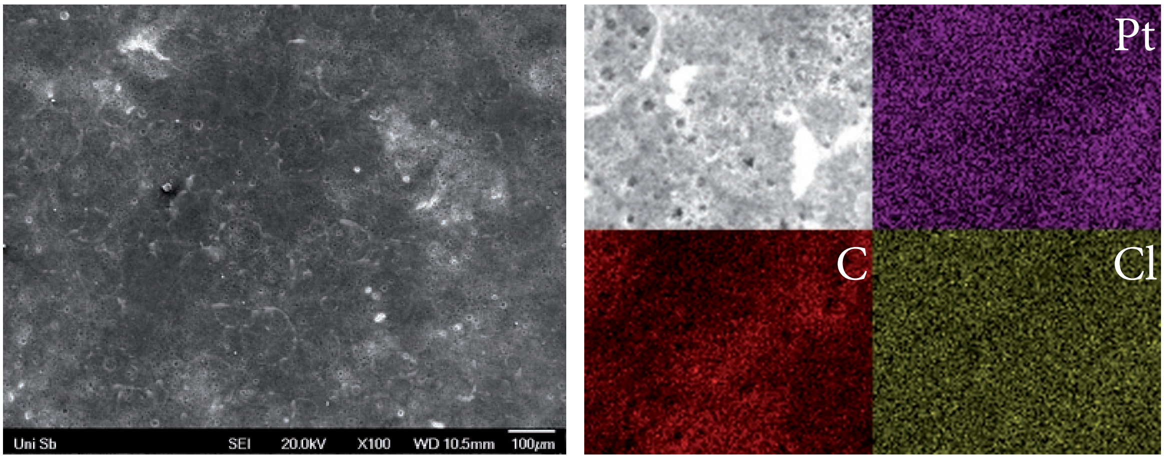

(a) (b)

Figure 57: (a) H23C8 MPL surface after the electrodeposition process. (b) Element mapping using the energy-dispersive X-ray spectroscopy. The pictures indicates an uniform platinum dispersion, but also a high quantity of Cl in the MPL network.

As can be observed in Figure 57a due to the slow solvent evaporation, the GDL surface presents circles formed after the spraying process. We suppose that the edge of this circles contains the ionomer. These can influence the electrodeposition process in a negative way. However, on the recorded SEM picture the pore structure is visible and unrestricted. The element mapping of the prepared GDE indicates a good platinum distribution on the MPL surface (Figure 57b). Unfortunately, during the analysis a high quantity of chlorine is found. Since the pictures are recorded after the electrodeposition process, the registered Cl can represent the not reduced

$PtCl_6^{2-}$ or Cl^-. In comparison to a bath electrodeposition process where the products remain in the liquid, here the ions are attaching on the platinum catalysts and on the carbon support. Even if the GDE is washed for at least three times the Cl^- ions are not removed.
The recorded polarization curves indicates an improved performance for the 50 cm^2 FC. Thus, the samples tested in the big cell illustrates an initial current density of 0.82 A cm^{-2} at 650 mV. Table 8 shows the performances of the GDE tested in these two developed fuel cell housings. Very interesting are the recorded results after the cell ageing. Both MEAs indicate a current density of 0.5 ± 0.05 A cm^{-2} at 650 mV. We assume that in the 50 cm^2 FC housing the water management is improved due to the long channels. So, the water is retained for longer times in the cell and the membrane is better humidified.

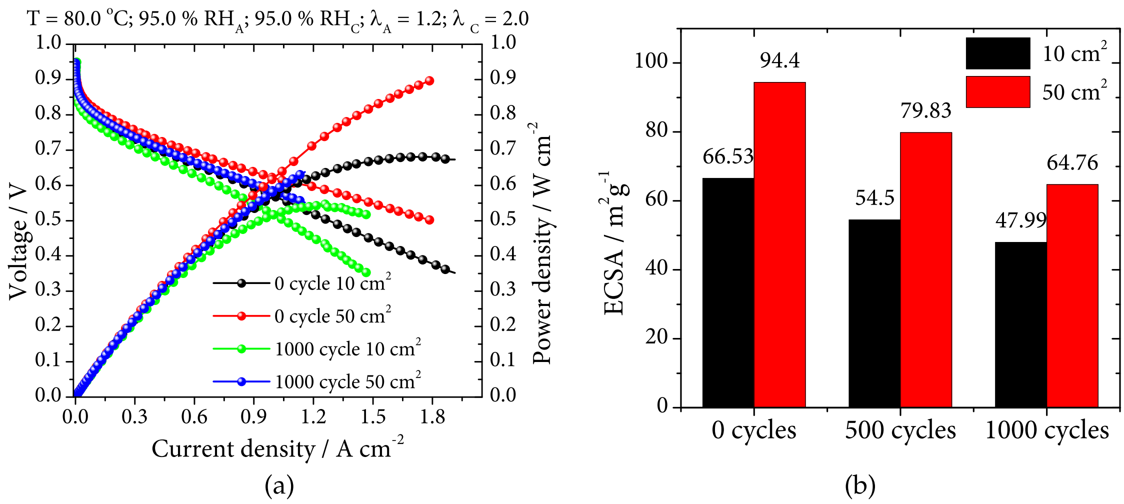

Figure 58: (a) Polarization curves of the up-scaled GDE, tested in two different FC housings. (b) ECSA of the same electrode, calculated at the initial state and after 1000 cycles ageing.

The calculated ECSA reveal a significant increase for the big cell (Figure 58b). This unexpected result can be explained by small catalyst variations along the GDE surface. Due to the big surface (over 225 cm^2), during the spraying process the GDL the temperature is not homogeneous and small ionomer agglomerates occur. Thus, the precursor and the ionomer does not penetrate to the same depth and a part of the $PtCl_6^{2-}$ cannot be electrochemically reduced.

We consider that the 50 cm^2 FC housing distributes the humidified gas better in the GDE structure. Moreover, due tot the large active area no significant influences of the catalyst loadings variations can be observed. Additionally, because of the optimum water management the catalyst sites remain free to reduce the oxygen even at high current densities.

7.5 IONOMER LOADING OPTIMIZATION

A fundamental requirement for the FC marketing is the operation with the O_2 from the atmospheric air. Nevertheless, this configuration implies a new GDL architecture and a better electrocatalyst. One of the big problems is the low ORR and

		$10\,cm^2$	$50\,cm^2$
initial	j at $650\,mV$	0.64	0.82
	$A\,mg^{-1}$ at $650\,mV$	3.2	4.1
	j at $900\,mV$	$1.2 \cdot 10^{-3}$	$3.8 \cdot 10^{-3}$
	$A\,mg^{-1}$ at $900\,mV$	$6.3 \cdot 10^{-3}$	$1.9 \cdot 10^{-2}$
aged	j at $650\,mV$	0.52	0.57
	$A\,mg^{-1}$ at $650\,mV$	2.6	2.88
	j at $900\,mV$	$2.9 \cdot 10^{-3}$	$3.5 \cdot 10^{-3}$
	$A\,mg^{-1}$ at $900\,mV$	$1.4 \cdot 10^{-2}$	$1.7 \cdot 10^{-2}$
	j losses at $650\,mV$ (%)	18.75	29.75

Table 8: Performances of the GDEs tested on two different cell housings. The samples tested in the $50\,cm^2$ cell indicates an improved operation.

O_2 quantity in the air (~21 %). In addition, due to the accumulation of nitrogen in the cathode pores concentration polarization appears [171]. A solution for this impediments is to increase the reactant pressure and the flow rate. Therefore, the FC housing tightness and membrane thickness should be considered. More over, the cathodic GDE needs to be structured with enough pores and reactant paths. Along to these problems, the impurities in the air stream can affect in a negative way the FC performance [27]. According to Lee et al. to increase the catalyst efficiency the CL thickness should be very small and the loading needs to be reduced [172]. For an optimum FC operation also the ionomer quantity need to be appropriate [173].

As result of previously optimizations, GDEs are produced and tested in a H_2/air system. Each one contains a loading of $0.4\,mg\,cm^{-2}$ platinum and a distinct ionomer loading of $0.1\,mg\,cm^{-2}$, $0.2\,mg\,cm^{-2}$ and $0.3\,mg\,cm^{-2}$. The performance analysis are performed by ZBT in a $25\,cm^2$ fuel cell housing, at an absolute pressure of $2.5\,bar$ (H_2/air). Furthermore, the prepared GDE are supposed to an ageing procedure.

Figure 59a shows the performance of the prepared samples. As can be observed the samples with a Nafion™ loading of $0.1\,mg\,cm^{-2}$ and $0.2\,mg\,cm^{-2}$ shows current densities over $0.7\,A\,cm^{-2}$ at $650\,mV$. The sample with $0.3\,mg\,cm^{-2}$ Nafion™ provide a current density of $0.34\,A\,cm^{-2}$. A explanation for this large voltage fall is the high Nafion™ loading. During the spraying process most of the pores are covered by the ionomer and the gas paths are obstructed. A performance summary of the prepared samples is presented in details in Table 9.

The electrochemical impedance measurements at $0.66\,A\,cm^{-2}$ sustain these hypothesis (Figure 60a). As can be observed, the total resistance of the sample containing $0.3\,mg\,cm^{-2}$ Nafion™ is with $0.1\,\Omega\,cm^{-2}$ higher than other two. The catalyst and diffusion resistance of all three samples are comparable but on the sample that incorporates a larger Nafion™ amount, the membrane resistance increase. This indicate a considerable ionomer quantity at the electrolyte/GDE interface.

The ageing process indicates a good stability for all prepared samples, with a loss at $650\,mV$ under 33 %. The large current density loss is observed for the sample

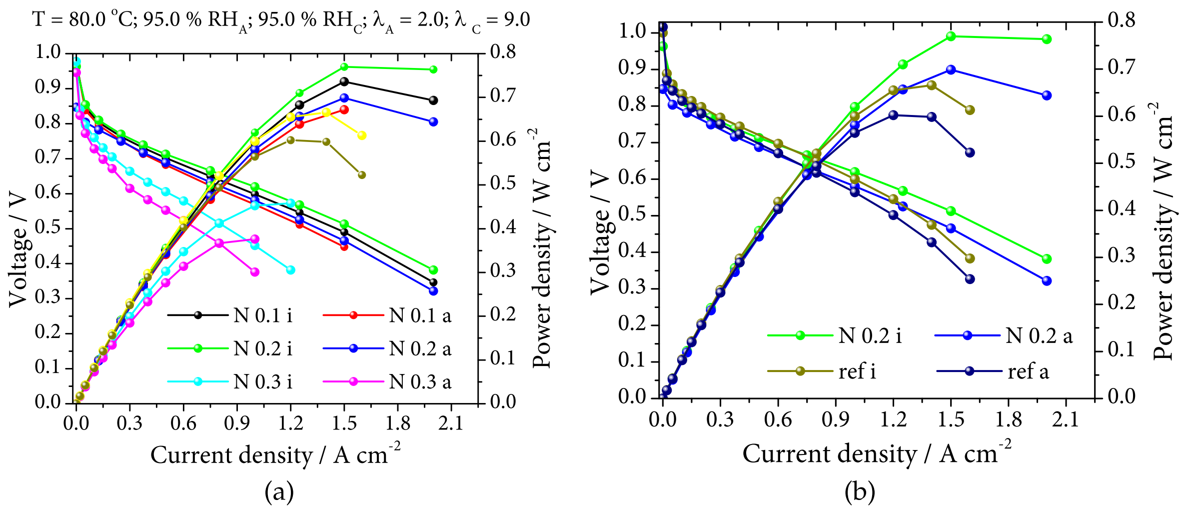

Figure 59: (a) Polarization curves of the GDE containing different Nafion™ loading. (b) Comparison of the self-prepared GDE and a commercial one, containing the catalyst form JM. All polarization curves, before and after ageing are recorded at 2.5 bar.

prepared with $0.3\,\mathrm{mg\,cm^{-2}}$ Nafion™. Additionally, this GDE indicates the lowest ECSA loss (4.9 %). We consider that due to the thicker Nafion™ layer the catalyst is better protected. Thus, the ionomer prevents the platinum ions moving and agglomeration in large clusters. After the ageing procedure, all the samples shows an increased total resistance, especially that with $0.2\,\mathrm{cm^2}$ ionomer loading. This indicates a clearly R_{diff} increase due to the partially platinum and ionomer intercalation. Also the GDE containing $0.1\,\mathrm{mg\,cm^{-2}}$ ionomer exhibit an increase of cathodic charge transfer resistance, a fact that indicates the catalyst migration.

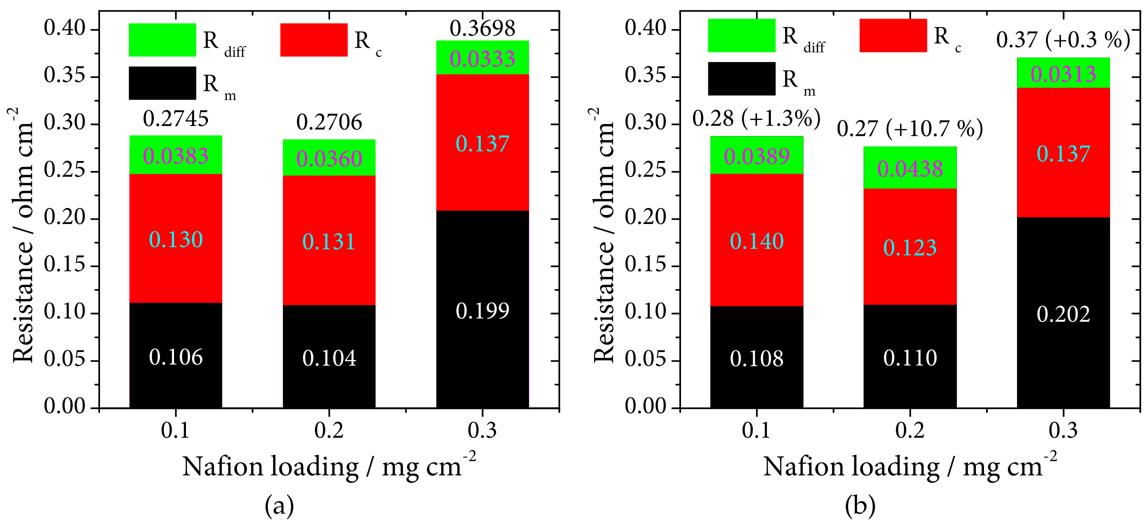

Figure 60: Resistances obtained for the prepared electrode by fitting the EIS curves recorded at a current density of $0.1\,\mathrm{A\,cm^{-2}}$ at (a) initial state and (b) after ageing. The used circuit is exemplified on Figure 9a.

In order to compare the prepared catalyst properties with a commercial electrocatalyst, a MEA containing at anode and cathode catalysts from JM (HiSPEC4000), with a loading of $0.36\,\mathrm{mg\,cm^{-2}}$ is produced. Although the electrocatalyst loading difference is very small, the self-prepared electrodes exhibit the same performance (Figure 59b). In detail, the commercial electrode displays a current density of $0.8\,\mathrm{A\,cm^{-2}}$ at $650\,\mathrm{mV}$ while the self-produced GDE exhibit $0.83\,\mathrm{A\,cm^{-2}}$. However, after the ageing procedure both systems manifest a current density of $0.67\,\mathrm{A\,cm^{-2}}$ at $650\,\mathrm{mV}$. Another surprising property of the developed GDE is the mass activity of $0.72\,\mathrm{A\,mg^{-1}}$ at $0.9\,\mathrm{V}$ which is with $30\,\%$ higher than that of the commercial catalyst.

		Nafion$^{\text{TM}}$ 0.1	Nafion$^{\text{TM}}$ 0.2	Nafion$^{\text{TM}}$ 0.3
initial	ECSA ($\mathrm{m^2g^{-1}}$)	29.67	35.33	14.91
	$\mathrm{A\,mg^{-1}}$ at $650\,\mathrm{mV}$	1.87	2.07	0.85
	j at $650\,\mathrm{mV}$	0.74	0.83	0.34
aged	ECSA ($\mathrm{m^2g^{-1}}$)	24.58	31.58	14.18
	$\mathrm{A\,mg^{-1}}$ at $650\,\mathrm{mV}$	1.5	1.67	0.57
	j at $650\,\mathrm{mV}$	0.63	0.67	0.23
	losses at $650\,\mathrm{mV}$ (%)	15.88	19.27	32.35
	ECSA loss (%)	17.14	10.57	4.87

Table 9: Performances of the GDEs tested on two different cell housings. The samples tested in the $50\,\mathrm{cm^2}$ cell indicates an improved operation.

7.6 SUMMARY

The developed spray and deposition methods are applied to produce GDE for PEMFC cathode. Therefore, the tuned parameters obtained on the Chapter 6 are utilized to coat GDLs with distinct platinum and ionomer loadings. In order to investigate the PEMFC performances over long times an accelerated procedure is proposed. Thus, the cell potential is swept between $0.4-1.4\,\mathrm{V}$ vs. DHE for 500 times and then for another 500 times between $0.05-1.4\,\mathrm{V}$ vs. DHE.
To prove the capability and the flexibility of the developed deposition method a new CL architecture is introduced. A multilayer structure with three distinct layers, each one with $0.1\,\mathrm{mg\,cm^{-2}}$ catalyst and ionomer loading is produced. The results indicate that the proposed structure influences in a positive way the PEMFC performance. Furthermore, the produced structure indicates a strong dependence on the reactants humidity. The calculations have revealed that the ORR of the new created structure increases by reducing the inlet gas RH.

A factor which affects the GDE performance is its substrate type. For a better overview, different commercial GDLs are studied as catalyst support. GDLs from Freudenberg and SGL are coated with the same electrocatalyst loading and tested under the similar conditions in the self-developed test station (see Chapter 4). Moreover, to reduce the hydrophobicity of the substrate, plasma treated GDL from Freudenberg are employed as substrate. According to the recorded curves no significant power decrease is observed. Likewise, all prepared GDEs show the same catalyst loading. The CV measurements illustrate a high ECSA, with a maximum of $53.38\,m^2g^{-1}$ for the H23C8 from Freudenberg. The prepared catalysts show a high stability. After the ageing process the ECSA losses are under 21 % for all produced samples. To study in detail how the catalyst loading influences the cell performance four different electrocatalyst loadings are investigated ($0.05\,mg\,cm^{-2}$, $0.1\,mg\,cm^{-2}$, $0.2\,mg\,cm^{-2}$ and $0.4\,mg\,cm^{-2}$). It should be emphasized that the proposed method is suitable to prepare GDE with a catalyst loading $\leqslant 0.2\,mg\,cm^{-2}$. However, the Nafion^{TM} loading affect at most the quantity of deposited platinum. A outstanding positive result is obtained for the sample prepared with $0.05\,mg\,cm^{-2}$ platinum which shows a mass activity at $650\,mV$ of $13.28\,A\,mg^{-1}$.

Along the physical parameters optimization, the upscaling possibilities of this new method are investigated. Therefore, using the deposition cell developed in Chapter 7, samples with an active area of $225\,cm^2$ are prepared. The study has revealed a performance comparable with the small electrodeposition cell ($50\,cm^2$). Moreover, the performed test on two different fuel cell housing ($10\,cm^2$ and $50\,cm^2$) indicates an improvement on the FC with an active area of $50\,cm^2$ in comparison to the $10\,cm^2$ cell.

A fundamental requirement for future PEMFC applications is the operation with the atmospheric air. With the help of colleagues from ZBT Duisburg, multiple samples are investigated in a H_2/air configuration at a pressure of $2.5\,bar$ absolute. The research has revealed that an ionomer loading in the range of $0.1-0.2\,mg\,cm^{-2}$ provides the best results. An increase in the Nafion^{TM} loading indicates the pore obstruction and a significant FC performance decrease. Additionally, the obtained results indicate that the electrochemically prepared catalyst provides a better activity than the commercial electrocatalyst (HiSPEC4000) from JM.

Thus, the electrodeposition method has been successfully applied to produce highly electrochemically active catalysts for ORR. Platinum utilisation and therefore catalyst loading under $0.1\,mg\,cm^{-2}$ can be achieved, with an improved PEMFC performance.

8 CONCLUSION AND FUTURE WORK RECOMMENDATIONS

In the focus of this study was the development of GDEs with as low as possible catalyst loading, using an electrochemically technique. In order to boost the electrocatalyst performances, the electrodeposition process takes place in-situ, so that most of the produced catalyst particles are situated at the triple-phase-boundary. Due to the rigorous electrodeposition profile the morphology of the created electrocatalyst can be precisely controlled. Thus, during the first step the precursor ions are assembled in nuclei. In the next pulse, according to the growth time, the cores grow by collecting more precursor ions and finally create a nanoparticle. In order to produce GDEs with a reduced loading, a new spraying device is developed. A commercial 3D printer produced by Velleman is modified by replacing the printing head with an in-house designed spraying equipment. Using the developed system, samples with an area up to $400\,\mathrm{cm}^2$ can be sprayed in a semi-automatic way. Along that, the system can spray different solutions without corrosion risks. Simultaneously, the self-built LV software offer a high precise movement and dosing control. So, the precursor and the ionomer can be homogeneously distributed over the surface of a commercial GDL. To find the best spraying and deposition parameters an intense effort was made to tune up these systems. Therefore, the influence of multiple physical parameters as temperature, pressure and relative humidity is examined.

For an easier and efficient PEMFC characterisation, a test station is developed. In addition to the commercial parts (thermostats, mass flow controllers, heating cartridge, etc.), the produced system contains a powerful controlling board, with over 20 inputs/outputs. A self-developed firmware manage all the components. Having the control in a centralized unit offers a higher safety degree and a simple device management. Simultaneously, the LV developed program displays in a styled mode the recorded data. Additionally, it contains a flexible experiment organizer with more that 30 possible techniques. An high attention is provided to the humidification system which contains a Nafion™ tube. So, relative humidities up to $100\,\%$ can be achieved with an accurate control. Moreover, the developed test station can be used for PEMFC with different sizes and can perform current measurements up to $80\,\mathrm{A}$. Together with the company Gamec Analysentechnik one testing platform is commercialized.

In addition to these two devices a new fuel cell housing with an active area of $10\,\mathrm{cm}^2$ is designed. For a better reactant distribution it contains four channels, each one with a width of $0.8\,\mathrm{mm}$ and a length of $175\,\mathrm{mm}$. To avoid the water accumulation, the proposed flow field presents four bends. Due to successful tests, the $10\,\mathrm{cm}^2$ cell architecture is upscaled to $50\,\mathrm{cm}^2$. Both models can be very easy connected on the self-constructed FC test station using $6\,\mathrm{mm}$ Swagelok connections. During the PhD period, over ten cells with distinct sizes are produced, all of them offering precisely and valuable data.

Following the same principle, an improved electrodeposition cell is constructed. In comparison to a fuel cell housing, the cathode side is reshaped, so that the sample is uniformly pressed on the electrolyte. Thus, the GDL containing the precursor establish an optimum contact with the electrolyte and the protons path is improved. The deposition cell contains simultaneously an improved sealing and membrane stretching system. The last feature makes possible the use of the electrolyte over many electrodeposition processes. Another cell advantage is the possibility to use the same electrodeposition cell for GDLs with distinct thicknesses. More over, the developed cell can be employed on the electrodeposition of any type of metals precursors in an anhydrous form. Additionally, the developed deposition cell permits a precise temperature control. For an accurate gas humidity management a Nafion^{TM} humidification system is implemented. Considering the necessitate of bigger GDEs, in actual work the spraying and electrodeposition process was upscaled to produce GDE with a size of $225\,\mathrm{cm}^2$.

With all the above mentioned studies, some important results and findings are summarized by the following:

1. As result of in-situ electrochemical reduction of hexachloroplatinic acid, most of the particles are situated at the triple-phase-boundary. Using a commercial GDL from Freudenberg the implicated physical parameters on catalyst creation have been studied. For a simple electrocatalyst evaluation the prepared GDE were tested as anode in the self developed fuel cell housing.
    - Ahead the electrodeposition process, the GDL need to contain the precursor in an anhydrous state. Thus, two different methods to apply the ionomer and the precursor on the GDL surface are examined. The use of an impregnation method has revealed a very bad catalyst formation, with particle sizes of $19 \pm 6\,\mathrm{nm}$. In order to increase the particle density and to reduce its size, the commercial GDL was coated with a mixture of carbon, Teflon and ionomer. By applying the electrodeposition technique a significant improvement on the catalyst morphology was observed. Additionally, the FC investigations have disclosed a current density improvement of $\geqslant 60\,\%$ at a voltage of $650\,\mathrm{mV}$, versus the initial approach. The experiments have illustrated that due to the high MPL hydrophobicity and small pore size the impregnation method is not suitable. Furthermore, due to the small GDL thickness the necessary solvent volume is limited to few $\mu\mathrm{l}$, affecting the precursor distribution on the MPL structure.
    - It was observed that by using a spraying technique the catalyst particles have a size of $4 \pm 0.6\,\mathrm{nm}$. Moreover, the created structure indicates a current density increase at $650\,\mathrm{mV}$ of $10\,\%$ in comparison to the impregnated one.
    - In order to reduce the catalyst loading and to maintain a high PEMFC performance the parameters involved in the spraying and electrodeposition processes are in detail optimised. Thus, it was found that the spraying order of both components (precursor and ionomer) affects the catalyst layer structure. The investigations on six distinct configurations have shown

that by mixing the Nafion™ with the precursor before spraying provides the highest power density. The research indicates that when the ionomer is sprayed on the fist layer the GDL pores are obstructed and the precursor cannot go deep in the MPL network. So, most of the $PtCl_6^{2-}$ are not electrochemically reduced and the platinum is wasted.

- Other parameters which influence the CL architecture are the GDL temperature and the driving gas pressure during the spraying process. By modifying the first parameter, the solvent evaporation rate can be controlled. So, the ionomer and the precursor can permeate deeper in the MPL structure. The variation of this parameter has revealed that for a higher spraying temperature the obtained CL exhibit improved electrochemical proprieties. By positioning the catalyst at the top of the MPL, a directly contact between the catalyst and electrolyte is accomplished. To arrange the electrocatalyst deeper in the MPL the driving gas pressure was varied in a range of $1.5 - 3.5\,\mathrm{bar}$. The examinations indicate a maximum performance for the precursor sprayed at a pressure of $2\,\mathrm{bar}$. Additionally, a significant decrease of the catalyst loading and FC performance is observed by growing the spraying pressure. At the maximum pressure of $3.5\,\mathrm{bar}$ the high gas flow evaporates the solvent very fast, so that a small amount of $PtCl_6^{2-}$reaches the GDL surface. Additionally, the high gas flow blows most of the precursor and ionomer from the MPL surface. The analysis on the GDEs transversal section have revealed a CL thickness of $\sim 2\,\mu m$ for the samples prepared at $2\,\mathrm{bar}$ and only $\sim 0.5\,\mu m$ for those produced at $3.5\,\mathrm{bar}$. Thus a pressure of $2\,\mathrm{bar}$ was found to be optimum for the spraying process.
- To obtain a precise catalyst layer thickness, the influence of solvent composition was investigated. Thus, the boiling point of the solvent was increased from 82.6 °C to 100 °C by adding water. According to the recorded polarization curves the PEMFC performance increases by growing the IPA concentration, until its reaches a maximum at 40 % IPA. Up to this point the measured current density at 650 mV remains constant at a value of $1.0 \pm 0.01\,\mathrm{A\,cm^{-2}}$. Besides, at low IPA concentrations the catalyst loading is reduced, followed by a slight increase at IPA concentrations over 40 %. This strange behaviour can be described as a reduced catalyst layer thickness. Due to the high MPL hydrophobicity and the slowing evaporation rate, the precursor remains at the GDL surface. The analysis of the GDE transversal section indicates a catalyst layer with a thickness of $\sim 6\,\mu m$.

2. An great emphasis was placed on the catalyst morphology. Therefore, the importance of electrodeposition parameters (electrolyte humidity, deposition temperature and pulse amplitude) was analysed.
   - Thus, by variation of deposition cell relative humidity it was observed that the deposited platinum quantity increases exponentially with the RH. Also, at low humidities ($\leqslant$ 80%) the created catalyst particles exhibit agglomerations. The test station measurements indicate a signifi-

cant current density increase at the working voltage of 650 mV with the RH (~30 %).

- For an improved proton kinetics, the deposition cell temperature was increased up to 70 °C. The examinations have revealed that the cell performance remains constant up to a temperature of 50 °C. Additionally, by increasing the temperature a boost of the deposited catalyst quantity is observed. So, at 70 °C the electrocatalyst loading is twice of the platinum quantity deposited at 25 °C. According to the recorded polarisation curves, the performance is boosted with ⩾35 %, in comparison to the samples prepared at room temperature.
- The nucleation pulse variation indicates that the $PtCl_6^{2-}$ are reduced at a potential under −0.3 V vs. DHE. A maximum catalyst loading was obtained by a potential of −0.8 V vs. DHE. The recorded SEM images indicate a catalyst thickness of 1 µm for a nucleation pulse of −0.3 V and −1 V vs. DHE. Additionally, at this two potentials catalyst agglomerations at the MPL top side are observed.

3. PEMFC operation depends not only on hydrogen oxidation at the anode but in particular on oxygen reduction at the cathode. Therefore a methodical examination of the electrochemically prepared catalyst on ORR was realized. Additionally, the electrocatalyst stability was evaluated by applying an ageing protocol. So, the cell potential was swept between 0.4 − 1.4 V for 500 times and then for another 500 times between 0.05 − 1.4 V.
   - By combining the spraying and electrodeposition methods multiple CL can be created. Thus, a multilayer catalyst configuration containing three distinct electrocatalyst layers was generated. The investigations as cathode have revealed an improved ORR activity and a high stability. However, this kind of structure exhibit extended particles growth due to the multiple deposition steps. In comparison to a commercial GDE from JM, the developed structure indicates a doubling of its mass activity. Moreover, the measurements at different RHs reveal that the FC performances increases by reducing the RH. According to the theory the prepared catalyst ORR kinetics is better at lower RH.
   - The electrodeposition method applicability on other commercial GDL types was investigated. Thus, six different GDL from two distinct producers were coated with the same catalyst and ionomer loading. The research has revealed that the MPL hydrophobicity influence at most the FC performance. So, all prepared GDEs present a ECSA $\geqslant 44\,m^2g^{-1}$, with a maximum of $50.1\,m^2g^{-1}$. After the ageing procedures the prepared catalyst structures indicates a high stability, with a maximum ECSA losses of 30 %. Even if the six GDLs presents a different MPL structure and hydrophobicity the deposited platinum quantity was the same. Additionally, the FC tests show the same behaviour and relatively the same current density at the proposed working potential of 650 mV.
   - The influence of the catalyst loading on the PEMFC cathode was investigated. The analysis has confirmed the possibility to use catalyst load-

ings under $0.1\,\mathrm{mg\,cm^{-2}}$ platinum at the PEMFC cathode. The lowest loading ($0.05\,\mathrm{mg\,cm^{-2}}$) indicates the highest ECSA. In addition it shows the largest losses after the ageing process. However, the recorded current density at $650\,\mathrm{mV}$ is comparable with that registered by other catalyst loadings. By computing the necessary platinum quantity per kW for a loading of $0.1\,\mathrm{mg\,cm^{-2}}$ a remarkable result of $0.12\,\mathrm{g\,kW^{-1}}$ is obtained. To understand in detail the kinetics and the mass transport losses from the polarization curves, a semiempirical model is approached. The fit indicates a Tafel slope for all prepared samples under $70\mathrm{mVdec^{-1}}$. This confirms the electrons ORR mechanism. According to the obtained results we have found that the in-situ electrodeposition method is suitable for catalysts depositions with a loading $\leqslant 0.2\,\mathrm{mg\,cm^{-2}}$.

- To prove the scalability and the possibility of use in an industrial process, the developed method was upscaled to $225\,\mathrm{cm^2}$. The produced GDEs were tested in two cell housing configurations ($10\,\mathrm{cm^2}$ and $50\,\mathrm{cm^2}$). The FC investigations indicates an increased performance for the cell housing with an active area of $50\,\mathrm{cm^2}$. This improvement was attributed to a slight catalyst variation along the GDE surface. Additionally, due to the longer flow field channel on the $50\,\mathrm{cm^2}$ cell the water management is improved and the electrolyte is better humidified. Surprisingly, after the ageing procedure both MEAs show the same current density ($0.5 \pm 0.05\,\mathrm{A\,cm^{-2}}$) at the operation voltage of $650\,\mathrm{mV}$. According to the element mapping analysis the prepared electrodes contains a larger amount of chlorine. This can be a negative factor for the catalyst activity and stability.
- Another requirement for large FC applications is the air operation. Together with the ZBT Duisburg the prepared GDEs were tested at an absolute pressure of $2.5\,\mathrm{bar}$. Additionally, the effect of the ionomer loading was monitored. According to the polarization curves the samples containing a $\mathrm{Nafion^{TM}}$ loading of $0.1\,\mathrm{mg\,cm^{-2}}$ and $0.2\,\mathrm{mg\,cm^{-2}}$ indicate a current density of $0.7\,\mathrm{A\,cm^{-2}}$ at $650\,\mathrm{mV}$. By increasing the $\mathrm{Nafion^{TM}}$ loading a significant decrease on the performance was observed. The electrochemical impedance spectroscopy measurements have revealed that the high $\mathrm{Nafion^{TM}}$ quantity increase the cell ohmic resistance. In comparison to the GDE prepared with a commercial catalyst the electrochemical deposited electrocatalyst indicates a clearly higher ORR activity. Additionally, the mass activity at $0.9\,\mathrm{V}$ provides an increase of $30\,\%$. After ageing procedure, both systems have shown the same current density of $0.67\,\mathrm{A\,cm^{-2}}$ at $650\,\mathrm{mV}$.

As it was presented, the electrochemical deposition method is a flexible and efficient technique which can be applied with success on the GDE preparation. Additionally, the developed spraying process and the optimized steps makes the combined method the right tool to manipulate the CL layer structure. According to our study this approach can be applied to any GDL type, with a high reproducibility. Moreover, the investigated procedure can be very easily upscaled, the only limitation is the electrolyte stability.

Even though a multitude of parameters and a variety of combinations were studied, the method can be further improved. As it was presented, the catalyst loading is not all the time the desired one. Therefore, a further optimization need to be done on the spraying process. Here the temperature of the moving plate need to be gradually varied in smaller steps and the influence on the FC performance studied. Also, in order to short the spraying process the pump rate can be increased. In the same time, to reduce the local GDL cooling, new moving patterns need to be considered. Along the spray process, the electrodeposition can be further extended for other metal precursors. It is know that many researcher work intensively to replace the expensive platinum catalyst with other electrocatalyst like Ni, Fe, Co or platinum alloys. Along that, the developed method can be used for other electrochemical systems as batteries or CO_2reduction.

Moreover, new catalyst structures can be created. For example a multilayered CL with distinct catalyst on each layer. It is known that the platinum-ruthenium catalyst is more tolerant to CO in the fuel cell stream than platinum alone. Thus, by placing this one very deep in the CL will filter most of the reactants impurities. Additionally, using the spraying method a completely new MPL structure can be generated, with a defined interlaced network. To increase the structure porosity pore forming elements as carbonates compounds ($Na_2CO_3, (NH_4)_2CO_3, NH_4HCO_3$) and glycerol can be incorporated. To improve the catalyst activity and to reduce its quantity a multilayer architecture containing the carbon support and the precursor are recommended.

During the actual studies a very thin CL structures were produced, directly on the MPL surface. This provides not only a good contact with the electrolyte but also a challenge for water removing. Therefore for a better water management on cathode applications it is recommended to add an additional Teflon layer after the electrodeposition process.

The developed technique make possible the structuring of MPL network, by spraying the ink over the GDL. Therefore, to precisely organize the CL, the precursor can be sprayed between the carbon layers. Additionally, the structure can include pore forming elements.

In order to avoid the catalyst poisoning with the chloride, another precursor can be applied ($H_2\,Pt(NO_2)_2\,SO_4$, $Na_2\,(Pt(OH)_6) \cdot 2H_2O$ and $K_2\,Pt(OH)_6$). Thus, the catalyst will show an improved activity and a higher stability.

BIBLIOGRAPHY

[1] IEC. Executive summary. Technical report, International Electrotechnical Commission, 2009.

[2] T. D. Gierke, G. E. Munn, and F. C. Wilson. The morphology in nafion perfluorinated membrane products, as determined by wide- and small- angle X-ray studies. *J. Polym. Sci. Polym. Phys. Ed.*, 19(11):1687–1704, 1981.

[3] Pure Perma. Series Fuel Cell Humidifiers - Perma Pure, 2016.

[4] Brian D. James and Andrew B. Spisak. Mass production cost estimation of direct H2PEM fuel cell systems for transportation applications: 2012 update. *U.S. Dep. Energy - Off. Energy Effic. Renew. Energy*, pages 1 – 62, 2012.

[5] Donald W Aitken. Transitioning to a Renewable Energy Future. *Int. Sol. Energy Soc.*, page 59, 2003.

[6] Shin-Ichi Inage. Prospects for large-scale energy storage in decarbonised power grids. *Int. Energy Agency*, pages 15–20, 2009.

[7] United Nations/Framework convention on climate change. Paris agreement. *21st Conf. Parties*, page 3, 2015.

[8] Travis Madsen, Rob Sargent, Tony Dutzik, Gideon Weissman, Kim Norman, and Alana Miller. We have the power: 100% renewable energy for a clean, thriving America. Technical report, Environment America Research & Policy Center, 2016.

[9] ECOFYS. Energy storage opportunities and challenges. Technical report, Ecofys, 2014.

[10] Europe Hydrogen. The ultimate guide to fuel cells and hydrogen technology. Technical report, hydrogen Europe, Brussels, 2016.

[11] International Energy Agency. Hydrogen production and storage. R&D priorities and gaps. *Hydrog. Implement. Agreem.*, 13:392–392, 2006.

[12] Center for Climate and Energy Solutions. Hydrogen fuel cell vehicles. Technical report, Pew center on Global Climate Change, 2011.

[13] Canan Acar and Ibrahim Dincer. Impact assessment and efficiency evaluation of hydrogen production methods. *Int. J. Energy Res.*, 39(13):1757–1768, 2015.

[14] J Larminie and A Dicks. *Fuel Cell Systems Explained*. John Wiley & Sons Ltd., 2003.

[15] Chris. Rayment and Scot Sherwin. Introduction to fuel cell technology, 2003.

[16] Wolf Vielstich, Arnold Lamm, and Hubert A Gasteiger, editors. *Handbook of Fuel Cells Fundamentals Technology and Applications Volume 5*, volume 5. John Wiley & Sons Ltd., 2003.

[17] Zero-emission vehicle standards for 2018 and subsequent model year passenger cars, light-duty trucks, and medium-duty vehicles. Technical Report 9, 2016.

[18] Zero-emission vehicle standards for 2009 through 2017 model year passenger cars, light-duty trucks, and medium-duty vehicles. Technical report, 2016.

[19] Paul E. Dodds, Paul Ekins, Adam D. Hawkes, Francis Li, Will McDowall, Philip Grünewald, Tia Kansara, and Paolo Agnolucci. The role of hydrogen and fuel cells in providing affordable, secure low-carbon heat. Technical Report May, UK Hydrogen and Fuel Cell, 2014.

[20] Sandra Curtin and Jennifer Gangi. State of the states: fuel cells in America 2014, 2013.

[21] Amaury Laporte and Rachael Shook. Fuel cells. Technical Report November, Enviromental and Energy Study Institute, 2015.

[22] A J Appleby and F R Foulkes. *Fuel cell handbook*. U.S. Department of Energy, 1998.

[23] Niancai Cheng, Yuyan Shao, Jun Liu, and Xueliang Sun. Electrocatalysts by atomic layer deposition for fuel cell applications. *Nano Energy*, pages 1–23, 2016.

[24] Wolf Vielstich, Arnold Lamm, and Hubert A Gasteiger, editors. *Handbook of Fuel Cells Fundamentals Technology and Applications Volume 1*, volume 1. John Wiley & Sons Ltd., 2003.

[25] Ge Zhou, Lea Der Chen, and James P. Seaba. CFD prediction of shunt currents present in alkaline fuel cells. *J. Power Sources*, 196(20):8180–8187, 2011.

[26] EG & G services, Ralph M. parsons company., and Science applications international corporation. *Fuel cell handbook*. U.S. Department of Energy, 2000.

[27] F. Uribe, W. Smith, M. Wilson, J. Valerio, T. Rockward, and F. Garzon. Electrodes for polymer electrolyte membrane operation on hydrogen/air and reformate/air. Technical Report 2, Hydrogen, Fuel Cells, and Infrastructure Technologies, 2003.

[28] Advanced Research Projects Agency-Energy. $1/W Photovoltaic systems. Technical report, U.S. Department of Energy, 2010.

[29] Dimitrios Papageorgopoulos. PEMFC R & D at the DOE fuel cell technologies program. *Fuel Cell*, 2011.

[30] M. Crouch. Fuel cell systems for base stations : deep dive study. *GSMA Green Power Mob.*, pages 1–27, 2011.

[31] Robert Remick, Douglas Wheeler, and Singh Prabhakar. MCFC and PAFC R & D workshop summary report. Technical report, U.S. Department of Energy Prepared, 2009.

[32] Jacob Spendelow and Jason Marcinkoski. DOE Hydrogen and Fuel Cells Program Record -2011. Technical report, U.S. Department of Energy, 2011.

[33] Xiaozi Yuan, Haijiang Wang, Jian Colin Sun, and Jiujun Zhang. AC impedance technique in PEM fuel cell diagnosis - a review. *Int. J. Hydrogen Energy*, 32(17):4365–4380, 2007.

[34] Sang Hyun Ahn, Sunyeol Jeon, Hee Young Park, Soo Kil Kim, Hyoung Juhn Kim, Eunae Cho, Dirk Henkensmeier, Sung Jong Yoo, Suk Woo Nam, Tae Hoon Lim, and Jong Hyun Jang. Effects of platinum loading on the performance of proton exchange membrane fuel cells with high ionomer content in catalyst layers. *Int. J. Hydrogen Energy*, 38(23):9826–9834, 2013.

[35] Sarah Flick, Shankar R. Dhanushkodi, and Walter Merida. Transport phenomena in polymer electrolyte membrane fuel cells via voltage loss breakdown. *J. Power Sources*, 280:97–106, 2015.

[36] W Winkler and P Nehter. Thermodynamics of fuel cells. *Model. Solid Oxide Fuel Cells*, pages 25–37, 2008.

[37] Chee Kok Poh, Zhiqun Tian, Narissara Bussayajarn, Zhe Tang, Fabing Su, San Hua Lim, Yuan Ping Feng, Daniel Chua, and Jianyi Lin. Performance enhancement of air-breathing proton exchange membrane fuel cell through utilization of an effective self-humidifying platinum-carbon catalyst. *J. Power Sources*, 195(24):8044–8051, 2010.

[38] K. C. Neyerlin, H. A. Gasteiger, C. K. Mittelsteadt, J. Jorne, and W. Gu. Effect of relative humidity on oxygen reduction kinetics in a PEMFC. *J. Electrochem. Soc.*, 152(6):A1073, 2005.

[39] K. C. Neyerlin, Wenbin Gu, Jacob Jorne, and Hubert a. Gasteiger. Determination of catalyst unique parameters for the oxygen reduction reaction in a PEMFC. *J. Electrochem. Soc.*, 153(10):A1955, 2006.

[40] Hui Xu, Ying Song, H. Russell Kunz, and James M. Fenton. Effect of elevated temperature and reduced relative humidity on ORR kinetics for PEM fuel cells. *J. Electrochem. Soc.*, 152(9):A1828, 2005.

[41] Samuel Cruz-Manzo and Rui Chen. Electrochemical impedance study on estimating the mass transport resistance in the polymer electrolyte fuel cell cathode catalyst layer. *J. Electroanal. Chem.*, 702:45–48, 2013.

[42] Amir M. Niroumand, Oldooz Pooyanfar, Natalia Macauley, Jake Devaal, and Farid Golnaraghi. In-situ diagnostic tools for hydrogen transfer leak characterization in PEM fuel cell stacks part I: R&D applications. *J. Power Sources*, 278:652–659, 2015.

[43] B. Andreaus, A. J. McEvoy, and G. G. Scherer. Analysis of performance losses in polymer electrolyte fuel cells at high current densities by impedance spectroscopy. *Electrochim. Acta*, 47(13-14):2223–2229, 2002.

[44] E. Antolini, L. Giorgi, a. Pozio, and E. Passalacqua. Influence of Nafion loading in the catalyst layer of gas-diffusion electrodes for PEFC. *J. Power Sources*, 77(2):136–142, 1999.

[45] Rohit Makharia, Mark F. Mathias, and Daniel R. Baker. Measurement of catalyst layer electrolyte resistance in PEFCs using electrochemical impedance spectroscopy. *J. Electrochem. Soc.*, 152(5):A970–A977, 2005.

[46] Wenchao Sheng, Seung Woo Lee, Ethan J. Crumlin, Shuo Chen, and Yang Shao-Horn. Synthesis, activity and durability of Pt nanoparticles supported on multi-walled carbon nanotubes for oxygen reduction. *J. Electrochem. Soc.*, 158:B1398, 2011.

[47] A. Marinkas, R. Hempelmann, A. Heinzel, V. Peinecke, I. Radev, and H. Natter. Enhanced stability of multilayer graphene-supported catalysts for polymer electrolyte membrane fuel cell cathodes. *J. Power Sources*, 295:79–91, 2015.

[48] Masao Miyake, Takeshi Ueda, and Tetsuji Hirato. Potentiostatic Electrodeposition of Pt Nanoparticles on Carbon Black. *J. Electrochem. Soc.*, 158(9):D590, 2011.

[49] F. Arena, J. Mitzel, and R. Hempelmann. Permeability and diffusivity measurements on polymer electrolyte membranes. *Fuel Cells*, 13(1):58–64, 2013.

[50] Ok-Hee Kim, Yong-Hun Cho, Dong Young Chung, Min Jeong Kim, Ji Mun Yoo, Ji Eun Park, Heeman Choe, and Yung-Eun Sung. Facile and gram-scale synthesis of metal-free catalysts: toward realistic applications for fuel cells. *Sci. Rep.*, 5:8376, 2015.

[51] S. J. Peighambardoust, S. Rowshanzamir, and M. Amjadi. Review of the proton exchange membranes for fuel cell applications. *Int. J. Hydrogen Energy*, 35(17):9349–9384, 2010.

[52] Frank A. de Bruijn, Robert C. Makkus, R. K A M Mallant, and G. J M Janssen. *Materials for state-of-the-art PEM fuel cells, and their suitability for operation above 100 C*, volume 1. Elsevier Ltd., 2007.

[53] Christian Schmidt, Tobias Glück, and Gudrun Schmidt-Naake. Modification of Nafion membranes by impregnation with ionic liquids. *Chem. Eng. Technol.*, 31(1):13–22, 2008.

[54] Ji Hye Won, Hyeon Ji Lee, Kyung Suk Yoon, Young Taik Hong, and Sang Young Lee. Sulfonated SBA-15 mesoporous silica-incorporated sulfonated poly(phenylsulfone) composite membranes for low-humidity proton exchange membrane fuel cells: Anomalous behavior of humidity-dependent proton conductivity. *Int. J. Hydrogen Energy*, 37(11):9202–9211, 2012.

[55] Jean-Marc Le Canut, Ruth Latham, Walter Mérida, and David a. Harrington. Impedance study of membrane dehydration and compression in proton exchange membrane fuel cells. *J. Power Sources*, 192(2):457–466, 2009.

[56] Mehdi Amirinejad, Soosan Rowshanzamir, and Mohammad H. Eikani. Effects of operating parameters on performance of a proton exchange membrane fuel cell. *J. Power Sources*, 161(2):872–875, 2006.

[57] Takahisa Suzuki, Hajime Murata, Tatsuya Hatanaka, and Yu Morimoto. Analysis of the Catalyst Layer of Polymer Electrolyte Fuel Cells. *R&D Rev. Toyota CRDL*, 39(3):33–38, 2003.

[58] Toby Astill, Zhong Xie, Zhiqing Shi, Titichai Navessin, and Steven Holdcroft. Factors influencing electrochemical properties and performance of hydrocarbon-based electrolyte PEMFC catalyst layers. *J. Electrochem. Soc.*, 156(4):B499, 2009.

[59] Satheesh Sambandam and Vijay Ramani. SPEEK/functionalized silica composite membranes for polymer electrolyte fuel cells. *J. Power Sources*, 170(2):259–267, 2007.

[60] Jason Marcinkoski, Jacob Spendelow, Adria Wilson, and Dimitrios Papageorgopoulos. DOE hydrogen and fuel cells program record - 2015. Technical report, U.S. Department of Energy, 2015.

[61] Ermete Antolini. Palladium in fuel cell catalysis. *Energy Environ. Sci.*, 2(9):915, 2009.

[62] Hui Wang, Xia Yuan, Dongwei Li, and Xiaohu Gu. Dendritic PtCo alloy nanoparticles as high performance oxygen reduction catalysts. *J. Colloid Interface Sci.*, 384(1):105–109, 2012.

[63] Yanguang Li, Wu Zhou, Hailiang Wang, Liming Xie, Yongye Liang, Fei Wei, Juan-Carlos Idrobo, Stephen J. Pennycook, and Hongjie Dai. An oxygen reduction electrocatalyst based on carbon nanotube-graphene complexes. *Nat. Nanotechnol.*, 7(6):394–400, 2012.

[64] Ahmad El-kharouf, Thomas J. Mason, Dan J.L. Brett, and Bruno G. Pollet. Ex-situ characterisation of gas diffusion layers for proton exchange membrane fuel cells. *J. Power Sources*, 218:393–404, 2012.

[65] Ahmad El-kharouf. *Understanding GDL properties and performance in polymer electrolyte fuel cells*. PhD thesis, University of Birmingham, 2014.

[66] S. Litster and G. McLean. PEM fuel cell electrodes. *J. Power Sources*, 130(1-2):61–76, 2004.

[67] Doo Sung Hwang, Chi Hoon Park, Sung Chul Yi, and Young Moo Lee. Optimal catalyst layer structure of polymer electrolyte membrane fuel cell. *Int. J. Hydrogen Energy*, 36(16):9876–9885, 2011.

[68] M. S. Wilson and S. Gottesfeld. Thin-film catalyst layers for polymer electrolyte fuel cell electrodes. *J. Appl. Electrochem.*, 22(1):1–7, 1992.

[69] Xiaoliang Cheng, Baolian Yi, Ming Han, Jingxin Zhang, Yaguang Qiao, and Jingrong Yu. Investigation of platinum utilization and morphology in catalyst layer of polymer electrolyte fuel cells. *J. Power Sources*, 79(1):75–81, 1999.

[70] Mallika Gummalla, Sarah Ball, David Condit, Somaye Rasouli, Kang Yu, Paulo Ferreira, Deborah Myers, and Zhiwei Yang. Effect of particle size and operating conditions on Pt3Co PEMFC cathode catalyst durability. *Catalysts*, 5(2):926–948, 2015.

[71] Atilla Biyikoglu. Review of proton exchange membrane fuel cell models. *Int. J. Hydrogen Energy*, 30(11):1181–1212, 2005.

[72] Roswitha Zeis. Materials and characterization techniques for high-temperature polymer electrolyte membrane fuel cells. *Beilstein J. Nanotechnol.*, 6(1):68–83, 2015.

[73] Hong Hua Chen and Min Hsing Chang. Effect of cathode microporous layer composition on proton exchange membrane fuel cell performance under different air inlet relative humidity. *J. Power Sources*, 232:306–309, 2013.

[74] Andrew P Saab, Fernando H Garzon, and Thomas A Zawodzinski. Determination of ionic and electronic resistivities in carbon/polyelectrolyte fuel-cell composite electrodes. *J. Electrochem. Soc.*, 149(12):A1541, 2002.

[75] Jiankui Chen, Huimin Liu, YongAn Huang, and Zhouping Yin. High-rate roll-to-roll stack and lamination of multilayer structured membrane electrode assembly. *J. Manuf. Process.*, 23:175–182, 2016.

[76] T. Binninger, E. Fabbri, R. Kotz, and T J Schmidt. Determination of the electrochemically active surface area of metal-oxide supported platinum catalyst. *J. Electrochem. Soc.*, 161(3):H121–H128, 2013.

[77] S. Shukla, K. Domican, K. Karan, S. Bhattacharjee, and M. Secanell. Analysis of low platinum loading thin polymer electrolyte fuel cell electrodes prepared by inkjet printing. *Electrochim. Acta*, 156:289–300, 2015.

[78] Nejat Veziroglu, Svetlana Zaginaichenko, Dmitry Schur, B. Baranowski, Anatoliy Shpak, and Valeriy Skorokhod. *Hydrogen materials science and chemistry of carbon nanomaterials*, volume 172. Springer Sceince+Business Media, Inc, CarbonNanomaterials2005, 2005.

[79] Héctor R. Colón-Mercado and Branko N. Popov. Stability of platinum based alloy cathode catalysts in PEM fuel cells. *J. Power Sources*, 155(2):253–263, 2006.

[80] S. Martin, P. L. Garcia-Ybarra, and J. L. Castillo. Electrospray deposition of catalyst layers with ultra-low Pt loadings for PEM fuel cells cathodes. *J. Power Sources*, 195(9):2443–2449, 2010.

[81] Toyota. 2016 Mirai Product Information 2016 Mirai Product Information. pages 1–3, 2016.

[82] Allen Hermann, Tapas Chaudhuri, and Priscila Spagnol. Bipolar plates for PEM fuel cells: A review. *Int. J. Hydrogen Energy*, 30(12):1297–1302, 2005.

[83] Peter Odetola, Patricia Popoola, Olawale Popoola, and David Delport. *Electrodeposition of functional coatings on bipolar plates for fuel cell applications - a review*. InTech, 2016.

[84] S. Shimpalee, V. Lilavivat, H. McCrabb, Y. Khunatorn, H.-K. Lee, W.-K. Lee, and J.W. Weidner. Investigation of bipolar plate materials for proton exchange membrane fuel cells. *Int. J. Hydrogen Energy*, 41(31):13688–13696, 2016.

[85] E. Planes, L. Flandin, and N. Alberola. Polymer composites bipolar plates for PEMFCs. *Energy Procedia*, 20:311–323, 2012.

[86] A. Müller, P. Kauranen, A. Von Ganski, and B. Hell. Injection moulding of graphite composite bipolar plates. *J. Power Sources*, 154(2):467–471, 2006.

[87] Christine Minke, Thorsten Hickmann, Antonio R. Dos Santos, Ulrich Kunz, and Thomas Turek. Cost and performance prospects for composite bipolar plates in fuel cells and redox flow batteries. *J. Power Sources*, 305:182–190, 2016.

[88] Bingyan Jiang, Nacera Stübler, Wangqing Wu, Qingxin Li, Gerhard Ziegmann, and Dieter Meiners. Manufacturing and characterization of bipolar fuel cell plate with textile reinforced polymer composites. *Mater. Des.*, 65:1011–1020, 2015.

[89] Chunzhi He, Sanket Desai, Garth Brown, and Srinivas Bollepalli. PEM Fuel Cell Catalysts: Cost, Performance, and Durability. *Electrochem. Soc. Interface*, pages 41–44, 2005.

[90] Jens Mitzel, Francesco Arena, Harald Natter, Tanja Walter, Martin Batzer, Manfred Stefener, and Rolf Hempelmann. Electrodeposition of PEM fuel cell catalysts by the use of a hydrogen depolarized anode. *Int. J. Hydrogen Energy*, 37(7):6261–6267, 2012.

[91] K. Ignatova and L. Petkov. Electrodeposition and morphology of Ni-Co alloy powders by constant and pulsating overpotential electrolysis. *Powder Metall. Met. Ceram.*, 49(11-12):707–715, 2011.

[92] María Escudero-Escribano, Arnau Verdaguer-Casadevall, Paolo Malacrida, Ulrik Grønbjerg, Brian P Knudsen, Anders K Jepsen, Jan Rossmeisl, Ifan E. L. Stephens, and Ib Chorkendorff. Pt5Gd as a highly active and stable catalyst for oxygen electroreduction. *J. Am. Chem. Soc.*, 134(40):16476–9, 2012.

[93] Qian Sun, Zheng Ren, Rongming Wang, Ning Wang, and Xia Cao. Platinum catalyzed growth of NiPt hollow spheres with an ultrathin shell. *J. Mater. Chem.*, 21(6):1925, 2011.

[94] Fengjuan Zhu, Jaemin Kim, Kai Chieh Tsao, Junliang Zhang, and Hong Yang. Recent development in the preparation of nanoparticles as fuel cell catalysts. *Curr. Opin. Chem. Eng.*, 8:89–97, 2015.

[95] Ermete Antolini. Nitrogen-doped carbons by sustainable N- and C-containing natural resources as nonprecious catalysts and catalyst supports for low temperature fuel cells. *Renew. Sustain. Energy Rev.*, 58:34–51, 2016.

[96] Yan Xiang, Shanfu Lu, and San Ping Jiang. Layer-by-layer self-assembly in the development of electrochemical energy conversion and storage devices from fuel cells to supercapacitors. *Chem. Soc. Rev.*, 41(21):7291, 2012.

[97] A. Capelo, M.A. Esteves, A.I. de Sá, R.A. Silva, L. Cangueiro, A. Almeida, R. Vilar, and C.M. Rangel. Stability and durability under potential cycling of Pt/C catalyst with new surface-functionalized carbon support. *Int. J. Hydrogen Energy*, 41(30):12962–12975, 2016.

[98] R. R. Adzic, J. Zhang, K. Sasaki, M. B. Vukmirovic, M. Shao, J. X. Wang, A. U. Nilekar, M. Mavrikakis, J. A. Valerio, and F. Uribe. Platinum monolayer fuel cell electrocatalysts. *Top. Catal.*, 46(3-4):249–262, 2007.

[99] Ruizhi Yang, Jennifer Leisch, Peter Strasser, and Michael F. Toney. Structure of dealloyed PtCu3 thin films and catalytic activity for oxygen reduction. *Chem. Mater.*, 22(16):4712–4720, 2010.

[100] Ratndeep Srivastava, Prasanna Mani, Nathan Hahn, and Peter Strasser. Efficient oxygen reduction fuel cell electrocatalysis on voltammetrically dealloyed Pt-Cu-Co nanoparticles. *Angew. Chemie - Int. Ed.*, 46(47):8988–8991, 2007.

[101] Christian Kulp, Xingxing Chen, Andrea Puschhof, Stefanie Schwamborn, Christoph Somsen, Wolfgang Schuhmann, and Michael Bron. Electrochemical synthesis of core-shell catalysts for electrocatalytic applications. *ChemPhysChem*, 11(13):2854–2861, 2010.

[102] Waldemar Mróz, Bogusław Budner, Wojciech Tokarz, Piotr Piela, and Michael L. Korwin-Pawlowski. Ultra-low-loading pulsed-laser-deposited platinum catalyst films for polymer electrolyte membrane fuel cells. *J. Power Sources*, 273:885–893, 2015.

[103] Ju Chou, Shrisudersan Jayaraman, Asanga D. Ranasinghe, Eric W. McFarland, Steven K. Buratto, and Horia Metiu. Efficient electrocatalyst utilization: Electrochemical deposition of Pt nanoparticles using nafion membrane as a template. *J. Phys. Chem. B*, 110(14):7119–7121, 2006.

[104] J.-Y. Lin, Y.-T. Tsai, S.-Y. Tai, Y.-T. Lin, C.-C. Wan, Y.-L. Tung, and Y.-S. Wu. Pulse-reversal deposition of cobalt sulfide thin dilm as a counter electrode for dye-sensitized solar cells. *J. Electrochem. Soc.*, 160(2):D46–D52, 2012.

[105] Christian Kulp, Konrad Gillmeister, Wolf Widdra, and Michael Bron. Synthesis of CuCorePtShell nanoparticles as model structures for core-shell electrocatalysts by direct platinum electrodeposition on copper. *ChemPhysChem*, 14(6):1205–1210, 2013.

[106] Kyoung Hwan Choi, Han Sung Kim, and Tae Hee Lee. Electrode fabrication for proton exchange membrane fuel cells by pulse electrodeposition. *J. Power Sources*, 75(2):230–235, 1998.

[107] B.M.E. Baumgartner and C.J. Raub. The electrodeposition of platinum and platinum alloys. *Platin. Met. Rev.*, 32(4):188–197, 1988.

[108] Peter Odetola, Patricia Popoola, Olawale Popoola, and David Delport. Parametric variables in electro-deposition of composite coatings. Imtech.

[109] A. Egetenmeyer, I. Radev, D. Durneata, M. Baumgärtner, V. Peinecke, H. Natter, and R. Hempelmann. Pulse electrodeposited cathode catalyst layers for PEM fuel cells. *Int. J. Hydrogen Energy*, 2017.

[110] Zi Fan Song, Jun Wei, Xiang Li, Wei Yue Zhou, Zhen Qi Chang, and Christophe A. Serra. Synthesis of size-controlled Pt/C/PTFE hydrophobic catalyst pellets in a capillary-based microfluidic system. *Int. J. Hydrogen Energy*, 39(30):16944–16952, 2014.

[111] A. M. Chaparro, B. Gallardo, M. A. Folgado, A. J. Martin, and L. Daza. PEMFC electrode preparation by electrospray: Optimization of catalyst load and ionomer content. *Catal. Today*, 143(3-4):237–241, 2009.

[112] G. Sasikumar, J. W. Ihm, and H. Ryu. Dependence of optimum Nafion content in catalyst layer on platinum loading. *J. Power Sources*, 132(1-2):11–17, 2004.

[113] Josef Christian. *Degradation phenomena and design principles for stable and active Pt/C fuel cell catalysts*. PhD thesis, University Bochum, 2013.

[114] Xiao-Zi Yuan, Chaojie Song, Wang Haijiang, and Jiujun Zhang. *Electrochemical impedance spectrosopy in PEM fuel cells*, volume 1. Springer, 2015.

[115] Allen J Bard and Larry R Faulkner. *ELECTROCHEMICAL METHODS Fundamentals and Applications*. John Wiley & Sons, INC., 2001.

[116] Inc Scribner Associates. Electrochemical impedance spectroscopy (EIS): a powerful and cost-effective tool for fuel cell diagnostics. Technical report, Scribner Associates, 2016.

[117] Evgenij Barsoukov and J. Ross Macdonald. *Impedance Spectroscopy Theory, Experiment, and Applications*. Wiley-Interscience, second edi edition, 2005.

[118] Junbo Hou, Wei Song, Hongmei Yu, Yu Fu, Lixing Hao, Zhigang Shao, and Baolian Yi. Ionic resistance of the catalyst layer after the PEM fuel cell suffered freeze. *J. Power Sources*, 176(1):118–121, 2008.

[119] Bernard A. Boukamp and Henny J M Bouwmeester. Interpretation of the Gerischer impedance in solid state ionics. *Solid State Ionics*, 157(1-4):29–33, 2003.

[120] Anne-Kristine Meland, Dick Bedeaux, and Signe Kjelstrup. A gerischer phase element in the impedance diagram of the polymer electrolyte membrane fuel cell anode. *Am. Chem. Soc.*, pages 21380–21388, 2005.

[121] E. Bradley Easton and Peter G. Pickup. An electrochemical impedance spectroscopy study of fuel cell electrodes. *Electrochim. Acta*, 50(12):2469–2474, 2005.

[122] H. Tawfik, Y. Hung, and D. Mahajan. Metal bipolar plates for PEM fuel cell - a review. *J. Power Sources*, 163(2):755–767, 2007.

[123] F. Dundar, A. Uzunoglu, A. Ata, and K. J. Wynne. Durability of carbon-silica supported catalysts for proton exchange membrane fuel cells. *J. Power Sources*, 202:184–189, 2012.

[124] Thorsten Arnhol and Andreas Brinner. Explosion protection in the fuel-cell vehicle development of hydrogen-powered propulsion systems at DLR. *Ex-Magazine*, pages 1–4, 2005.

[125] Yuxiu Liu, Michael W. Murphy, Daniel R. Baker, Wenbin Gu, Chunxin Ji, Jacob Jorne, and Hubert a. Gasteiger. Proton conduction and oxygen reduction kinetics in PEM fuel cell cathodes: effects of ionomer-to-carbon ratio and relative humidity. *J. Electrochem. Soc.*, 156(8):B970, 2009.

[126] Dongmei Chen, Wei Li, and Huei Peng. An experimental study and model validation of a membrane humidifier for PEM fuel cell humidification control. *J. Power Sources*, 180(1):461–467, 2008.

[127] Elif Eker Kahveci and Imdat Taymaz. Effect of humidification of the reactant gases in the proton exchange membrane fuel cell. *J. Clean Energy Technol.*, 3(5):356–359, 2015.

[128] Thomas A. Zawodzinski, John Davey, Judith Valerio, and Shimshon Gottesfeld. The water content dependence of electro-osmotic drag in proton-conducting polymer electrolytes. *Electrochim. Acta*, 40(3):297–302, 1995.

[129] Yik Yang. *LabVIEW graphical programming cookbook*. Packt Publishing, Birningham, 2014.

[130] Marco Schwartz and Oliver Manickum. *Programming Arduino with LabVIEW*. Packt Publishing, Birningham, 2015.

[131] A. M. Chaparro, P. Ferreira-Aparicio, M. A. Folgado, A. J. Martin, and L. Daza. Catalyst layers for proton exchange membrane fuel cells prepared by electrospray deposition on Nafion membrane. *J. Power Sources*, 196(9):4200–4208, 2011.

[132] K. Scott, S. Pilditch, and M. Mamlouk. Modelling and experimental validation of a high temperature polymer electrolyte fuel cell. *J. Appl. Electrochem.*, 37(11):1245–1259, 2007.

[133] Walther Schwarzacher. Electrodeposition: a technology for the future. *Electrochem. Soc. Interface*, 15(1):32–35, 2006.

[134] Huichao He, Peng Xiao, Ming Zhou, Yunhuai Zhang, Yichao Jia, and Shujuan Yu. Preparation of well-distributed Pt-Ni nanoparticles on/into TiO 2NTs by pulse electrodeposition for methanol photoelectro-oxidation. *Catal. Commun.*, 16(1):140–143, 2011.

[135] G. Sandmann, H. Dietz, and W. Plieth. Preparation of silver nanoparticles on ITO surfaces by a double-pulse method. *J. Electroanal. Chem.*, 491(1-2):78–86, 2000.

[136] Jens Mitzel. *Gasdiffusionselektroden für Polymerelektrolytmembran-Brennstoffzellen mittels elektrochemischer Abscheidungsverfahren*. PhD thesis, Saarland University, 2012.

[137] Kaitlyn M. Yarrow, Nicole E. De Almeida, and E. Bradley Easton. The impact of pre-swelling on the conductivity and stability of Nafion/sulfonated silica composite membranes. *J. Therm. Anal. Calorim.*, 119(2):807–814, 2015.

[138] Kirt A. Page, Jae Wook Shin, Scott A. Eastman, Brandon W. Rowe, Sangcheol Kim, Ahmet Kusoglu, Kevin G. Yager, and Gery R. Stafford. In situ method for measuring the mechanical properties of nafion thin films during hydration cycles. *ACS Appl. Mater. Interfaces*, 7(32):17874–17883, 2015.

[139] Seyed Schwan Hosseiny. *Vanadium/air redox flow battery*. PhD thesis, University of Twente, 2011.

[140] Francesco Arena. *Cross - linked sPEEK and its application for High Temperature PEMFCs*. PhD thesis, Saarland University, 2014.

[141] Brian Krassenstein. Five 3D Printing Predictions For the Next Five Years, 2014.

[142] Hiroshi Iden, Satoshi Takaichi, Yoshihisa Furuya, Tetsuya Mashio, Yoshitaka Ono, and Atsushi Ohma. Relationship between gas transport resistance in the catalyst layer and effective surface area of the catalyst. *J. Electroanal. Chem.*, 694:37–44, 2013.

[143] L Giorgi, E Antolini, A Pozio, and E Passalacqua. Influence of the PTFE content in the diffusion layer of low-Pt loading electrodes for polymer electrolyte fuel cells. *Electrochim. Acta*, 43(24):3675–3680, 1998.

[144] Yan-Jie Wang, Baizeng Fang, Hui Li, Xiaotao T. Bi, and Haijiang Wang. Progress in modified carbon support materials for Pt and Pt-alloy cathode catalysts in polymer electrolyte membrane fuel cells. *Prog. Mater. Sci.*, 82:445–498, 2016.

[145] Da Li, Youpeng Qu, Jia Liu, Weihua He, Haiman Wang, and Yujie Feng. Using ammonium bicarbonate as pore former in activated carbon catalyst layer to enhance performance of air cathode microbial fuel cell. *J. Power Sources*, 272:909–914, 2014.

[146] Wolf Vielstich, Arnold Lamm, and Hubert A Gasteiger, editors. *Handbook of fuel cells fundamentals technology and applications volume 3*, volume 3. John Wiley & Sons Ltd., 2003.

[147] J. Mehta, V., Cooper. Review and analysis of PEM fuel cell design and manufacturing. *J. Power Sources*, 114(1):32–53, 2003.

[148] Ying Song, Yu Wei, Hui Xu, Minkmas Williams, Yuxiu Liu, Leonard J. Bonville, H. Russell Kunz, and James M. Fenton. Improvement in high temperature proton exchange membrane fuel cells cathode performance with ammonium carbonate. *J. Power Sources*, 141(2):250–257, 2005.

[149] Tatyana V. Reshetenko, Hee T. Kim, and Ho J. Kweon. Cathode structure optimization for air-breathing DMFC by application of pore-forming agents. *J. Power Sources*, 171(2):433–440, 2007.

[150] Gui-Cheng Liu, Yi-Tuo Wang, Jing Zhang, Meng Wang, Chao-Jie Zhang, and Xin-Dong Wang. Pore-forming technology and performance of MEA for direct methanol fuel cells. *J. Chem. Technol. Biotechnol.*, 88(5):818–822, 2013.

[151] Jishi Zhao, Xiangming He, Li Wang, Jianhua Tian, Chunrong Wan, and Changyin Jiang. Addition of NH4HCO3 as pore-former in membrane electrode assembly for PEMFC. *Int. J. Hydrogen Energy*, 32(3):380–384, 2007.

[152] Yuying Zheng, Zhengjie Dou, Yanxiong Fang, Muwu Li, Xin Wu, Jianhuang Zeng, Zhaohui Hou, and Shijun Liao. Platinum nanoparticles on carbon-nanotube support prepared by room-temperature reduction with H2 in ethylene glycol/water mixed solvent as catalysts for polymer electrolyte membrane fuel cells. *J. Power Sources*, 306:448–453, 2016.

[153] W. Zhu, D. Ku, J. P. Zheng, Z. Liang, B. Wang, C. Zhang, S. Walsh, G. Au, and E. J. Plichta. Buckypaper-based catalytic electrodes for improving platinum utilization and PEMFC's performance. *Electrochim. Acta*, 55(7):2555–2560, 2010.

[154] FREUDENBERG FCCT SE & CO. KG. Freudenberg gas diffusion layers for PEMFC and DMFC.

[155] Haoran Yu, Justin M. Roller, William E. Mustain, and Radenka Maric. Influence of the ionomer/carbon ratio for low-Pt loading catalyst layer prepared by reactive spray deposition technology. *J. Power Sources*, 283:84–94, 2015.

[156] André Wolz, Susanne Zils, Marc Michel, and Christina Roth. Structured multilayered electrodes of proton/electron conducting polymer for polymer electrolyte membrane fuel cells assembled by spray coating. *J. Power Sources*, 195(24):8162–8167, 2010.

[157] John J. Whalen, James D. Weiland, and Peter C. Searson. Electrochemical deposition of platinum from aqueous ammonium hexachloroplatinate solution. *J. Electrochem. Soc.*, 152(11):C738–C743, 2005.

[158] Ana M. Gómez-Marín, Ruben Rizo, and Juan M. Feliu. Some reflections on the understanding of the oxygen reduction reaction at Pt(111). *Beilstein J. Nanotechnol.*, 4(1):956–967, 2013.

[159] S.-Y. Lee, H.-J. Kim, K.-H. Kim, E Cho, I.-H. Oh, and T.-H. Lim. Gradient catalyst coating for a proton exchange membrane fuel cell operation under non-humidified conditions. *Electrochem. Solid-State Lett.*, 10(10):B166–B169, 2007.

[160] Daouda Fofana, Sadesh Kumar Natarajan, Jean Hamelin, and Pierre Benard. Low platinum, high limiting current density of the PEMFC (proton exchange membrane fuel cell) based on multilayer cathode catalyst approach. *Energy*, 64:398–403, 2014.

[161] M. Prasanna, E. A. Cho, H. J. Kim, I. H. Oh, T. H. Lim, and S. A. Hong. Performance of proton-exchange membrane fuel cells using the catalyst-gradient electrode technique. *J. Power Sources*, 166(1):53–58, 2007.

[162] Olivier Antoine, Yann Bultel, Patrick Ozil, and Robert Durand. Catalyst gradient for cathode active layer of proton exchange membrane fuel cell. *Electrochim. Acta*, 45(27):4493–4500, 2000.

[163] K. C. Neyerlin, Wenbin Gu, Jacob Jorne, Alfred Clark, and Hubert A. Gasteiger. Cathode catalyst utilization for the ORR in a PEMFC. *J. Electrochem. Soc.*, 154(2):B279, 2007.

[164] Dawn M Bernardi, Mark W Verbrugge, J Electrochem Soc, Dawn M Bernardi, and Mark W Verbrugge. A mathematical model of the solid-polymer-electrolyte fuel cell. 139(9):2477–2491, 1992.

[165] Nancy L Garland. Polymer DOE ′ s R & D electrolyte membrane fuel cell catalyst development activities. 2012.

[166] Information Technische. Sigracet 10 Series Gas Diffusion Layer.

[167] Information Technische. Sigracet 34 & 35 Series Gas Diffusion Layer.

[168] S. R. Dhanushkodi, S. Kundu, M. W. Fowler, and M. D. Pritzker. Study of the effect of temperature on Pt dissolution in polymer electrolyte membrane fuel cells via accelerated stress tests. *J. Power Sources*, 245:1035–1045, 2014.

[169] Junbom Kim, Charles Chamberlin, Junbom Kim, Seong-min Lee, Supramaniam Srinivasan, and Charles E Chamberlin. Modeling of proton exchange membrane fuel cell performance with an empirical equation. 142(February):2670–2674, 1995.

[170] M. D. Gasda, R. Teki, T.-M. Lu, N. Koratkar, G. a. Eisman, and D. Gall. Sputter-deposited Pt PEM fuel cell electrodes: particles vs layers. *J. Electrochem. Soc.*, 156:B614, 2009.

[171] A. Fischer, J. Jindra, and H. Wendt. Porosity and catalyst utilization of thin layer cathodes in air operated PEM-fuel cells. *J. Appl. Electrochem.*, 28(3):277–282, 1998.

[172] Myoungseok Lee, Makoto Uchida, Donald A. Tryk, Hiroyuki Uchida, and Masahiro Watanabe. The effectiveness of platinum/carbon electrocatalysts: Dependence on catalyst layer thickness and Pt alloy catalytic effects. *Electrochim. Acta*, 56(13):4783–4790, 2011.

[173] E. Passalacqua, F. Lufrano, G. Squadrito, A. Patti, and L. Giorgi. Nafion content in the catalyst layer of polymer electrolyte fuel cells: Effects on structure and performance. *Electrochim. Acta*, 46(6):799–805, 2001.

DECLARATION

I hereby declare that this dissertation is my own original work except where otherwise indicated. All data or concepts drawn directly or indirectly from other sources have been correctly acknowledged. This dissertation has not been submitted in its present or similar form to any other academic institution either in Germany or abroad for the award of any other degree.

Saarbrücken, 2017

Dan Iulian Durneata,